Entwurf eines elastischen Antriebssystems für eine gangunterstützende aktive Orthese für Menschen mit inkompletter Querschnittslähmung

Design of an Elastic Actuation System for a Gait-Assistive Active Orthosis for Incomplete Spinal Cord Injured Subjects

Masterthesis at the Institute for Mechatronic Systems in Mechanical Engineering at Technische Universität Darmstadt and the Biomedical Engineering Research Centre at Universitat Politècnica de Catalunya

Diese Arbeit wurde eingereicht von Florian Stuhlenmiller

TECHNISCHE UNIVERSITÄT DARMSTADT

Diese Arbeit wurde vorgelegt von
Florian Stuhlenmiller

Betreuer: Dr.-Ing. Philipp Beckerle, Assoc. Prof. Dr. Josep M. Font-Llagunes

Bearbeitungszeitraum: 02.11.2015 bis 02.05.2016

Darmstadt, den May 1, 2016

Thesis Statement

Hiermit versichere ich, die vorliegende Arbeit ohne Hilfe Dritter nur mit den angegebenen Quellen und Hilfsmitteln angefertigt zu haben. Alle Stellen, die aus Quellen entnommen wurden, sind als solche kenntlich gemacht. Diese Arbeit hat in gleicher oder ähnlicher Form noch keiner Prüfungsbehörde vorgelegen. In der abgegebenen Thesis stimmen die schriftliche und elektronische Fassung überein.

Darmstadt, den 30.04.2016

Unterschrift _____

Stuhlenmiller, Florian

I herewith formally declare that I have written the submitted thesis independently. I did not use any outside support except for the quoted literature and other sources mentioned in the paper. I clearly marked and separately listed all of the literature and all of the other sources which I employed when producing this academic work, either literally or in content. This thesis has not been handed in or published before in the same or similar form. In the submitted thesis, the written copies and the electronic version are identical in content.

Darmstadt, the 30.04.2016

Unterschrift _____

Stuhlenmiller, Florian

Abstract

A spinal cord injury severely reduces the quality of life of affected people. Following the injury, limitations of the ability to move may occur due to the disruption of the motor and sensory functions of the nervous system depending on the severity of the lesion. An active stance-control knee-ankle-foot orthosis was developed and tested in earlier works to aid incomplete SCI subjects by increasing their mobility and independence. This thesis aims at the incorporation of elastic actuation into the active orthosis to utilise advantages of the compliant system regarding efficiency and human-robot interaction as well as the reproduction of the phyisological compliance of the human joints. Therefore, a model-based procedure is adapted to the design of an elastic actuation system for a gait-assisitve active orthosis. A determination of the optimal structure and parameters is undertaken via optimisation of models representing compliant actuators with increasing level of detail. The minimisation of the energy calculated from the positive amount of power or from the absolute power of the actuator generating one human-like gait cycle yields an optimal series stiffness, which is similar to the physiological stiffness of the human knee during the stance phase. Including efficiency factors for components, especially the consideration of the electric model of an electric motor yields additional information. A human-like gait cycle contains high torque and low velocities in the stance phase and lower torque combined with high velocities during the swing. Hence, the efficiency of an electric motor with a gear unit is only high in one of the phases. This yields a conceptual design of a series elastic actuator with locking of the actuator position during the stance phase. The locked position combined with the series compliance allows a reproduction of the characteristics of the human gait cycle during the stance phase. Unlocking the actuator position for the swing phase enables the selection of an optimal gear ratio to maximise the recuperable energy. To evaluate the developed concept, a laboratory specimen based on an electric motor, a harmonic drive gearbox, a torsional series spring and an electromagnetic brake is designed and appropriate components are selected. A control strategy, based on impedance control, is investigated and extended with a finite state machine to activate the locking mechanism. The control scheme and the laboratory specimen are implemented at a test bench, modelling the foot and shank as a pendulum articulated at the knee. An identification of parameters yields high and nonlinear friction as a problem of the system, which reduces the energy efficiency of the system and requires appropriate compensation. A comparison between direct and elastic actuation shows similar results for both systems at the test bench, showing that the increased complexity due to the second degree of freedom and the elastic behaviour of the actuator is treated properly. The final proof of concept requires the implementation at the active orthosis to emulate uncertainties and variations occurring during the human gait.

Kurzzusammenfassung

Eine Verletzung des Rückenmarks beeinträchtigt die Lebensqualität betroffener Personen. Dabei ist eine mögliche Folge eine eingeschränkte Bewegungsfähigkeit aufgrund der Störung motorischer und sensorischer Funktionen des Nervensystems in Abhängigkeit des entsprechenden Schweregrades. Eine aktive Knie-Fuß-Orthese mit gesperrtem Kniegelenk während der Standphase wurde im Rahmen vorheriger Arbeiten entwickelt und getestet, um Personen mit inkompletter Rückenmarskverletzung zu unterstützen und ihnen Mobilität und Unabhängigkeit zu ermöglichen. Diese Thesis hat die Anwendung elastischer Antriebstechnik in der aktiven Orthese zum Ziel, um Vorteile nachgiebiger Antriebe hinsichtlich Mensch-Maschine Interaktion und Effizienz zu Nutzen. Für die Entwicklung wird ein modellbasiertes Vorgehen verwendet und die Bestimmung der optimalen Struktur und Parameter des Antriebs erfolgt mittels Optimierung verschiedener Modelle nachgiebiger Systeme. Die Minimierung der Energie, bestimmt aus positiver oder absoluter Leistung des Aktors für die Erzeugung eines Gangzyklus, ergibt eine optimale, serielle Steifigkeit, die der physiologischen Steifigkeit des Knies während der Standphase ähnelt. Die Berücksichtigung der Wirkungsgrade verschiedener Komponenten, allen voran die Berücksichtigung des elektschen Motormodells, ergibt weitere Erkentnisse. Da ein natürlicher Gangzyklus hohe Momente bei geringen Geschwindigkeiten in der Standphase und geringere Momente aber hohe Geschwindigkeiten während der Schwungphase enthält, ergeben sich für einen elektrischen Motor mit Getriebe zwei Bereiche, von denen sich allerdings nur einer im Bereich optimaler Effizienz befindet. Somit erfolgt die Entwicklung eines Konzepts mit blockiertem Aktor während des Standes. Dies erlaubt, die Nachbildung eines natürlichen Ganges während der Standphase aufgrund der seriellen Nachgiebigkeit. Eine Entsperrung des Aktors für die Schwungphase und Auswahl eines optimalen Übersetzungsverhältnisses des Getriebes führt zu einer Maximierung der Rekuperation. Ein Prototyp des vorgeschlagenen Konzepts, bestehend aus elektrischem Motor, Harmonic-Drive-Getriebe, Torsionsfeder und elektromagnetischer Bremse, wird entwickelt. Zudem wird eine Regelstrategie, basierend auf Impedanzregelung und Zustandsautomaten für die Kontrolle der Bremse untersucht. Der Prototyp und die Regelstrategie werden in einen Prüfstand implementiert, der Unterschenkel und Fuß als Pendel modelliert. Eine Parameterbestimmung ergibt hohe und nicht-lineare Reibung als Schwachpunkt des Systems, da dies die Effizienz stark reduziert eine entsprechende Kompensation erfordert. Ein Vergleich zwischen direktem und elastischem Antrieb zeigt ähnliche Ergebnisse am Prüfstand für beide Systeme, sodass die erhöhte Komplexität aufgrund des zweiten Freiheitsgrades und der Nachgiebigkeit des elastischen Systems entsprechend gehandhabt wird. Eine endgültige Bewertung des Antriebskonzepts erfordert die Implementierung in die aktive Orthese, um Variationen und mögliche Störungen des natürlichen Ganges berücksichtigen zu können.

Contents

Notation

Abbreviations

A-SCKAFO	Active Stance-Control Knee-Ankle-Foot Orthosis
BIBO	Bounded Input, Bounded Output
CREB	Biomedical Engineering Research Centre
CSEA	Clutched Series Elastic Actuator
DA	Direct Actuator
EC	Electronically Commutated
EMB	Electro-Magnetic friction Brake
FES	Functional Electrical Stimulation
FSM	Finite State Machine
GRF	Ground Reaction Force
ISP	Input Strictly Passive
IMU	Inertial Measurement Unit
SCI	Spinal Cord Injury
SEA	Series Elastic Actuator
UPC	Universitat Politècnica de Catalunya
OSP	Output Strictly Passive
PEA	Parallel Elastic Actuator
VSP	Very Strictly Passive

Symbols

$\dot{x}$	denotes the time derivative of x
$\ddot{x}$	denotes the second time derivative of x
$\|\|x\|\|$	denotes the L_p norm of x
$\tilde{x}$	denotes the error of x
x_{max}, x_{min}	denotes maximum, minimum value of x
x_d	denotes desired x
$\mathbf{RE}[x]$	denotes the real part of x
a_{EMB}	activation signal of the EMB
a_n	nth parameter in the Fourier Series
b_n	nth parameter in the Fourier Series

d_a	damping of the actuator
d_p	damping of the pendulum
d_d	desired damping impedance control
$d_{d,cr}$	desired critical damping impedance control
g	gravitational acceleration
$\Delta\theta_s$	deflection of a series spring
$\Delta\theta_p$	deflection of a parallel spring
E_{gc}	energy per gait cycle from absolute power
$E_{gc,rec}$	energy per gait cycle including recuperation
$E_{gc,+}$	energy per gait cycle from positive power
$E_{gc,-}$	energy per gait cycle from negative power
η	total efficiency factor
η_x	efficiency factor of component x
$eta_{x,r}$	resulting efficiency factor of component x
$F_{ndyn,min}$	minimum allowable dynamic normal force of a compression spring
I	electrical current
I_a	moment of inertia of the actuator
$I_{a,d}$	desired moment of inertia of the actuator impedance control
I_{EC}	moment of inertia of an EC-motor
I_{ext}	moment of inertia of the external system
I_{nl}	no load current
I_p	total moment of inertia of the pendulum
$I_{p,cg}$	moment of inertia with respect to the centre of mass of the pendulum
i_G	gear ratio
k_s	series stiffness
k_b	speed constant
k_{cp}	spring constant compression spring
k_d	desired stiffness impedance control
k_o	optimal stiffness
k_m	motor constant
k_p	parallel stiffness
k_s	series stiffness
k_t	total stiffness
k_τ	torque constant
l_h	body height
$l_{p,cg}$	distance between centre of mass and axis of rotation of the pendulum
l_{cp}	length compression spring

m_h	body mass
m_p	mass of the pendulum of the test bench
N	number of compression springs
ν_m	viscouos motor damping
P	power
P_a	actuator power
P_{el}	electrical power
P_k	knee power
P_{max}	peak power
R	terminal resistance
r	external input of a system
r_s	radius to compression spring
S	storage function
s	Laplace variable
t	time
t_{gc}	time for one gait cycle
u	input of a system
u_{ci}	control input
U	electrical voltage
θ	angle
θ_a	actuator angle
$\theta_{a,0}$	initial actuator angle
θ_k	knee angle
$\dot{\theta}_{nl}$	no load speed
θ_p	pendulum angle
τ	torque
τ_a	actuator torque
τ_{EMB}	torque of the friction brake
τ_{ext}	external torque
$\tau_{ext,dev}$	external deviation torque
τ_g	gravitational torque
τ_k	knee torque
τ_l	locking torque
$\tau_{s,a}$	allowable torque of the torsional spring
ω	angular frequency
ω_0	angular resonance frequency
y	output of a system

1 Introduction

1.1 Motivation

Spinal cord injuries (SCI) damage or sever the connections between body and brain thus interrupting motor and sensory functions. Hence, subjects are partly or completely paralysed depending on the severity of the injury. The quality of life of people, who experienced such an injury, is greatly reduced [1]. The reduced mobility can lead to dependence on caregivers and daily tasks can become challenging. The recovery of the mobility is rated as a highly desired goal for most subjects as examined in [2]. The World Health Organisation proposed in the *WHO global disability action plan 2014-2021*, among other things, to strengthen assistive technologies to allow people with disabilities to live in dignity and achieve their full potential [3]. A lower limb knee-ankle-foot orthosis has been developed within the framework of the national project *Design of an innovative gait-assistive active orthosis for SCI subjects based on motion analysis and prediction methods and complex musculoskeletal models* conducted at the Biomedical Engineering Research Centre (CREB) of the Universitat Politècnica de Catalunya (UPC). The prototype of the designed active orthosis is based on rigid actuation and enables a subject with incomplete spinal cord injury to walk with the help of crutches or parallel bars in a laboratory environment. To improve the orthotic device, the utilisation of compliant actuation is investigated during this thesis to improve the efficiency of the system and allow the device to reproduce a human-like locomotion of the subject. Thereby, elastic components are utilised in the actuation system to store and release energy, reduce impact loads and mimic the physiological stiffness of human joints, which can not or only with high effort be provided by rigid actuation. This is part of continuous refinement of the active orthosis, to develop a safe and affordable device increasing the quality of life of subjects limited by a spinal cord injury. As part of this project, the aim of the thesis is presented in the following.

1.2 Aim of the Thesis

Based on the motivation, the aim of this project is to design an elastic actuation system for an active orthosis, enabling spinal cord injured subjects to perform a healthy, human-like locomotion. Therefore, simulations of the compliant system are performed to analyse potentials and extract

optimal parameters. A conceptual actuation system is selected, designed and manufactured and an appropriate control strategy is analysed to provide stable and robust operation. Laboratory specimen of the concept and control scheme are implemented at a test bench to evaluate and compare the elastic system with standard, rigid actuation. The design process and experimental evaluation focuses on an efficient reproduction of a comfortable, healthy gait cycle as well as the safety of the user and is evaluated accordingly.

1.3 Structure of the Thesis

In the beginning, Chapter 2 presents the national project followed by a selection of exemplary gait data that is used throughout the analysis. In addition, an overview of the basis and state of the art for active orthoses and elastic actuators as well as an overview of the theoretical background utilised to design the control law is given. The applied procedure to design the elastic actuation system and to fulfil the aim of this work is presented in Chapter 3. The first step is the analysis of the potential of elastic actuators presented in Chapter 4, where respective criteria are defined followed by optimisations of models with increasing level of detail to extract the optimal structure and parameters for an elastic actuator. Chapter 4 finishes with a conceptual structure for the actuation system, which is designed in the following chapter. Thereby, concepts based on the results of the previous analysis are generated and analysed. Chapter 5 ends with a laboratory specimen, designed according to one selected concept as well as proposed components to fulfil the aim of the project. The selection, analysis and evaluation of a control strategy is presented in Chapter 6. An experimental evaluation of the laboratory specimen and control is performed in Chapter 7 and fulfilment of the aim of the project is analysed. Social and economic impact of this thesis are analysed in Chapter 8. Finally, a conclusion and discussion of this thesis is presented in Chapter 9.

2 State of the Art and Theoretical Background

This chapter presents the fundamentals used throughout this thesis, starting with a description of the project *Design of an innovative gait-assistive active orthosis for SCI subjects based on motion analysis and prediction methods and complex musculoskeletal models*. As the project is engaged in supporting SCI subjects to walk, biomechanical data of the human gait are given focused on the characteristics of the knee. Afterwards, a brief review of the history and state of the art of active ortheses is presented followed by an overview of elastic actuation systems. In the following, fundamentals for the control strategies examined in Chapter 6 are given and the challenges of the design of elastic actuators are summarised at the end of the chapter.

2.1 SCI Injuries and Project Description

This thesis is affiliated with the project *Design of an innovative gait-assistive active orthosis for SCI subjects based on motion analysis and prediction methods and complex musculoskeletal models* with grant number DPI2012-38331-C03-02 supported by the Ministry of Economy and Competitiveness of Spain. The project is undertaken in cooperation with the University of La Coruña, focused on control and experimental tests, the University of Extremadura working on muscle modelling, Electromyography and Functional Electrical Stimulation (FES) as well as the UPC, responsible for simulation and mechanical design. The project started in January 2012 and finished in December 2015 with successful testing of a prototypic active stance-control knee-ankle-foot orthosis (A-SCKAFO). The main aim of the project is to develop a gait-assistive active orthosis that is efficient and affordable to increase mobility and independence of SCI subjects. A continuation of the development of active orthosis occurs in the course of the project *Low-cost motor-FES hybrid orthosis for the gait of spinal cord injured subjects and simulation methods to support the design and adaptation (HYBOR)* with grand number DPI2015-65959-C3-2-R. Due to the SCI injury, paralysis or muscle atrophy occurs, which reduces the capabilities of the subject. To determine the required external support, a biomechanical multibody model is investigated, so that the human together with the device can walk with the help of crutches [4]. A prototypic active orthosis is presented in [4], which is able to support subjects classified by the ASIA Im-

pairment Scale with levels C or D. These levels describe an incomplete SCI and the preservation of motor and sensor functions below the injury [4].

2.2 Characteristics of the Human Gait

This section presents the characteristics of a healthy human walking gait, usually described by joint angles and torques. A common procedure to measure gait data is the motion capturing method, e.g., as described in [5]. Several markers are placed on distinctive points of the subject and their positions are recorded during the movement using several cameras. The resulting coordinates for every marker are then transformed to angular position of the joints. Forces and torques can be calculated by inverse dynamics using measured ground reaction forces, e.g., captured by force plates, and moments of inertia of the human body. This approach is widely used to analyse gait data, for example in [5, 6].
The resulting characteristics of the human gait can be described as several repetitive cycles, each segmented into a stance phase and a swing phase as presented in Figure 2.1. The stance phase, beginning with the heel strike, which induces a loading response, continues with mid- and terminal stance and ends with the pre-swing. The following swing phase is separated in initial, mid- and terminal swing. The stance phase lasts approximately 60 % of the gait cycle, the swing phase 40 %. Only one leg is loaded during the single support phase, which lasts from the mid-stance to the terminal stance.

Characteristic Trajectories of the Knee during Human Gait

As common for gait data, trajectories are given in percent of progress of the gait cycle and the torque of the knee τ_k as well as power P_k are presented normalized to the body weight. The

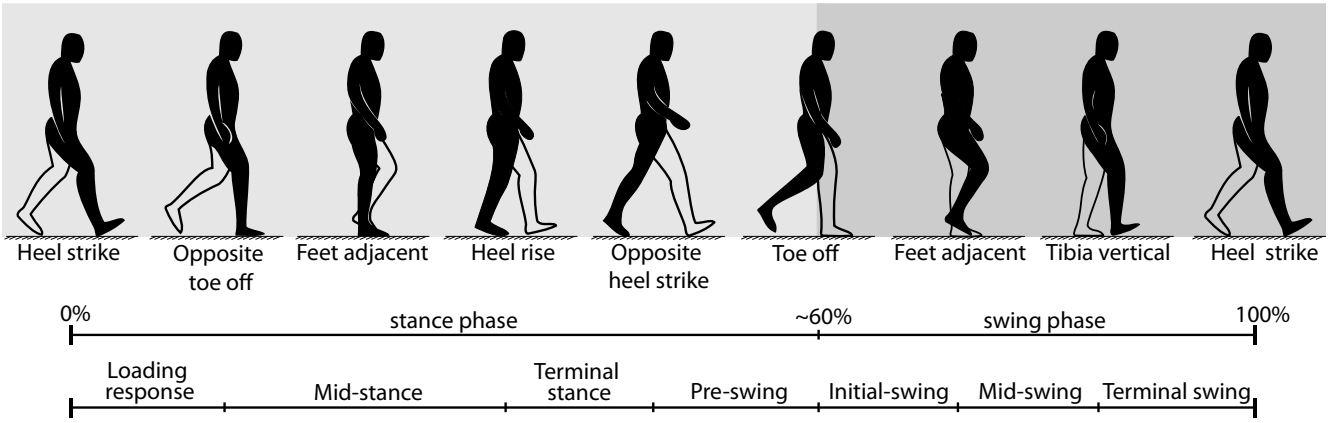

Figure 2.1: Phases of the Gait Cycle, as presented in [7]

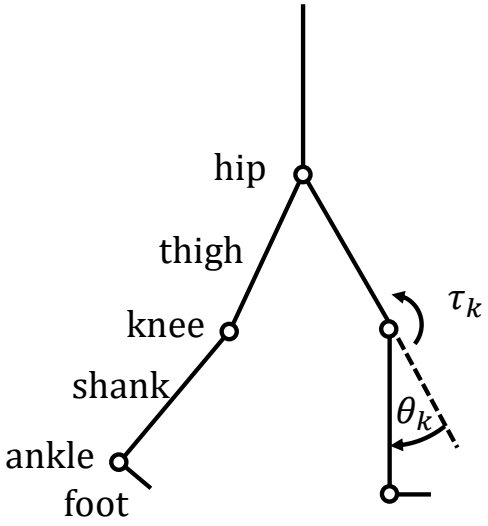

Figure 2.2: Definition of the knee angle and torque

knee angle θ_k is between thigh and shank and defined to be zero when fully extended as depicted in Figure 2.2. In the following, the characteristics of the knee are presented using data from [6]. In this study, a comparison of 20 young (6 to 17 years) and 20 adult (22 to 72 years) subjects performing different tasks is conducted. The authors of [6], not associated with this thesis, published the data of the experiments, which is used as a reference for healthy human gait in the following analyses. Figure 2.3 presents the characteristic trajectories for knee flexion and extension from healthy adult subjects walking at approximately $0.9\,\mathrm{m\,s^{-1}}$, described as very slow gait in [6]. The dashed lines for τ_k, knee angle θ_k and P_k represent the standard deviation of the mean value as given in [6]. The red segments of the curves in Figure 2.3 represent 0 % to 50 % of the gait cycle, from the heel strike until the end of the single support phase. High loads occur in the knee during this phase due to weight acceptance and the support with a single leg, which are approximately represented by the red part in the torque-angle characteristic illustrated in the bottom right of Figure 2.3. As discussed in [8], this section can be modelled as a linear torsional spring. A further analysis of the knee trajectories is presented in Section 4.1.

2.3 Active Orthoses

After presenting a healthy human gait, active exoskeletons and orthoses are presented in this section. These can be described as devices worn by an operator and fit closely to the body [9]. Exoskeletons enhance the capabilities of a healthy person, e.g., the *Berkeley lower extremity exoskeleton* [10] supports the user in transporting heavy loads. Orthoses are rehabilitation devices assisting in the ambulation of an operator with a limb pathology [9]. Active orthoses allow con-

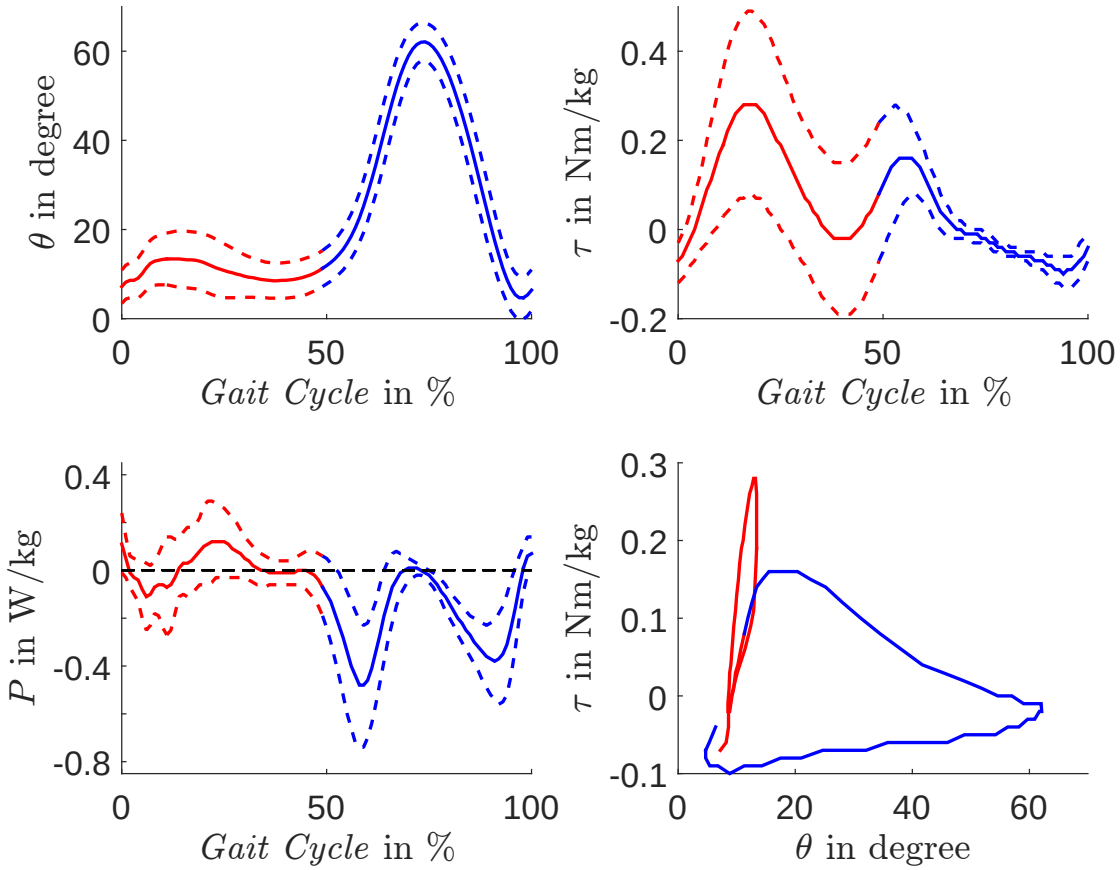

Figure 2.3: Gait Data for the Knee from [6] / top left: knee angle / top right: knee torque / bottom left: knee power / bottom right: torque-angle characteristic

trolling the joints as well as adding and dissipating energy [11]. Active orthotic devices can be distinguished based on the number and position of actuated joints and the portability. An exemplary non-portable device is the *Lokomat* [11], a treadmill-based robot used for rehabilitation. In virtue of the project goals described in Section 2.1, focus of this thesis are wearable orthoses. Devices operating the hip [12], knee [4, 13, 14] or ankle joint [15, 16] as well as combinations of knee and hip [17–19] are researched.

Active, wearable orthoses usually consist of an actuation system powered by batteries, a microcontroller running control algorithms as well as sensors to capture motion, forces and user intention. The actuator transfers forces via a a human-robot interface attached to the operator. The control strategy usually consists of three parts: a high level controller detecting environment and user intention, a mid level controller to transform this information into input variables for the actuation system and a low level controller executing the desired trajectories [20].

For generating or supporting a human-like gait, different strategies are used, e.g., variable damping of a knee orthosis is implemented in [21] via a rhelogical fluid to accelerate recovery in knee injury patients. Compliant actuation designs are utilized, e.g., in [12, 15, 17], to increase efficiency and human-robot-interaction by adding elasticity to the system. Further characteristics of elastic actuators are presented in Section 2.4. Advanced control strategies for the low level controller, e.g. force/torque control and impedance control are used in [12, 17] and [15, 22] respectively. Machine learning and adaptive control is used, e.g., for non-compliant actuated systems in [15, 23–25], to optimize the control for individual subjects.
Further strategies can be found in the field of active prostheses, which substitute a lost limb instead of providing support to the subject. They usually consist of the same components as active orthoses with differences in the human-robot interface. For example, the *CYBERLEGS Beta Prosthesis* [26] contains an elastic actuator and an elastic mechanism that takes the load during the weight acceptance phase. In the design proposed in [27], an elastic actuator is combined with a clutch to improve the energy efficiency and increase the distance the subject can walk with the device. As can be seen from the literature presented above, research aims at improving active orthoses to provide a human-like gait for individual subjects, however complexity increases as elastic actuation or intelligent control is applied.

2.4 Elastic Actuators

As presented above, elastic actuators are used to enhance efficiency and provide human-like gait in active orthoses and prosthesis. This chapter discusses the properties of elastic actuation and gives a basic model for the analysis performed in Chapter 4. The basic idea for series elastic actuators (SEA) is adding an elasticity in series between actuator and output, while for an parallel elastic actuator (PEA) the elasticity is connected in parallel to either actuator or output. A fundamental model of a SEA is depicted in Figure 2.4 and a PEA with spring parallel to actuator is presented in Figure 2.5. The actuator with moment of inertia I_a generates the torque τ_a while the output of each system is represented by the load τ_{ext} and includes all output torques loading the spring, e.g., inertial and gravitational torques as well as external disturbances. The stiffness of the spring is denoted by k_s for the SEA and k_p for the parallel spring and the deflection by $\Delta\theta_s$ and $\Delta\theta_{pa}$, respectively. An analysis of the depicted model of the SEA leads to a system with two degrees of freedom coupled by a spring according to the following equation:

$$\begin{bmatrix} I_a & 0 \\ 0 & 0 \end{bmatrix} \begin{bmatrix} \ddot{\theta}_a \\ \ddot{\theta}_{ext} \end{bmatrix} + \begin{bmatrix} k_s & -k_s \\ -k_s & k_s \end{bmatrix} \begin{bmatrix} \theta_a \\ \theta_{ext} \end{bmatrix} = \begin{bmatrix} \tau_a \\ -\tau_{ext} \end{bmatrix} \tag{2.1}$$

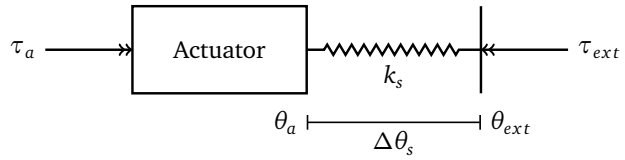

Figure 2.4: Model of an SEA

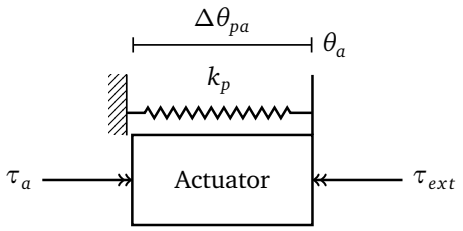

Figure 2.5: Model of an PEA with elasticity parallel to actuator

The inertial torque $I_{ext}\ddot{\theta}_{ext}$ is included in τ_{ext} and therefore only the moment of inertia of the actuator is present in the mass matrix. This representation allows the use of the equations in conjunction with arbitrary output systems, as just τ_{ext} and θ_{ext} need to be known to calculate the necessary actuator angle and torque. In contrast to the SEA, the PEA only has one degree of freedom. The deflection $\Delta\theta_{pa}$ composed of the actuator position θ_a and an offset $\theta_{a,0}$. Therefore, the system with an elasticity in parallel to the actuator is modelled according to the following equation:

$$I_a\ddot{\theta}_a + k_p(\theta_a - \theta_{a,0}) = \tau_a - \tau_{ext} \tag{2.2}$$

The parallel stiffness can be used to reduce the required actuator power [28, 29] thus improving the design by selecting a lower gear ratio or smaller actuator size in comparison to a directly driven system. For systems with harmonic trajectories, SEAs improve the efficiency [7, 30], as energy can be stored and released in the elasticity independent from the actuator. In addition, SEAs display high backdriveability of the output system and high shock tolerance due to the elasticity in series to the actuator [31]. As the torque at the output generated by a SEA depends on the position and not on the actual torque of the actuator, the stability and fidelity of force control is improved [31]. Furthermore, the compliance of SEA provides higher safety in robot-human interactions as mechanical deformation occurs and the deflection of the spring can serve as a cheap torque sensor [32, 33]. However, the complexity of elastic actuators is increased. Additional mechanical components and sensors are required, resulting in larger dimensions and increased weight. Furthermore, modelling and control is more complicated, as the differential equations of a SEA is of fourth order due to the two degrees of freedom and collocation may occur.

A further extension of elastic actuators by implementing an adaptable compliance leads to variable stiffness actuators. This allows for an adjustment of the characteristic behaviour of the actuation system to get optimal results. For example, in [7, 30] the natural dynamics of the system are adapted to the operating frequency to minimise the required mechanical energy. The compliance is reduced for high velocity operations in [32] to increase the safety

of human-robot interactions. The compliance can be equilibrium-controlled, which is based on a control law [34]. A physical adaptation of the stiffness is achieved via an antagonistic-controlled, mechanically-controlled or structure-controlled concept [34]. The antagonistic controlled stiffness is based on the utilisation of two SEAs with nonlinear springs working against each other [34]. A mechanism changing the structure of an elastic element, e.g., length of a spring is applied for a structure-controlled approach, while the pretension or preload of the spring is modified to mechanically control the stiffness [34].

2.5 Boundedness of Signals and Passivity of Systems

This section presents the theoretical background and a respective interpretation of the boundedness of signals and the passivity of systems. The definitions are used in Chapter 6 to design the control law of a non-linear system via a passivity approach. Proof and further definitions, examples as well as discussion can be found in [35].

Boundedness of Signals and Transfer Functions

In the following, definitions for the boundedness of signals and transfer functions are given.

Definition 1. *Bounded real transfer function (Definition 2.24 in [35]):*
A function $g(s)$ is said to be bounded real, if

1. $g(s)$ *is analytic in* $\mathbf{RE}[s] > 0$
2. $g(s)$ *is real for real and positive* s
3. $|g(s)| \leq 1$ *for all* $\mathbf{RE}[s] > 0$

A function $g(s)$ is analytic in a domain only if it is defined and infinitely differentiable for all points in the domain [35]. This means that a bounded real function $g(s)$ does not have poles with a positive real part. If condition 1 in Definition 1 is extended to $g(s)$ *is analytic in* $\mathbf{RE}[s] \geq 0$, the function $g(s)$ is asymptotically stable.

Definition 2. *Definition of the norms L_p norms (Section 4.2 in [35]):*
The most common signal norms are L_1, L_2, L_p and L_∞, which are defined as:

1. L_1: $||x||_1 \equiv \int |x(t)| \, \mathrm{d}t$
2. L_2: $||x||_2 \equiv \left(\int |x(t)|^2 \, \mathrm{d}t \right)^{\frac{1}{2}}$
3. L_p: $||x||_p \equiv \left(\int |x(t)|^p \, \mathrm{d}t \right)^{\frac{1}{p}}$ *for* $2 \leq p < +\infty$

4. L_∞: $||x||_\infty \equiv \sup|x(t)|$ *for* $t > 0$

Regarding the notation: A function f belongs to the norm L_p if f is locally Lebesgue integrable $\left(|\int_a^b f(t)\,\mathrm{d}t| < +\infty\right)$ for any $b > a$ and $||f||_p < +\infty$. By using one of the presented norms, limits of $f(t)$ can be examined. An example is given in [35] for the system

$$\dot{x} = Ax(t) + Bu(t) \tag{2.3}$$

with A exponentially stable. If $u \in L_2$, then $x \in L_2 \cap L_\infty$, $\dot{x} \in L_2$ and $\lim_{t\to+\infty} x(t) = 0$. Thus, the examination of the L_p norm of the output for a respective input allows the analysis of the stability of a system. For example, a system for which $||y||_p \leq C||u||_p$ is called bounded-input bounded-output (BIBO) stable for an arbitrary but finite $C > 0$, which means that the output y of this system never becomes infinite for a finite input u and the system is stable.

Passivity of Systems

A definition of a passive system according is given in [35], regarding the following system:

$$\Gamma = \begin{cases} \dot{x}(t) = f(x(t)) + g(x(t))u(t) \\ y(t) = h(x(t)) \\ x(0) = x_0 \end{cases} \tag{2.4}$$

Definition 3. *Dissipative System (Definition 4.20 in [35]):*
The system Γ *is said to be dissipative if there exists a so called storage function* $S(x) > 0$*, such that the following inequality holds:*

$$S(x(t)) \leq S(x(0)) + \int_0^t w(y(s)u(s))\,\mathrm{d}s \tag{2.5}$$

along all possible trajectories of Γ *starting at* $x(0)$*, for all* $x(0)$*,* $t \geq 0$ *(said differently: for all admissible controllers* $u(\cdot)$ *that drive the state from* $x(0)$ *to* $x(t)$ *on the interval* $[0, t]$*).*

For this definition, it is assumed that the supply rate $w(y(s)u(s))$ is locally Lebesgue integrable independently of the input and the initial conditions [35]. A physical representation of the storage function S is the energy of the system and the supply rate $y(s)u(s)$ is described as the power added to the system. The single terms in Equation (2.5) are however not limited to

satisfy a physical representation. Equation (2.5) can also be written in terms of power along the trajectory of the system, which gives the definition for passive systems:

Definition 4. *Passive System (Corollary 2.3 in [35]):*
Assume there exists a continuously differentiable function $S(\cdot) \geq 0$, such that $\int_0^t d(s)\,\mathrm{d}s \geq 0$ for all $t \geq 0$. Then

1. *If*

$$\dot{S}(t) \leq y^T(t)u(t) - d(t) \tag{2.6}$$

   for all $t \geq 0$ and all functions $u(\cdot)$, the system is passive.

2. *If there exists a $\delta \geq 0$, such that*

$$\dot{S}(t) \leq y^T(t)u(t) - \delta u^T(t)u(t) - d(t) \tag{2.7}$$

   for all $t \geq 0$ and all functions $u(\cdot)$, the system is input strictly passive (ISP).

3. *If there exists a $\epsilon \geq 0$, such that*

$$\dot{S}(t) \leq y^T(t)u(t) - \epsilon y^T(t)y(t) - d(t) \tag{2.8}$$

   for all $t \geq 0$ and all functions $u(\cdot)$, the system is output strictly passive (OSP).

4. *If there exists $\delta \geq 0$ and a $\epsilon \geq 0$, such that*

$$\dot{S}(t) \leq y^T(t)u(t) - \delta u^T(t)u(t) - \epsilon y^T(t)y(t) - d(t) \tag{2.9}$$

   for all $t \geq 0$ and all functions $u(\cdot)$, the system is very strictly passive (VSP).

In addition to the definition of passive systems, the behaviour of interconnected systems is discussed in [35].

Definition 5. *Stability of Feedback Systems (Corollary 5.3 in [35]):*
The system with a feedback loop $\frac{y(s)}{r(s)} = \frac{H_1}{1+H_2}$ as depicted in Figure 2.6 with the external input r is L_2-finite-gain stable, if

1. *H_1 is passive and H_2 is ISP*

2. *H_1 is OSP and H_2 is passive*

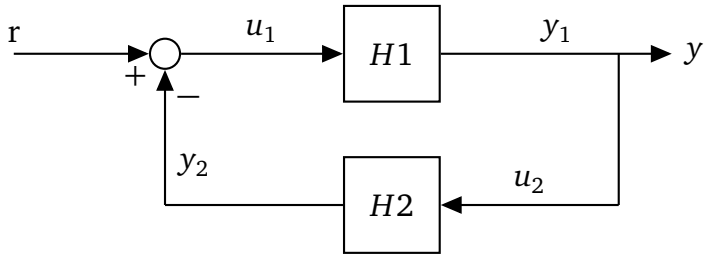

Figure 2.6: Block Diagram of a Feedback System as presented in [35]

This definition and the respective proof in [35] show the stability of a feedback system under certain requirements regarding the passivity of each transfer function. As only the passivity attribute is required, the exact transfer function is not necessary and thus Definition 5 can be used for nonlinear systems. The resulting stability is similar to the concept of the BIBO-stability and yields $||y||_2 \leq C||u||_2$, so $u \in L_2$ is necessary. In addition, L_2-finite-gain stability is related to the positive realness of transfer functions presented in Definition 1, showing that the system does not have poles with a negative real part. This is discussed via the Nonlinear Kalman-Yakubovich-Popov Lemma for a general case (Lemma 4.87) in [35].

To summarise, Definitions 3 to 5 provide criteria and a description regarding the passivity of systems. The determination of a nonlinear system to be passive yields a criterion for the stability, as the output is bounded for a bounded input according to Definitions 1 and 2, and therefore does not reach infinite values. Hence, a nonlinear, passive system either approaches a certain, finite value or oscillates continuous with a bounded amplitude.

2.6 Design Challenges

A review of the state of the art shows that elastic actuation has a high potential for the improvement of active orthoses to increase energy efficiency and provide safe and comfortable human-robot interaction. The successful implementation is thereby a challenge, as the complexity is higher compared to a directly actuated system. For example, the second degree of freedom due to the compliant behaviour influences the natural dynamics of the system and can lead to unstable operation. Hence, additional components, e.g., elastic elements with respective mounting, have to be designed, and a more advanced control approach to ensure 5stability of the system, which is often nonlinear, is required as well.

3 Approach to the Design of an Elastic Actuation System

The goals introduced in Section 1.2 are described and broken down into different phases to select a procedure to achieve the objectives. Thus, this section creates a basis for the development of the elastic actuator as design criteria are selected in reference to the presented goals.

3.1 Goals of Thesis in Detail

The importance of enabling SCI-subjects to walk and participate in daily life is motivated in Chapter 1. This work is based on the active orthosis presented in Section 2.1 and potential improvements by adding elasticity to the system are analysed. This leads to the definition of goals, which are given a priority and summarized in Table 3.1. Of most importance is the generation of a human-like gait-cycle described by characteristic trajectories for the position and the torque of the natural gait. The data given in [6] and presented in Section 2.2 is utilised as a reference. It is assumed that by achieving this goal, the active orthosis enables the subject to perform a natural gait, which leads to a stable and safe motion. This has to be assured in the presence of disturbances and uncertainties, e.g., the system has to work for a variety of different subjects with distinctive masses, heights, walking speeds and gait characteristics. Thus, the system has to be robust in respect to the mechanical design and the design of the controller. In

Table 3.1: Design Goals for the Elastic Actuator

Priority	Description	Attribute
1	Human-like gait-cycle	Generate position and torque according to natural gait data, representative gait data from [6] is used
2	Robustness	Stable against disturbances, fulfil function for range of biological parameters
3	Comfort	Smooth trajectories during the gait, absorption of shocks
4	Energy efficiency	Reduced energy consumption in comparison to a directly-driven system

addition, the comfort of the orthosis has to be high for each individual. As the system is mobile, the energy efficiency should be high to allow operation for long period of time. This is given the lowest priority, as it does not influence the basic function and safety of the subject. The goals have to be achieved by designing an elastic actuation system with an appropriate control law. Hence, a design procedure is selected and presented in the next chapter to provide a structured approach during the project.

3.2 Model-Based Design Procedure

A human-machine-centred design framework as presented in [7] can be used to structure the design approach. During this procedure, technical factors are generated from biomechanical data and combined with human factors from questionnaires as well as literature and a quality-function deployment method is applied to generate a respective mechatronic design. However a literature research has not resulted in reliable data to generate human factors for active orthoses for SCI-subjects. Only one subject participates in the national project described above and is still training with the developed prototype, thus some experience is available, but the evaluation of the data is not finalised at the date of this thesis. Therefore, human factors are not included directly in the selection of criteria as proposed in [7].
Consequently, instead of a human-machine-centred design framework, a model-based design procedure according to VDI 2206 [36] is selected. During this project, the first macro-cycle of [36] is completed, leading to a laboratory specimen. Therefore, a prototype of an elastic actuator is designed to perform experimental evaluation at a test bench. The macro-cycle is processed according to the V model [36], beginning with the definition of requirements and followed by the system design. In this phase, necessary functions of the system are analysed to generate a concept for the product, which is further specified in the domain-specific design phase and a solution of each function is specified. Each solution is afterwards combined to the laboratory specimen during the system integration and evaluated with respect to the requirements.
The V model is applied to the development of an elastic drive train for an active orthosis, which leads to the model-based design procedure depicted by Figure 3.1. In the beginning, the objectives are specified, which is presented in Section 3.1. In the next chapter, the functions and concept are selected based on a model-based analysis of the potential of an elastic actuation system. The details of the solution and the design as well as the selection of components is conducted in Chapter 5 as part of the domain-specific design. A second part of this phase is the selection of an appropriate control law, presented in Chapter 6. The system integration and evaluation is performed afterwards and presented in Chapter 7.

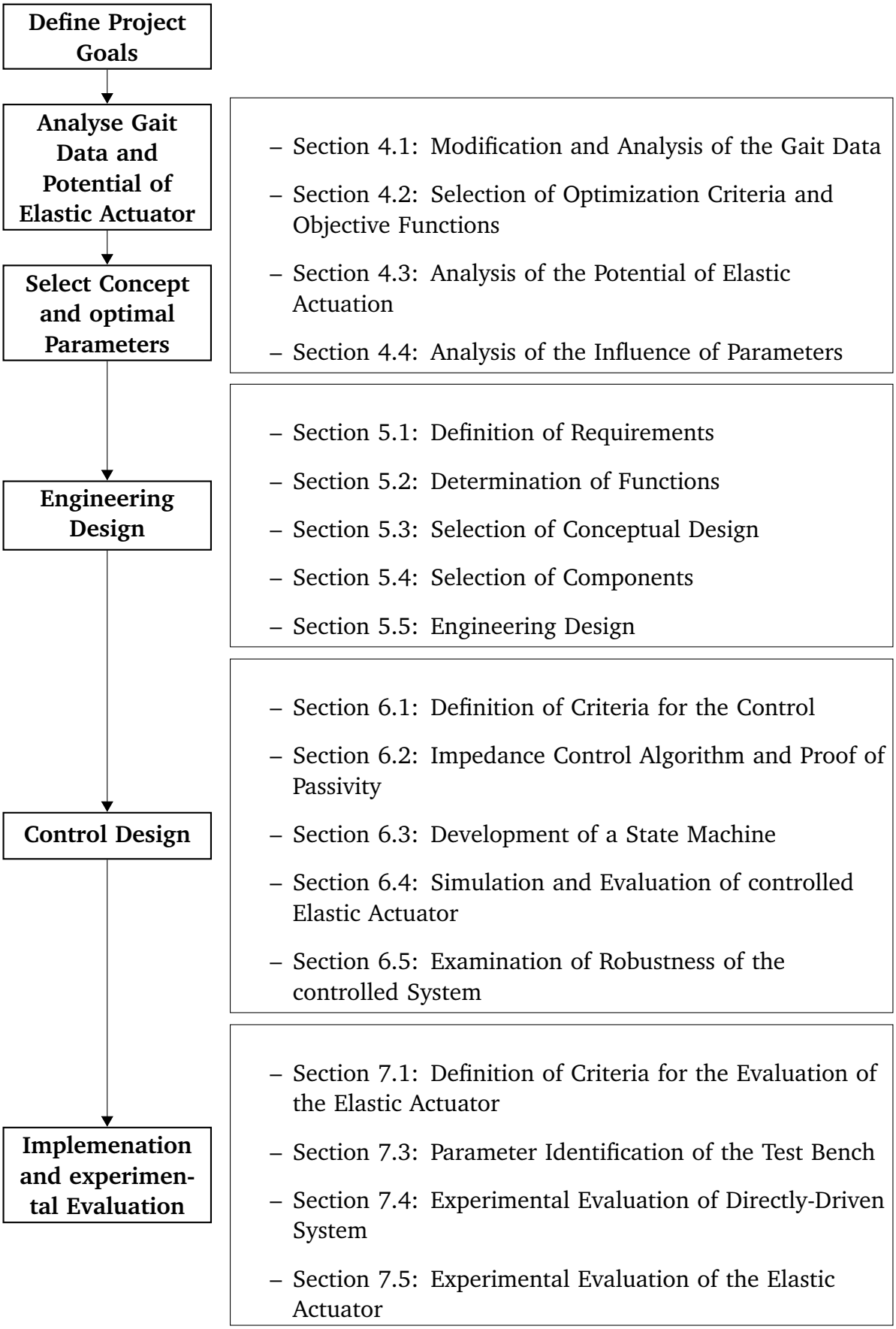

Figure 3.1: Design procedure for the elastic actuation system

4 Analysis of the Potential of Elastic Actuators

The potential of elastic actuated systems is investigated in the course of Chapter 4. In the beginning, the gait data presented in Section 2.2 is analysed and a system with direct actuation (DA) is investigated for a comparison to the compliant system. The analysis of the potential of systems with elastic components focuses on the energy efficiency of compliant actuators providing a healthy gait for SCI subjects. Therefore, criteria and objective functions for an optimisation of parameters are discussed using the analysed gait data in combination with different models of elastic actuation. The performed optimisations are analysed and concepts for the design of an efficient actuation system are proposed based on the results at the end of the chapter.

4.1 Modification and Analysis of the Gait Data

The gait data presented [6] is modified in the beginning of this chapter to improve the results of the following analyses and simulations. The data in Figure 2.3 shows curves captured from several subjects and gait cycles. In [6], the duration of the gait cycle is presented from 0 % to 100 %. Mean values and standard deviation for angular position, torque and power of the knee are given in increments of 1 %. However, the gait data can not be used to simulate several gait trials, as start values for angle and torque do not coincide with the respective end values. In addition, due to the number of values given per gait cycle, numerical derivation of the signals does not yield smooth curves, which are necessary to provide further data, e.g., for velocity and acceleration used for the analysis. Also, the first and last values of the derivated signals can not be evaluated due to unknown boundary conditions of velocity and acceleration. Thus, in the following, a modification of the gait data is conducted to achieve smooth trajectories for the following investigations. All adjustments are made via available algorithms in *Matlab*.
The fist modification is a spline-interpolation to increase the values per gait cycle from 100 to 1000, utilised to increase the quality of the following fit to a Fourier Series of the 8th order, which is applied to the interpolated data. This is advantageous as the resulting trajectories after numerical derivation are smooth. However, this still results in missing boundary conditions. These are obtained by repeating the gait cycle three times and applying the fit to a Fourier Series. The resulting trajectories and numerical derivations are calculated and data of the first

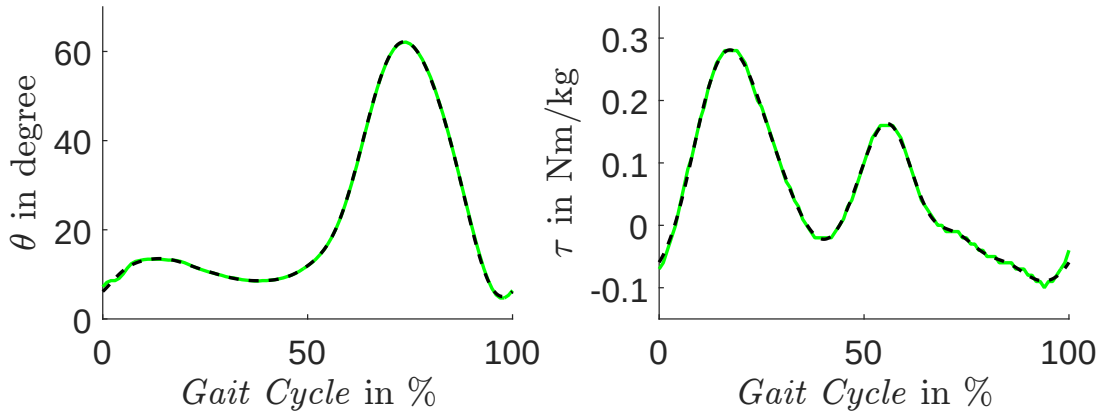

Figure 4.1: Comparison of original and modified mean data / left: original (green) and modified (dashed-black) knee angle / right: original (green) and modified (dashed-black) knee torque

and third gait cycle are neglected to get data with boundary conditions for one gait cycle. This also ensures smooth transition between gait cycles for the simulations performed in Section 6.4. In Figure 4.1, a comparison of original data from [6] in green and the Fourier Series in dashed black shows high accordance between the characteristics while the modified trajectories are smoother, especially at the beginning and end of the gait cycle. The details and the parameters of the obtained Fourier Series are listed in Appendix A.1. Figure 4.2 is additionally presenting characteristics of the knee from [6] after interpolation and fit to a Fourier Series in the layout of Figure 2.3. Noticeable is a continuous trajectory of τ_k over θ_k in the bottom-right of Figure 4.2 compared to Figure 2.3 as a result of smooth and continuous trajectories.

Analysis of the Gait Data

Observing the gait data in Figure 4.2, the stance phase in red is composed of high torques and small movements while the swing phase is characterized by lower torques and high angles and thus high velocities. The power of the knee is balanced during the stance phase but exhibits two distinct negative peaks during the swing phase. As positive power corresponds to required power and negative power represents dissipation, the knee mainly dissipates energy during ground level walking. However, hip and ankle add power to the joints, as presented in [5, 6], so in total, walking still requires power. A further characteristic of the knee trajectories is a base frequency ω, extracted from the Fourier Series $F(t) = a_0 + \sum a_n \cos n\omega t + \sum b_n \sin n\omega t$ for $n = 0,...,8$. The resulting parameters of the series fitted to the gait data are presented in Appendix A.1 and show a base frequency of $\omega = 0.0628 \frac{\text{rad}}{\text{\% of gait cycle}}$. Thus the knee trajectories contain the frequencies nw for $n = 0,...,8$, which can be utilised to determine the operating frequencies and match the properties of an elastic actuation system to minimise energy con-

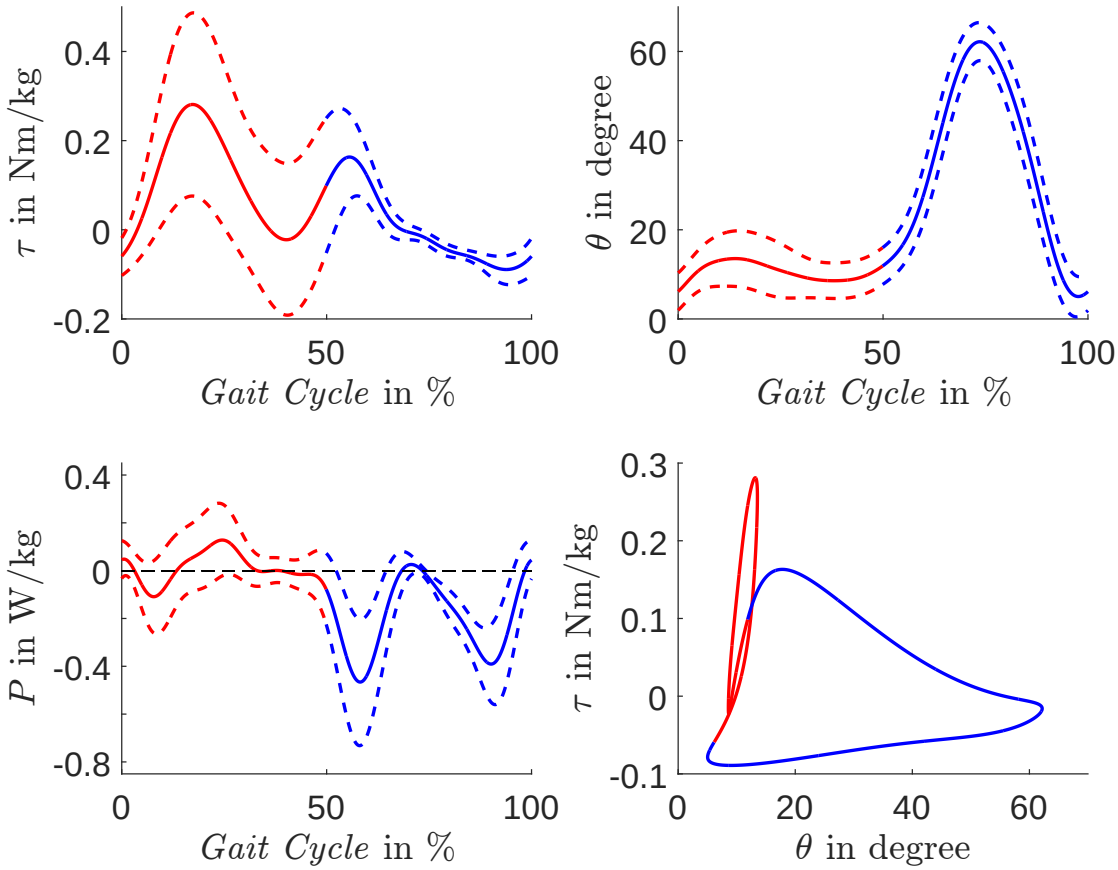

Figure 4.2: Modified gait data including standard deviations / top left: knee angle / top right: knee torque / bottom left: knee power / bottom right: torque-angle characteristic

sumption, as proposed in [7]. The base frequency coincides for the data of knee angle and knee torque including the standard deviation. A transformation of the frequency in Hz requires the duration of the gait cycle in seconds instead of percent of gait cycle.

For further use, distinctive parameters of the modified gait characteristics are summarized in Table 4.1. The values for maximum torque $\tau_{k,max}$, the range of motion θ_k as well as the peak power $P_{k,max}$ and $P_{k,min}$ are directly read from the data depicted in Figure 4.2. The maximum angular velocity $\dot{\theta}_{k,max}$ is taken from the numerical derivation of θ_k.

Table 4.1: Characteristic parameter of the knee [6]

Description	Parameter	Value
maximum torque	$\tau_{k,max}$	$0.49\,\mathrm{N\,m\,kg^{-1}}$
range of motion	φ_k	0° to 66.5°
maximum angular velocity	$\dot{\theta}_{k,max}$	286.8 °/s
maximum peak power	$P_{k,max}$	$0.29\,\mathrm{W\,kg^{-1}}$
minimum peak power	$P_{k,min}$	$-0.73\,\mathrm{W\,kg^{-1}}$

For the active orthosis, the presented knee trajectory is generated by an actuator. To analyse the potential of an elastic actuator, a DA is investigated to allow comparison with a reference system in addition to the natural gait data. The directly-actuated system has to provide the knee trajectory and knee torque and can be modelled according to Figure 4.3. The equation of motion results to:

$$I_a \ddot{\theta}_a = \tau_a - \tau_{ext} \tag{4.1}$$

with $\tau_{ext} = \tau_k$ and $\theta_a = \theta_k$. The necessary mechanical power of the actuator to generate the knee trajectory is calculated according to:

$$P_a = \tau_a \dot{\theta}_a \tag{4.2}$$

Inserting Equation (4.1) into Equation (4.2) and expressing the power in dependency of the knee data yields:

$$P_a = (I_a \ddot{\theta}_k + \tau_k)\dot{\theta}_k \tag{4.3}$$

Thus the moment of inertia of the actuator increases the necessary power for the generation of the desired knee motion. In Figure 4.4, the resulting power is depicted for the knee and the DA with increasing actuator inertia. The transition between single support and double support at 50 % of the gait cycle is marked by a grey dashed line and marks a transition to a phase with higher positive and negative power.

The calculation of the power utilises the moment of inertia of an exemplary 70 W electronically commutated (EC) motor (*EC45 flat*) (*Maxon Motor AG, Sachseln, Switzerland*, Appendix B.6) with a rotor inertia of $I_{EC} = 1.81 \times 10^{-5}\,\mathrm{kg\,m^2}$ and gear ratios of $i_G = 60$, 120 and 160, thus the reflected actuator inertia is $I_a = I_{ec} i_G^2$. Moments of inertia of the gear drive and the active orthosis are neglected as they are assumed to be considerably smaller than the reflected actuator inertia. To be able to calculate the power and energy, the knee torque τ_k presented in Section 2.2 is scaled to a human with mass $m_h = 75\,\mathrm{kg}$ and a duration of one gait cycle $t_{gc} = 1.3\,\mathrm{s}$. The acceleration of the knee $\ddot{\theta}_k$ is obtained by numerical derivation.

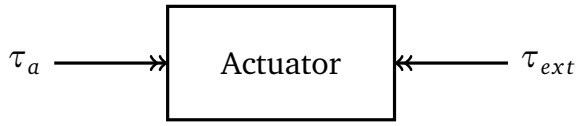

Figure 4.3: Model of the directly-actuated System

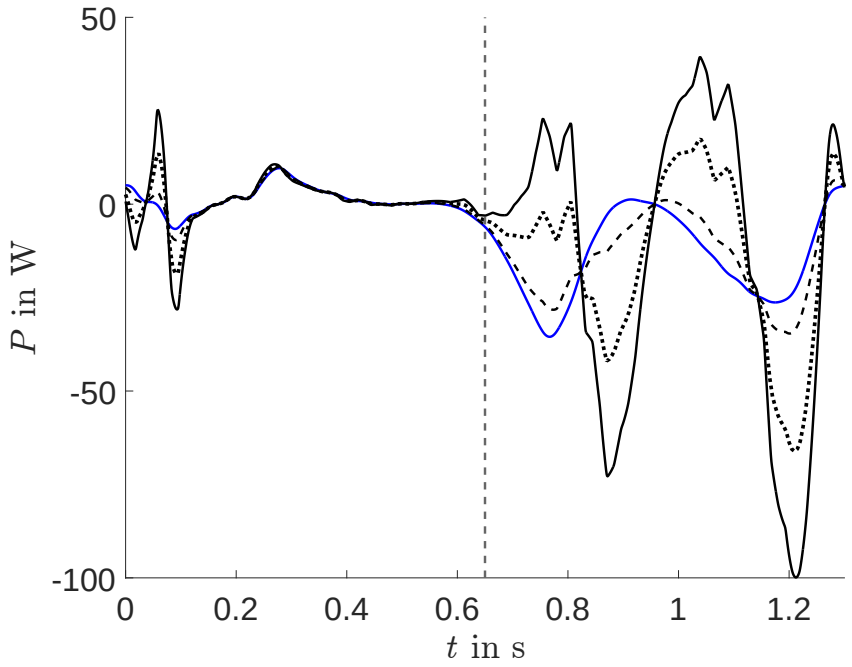

Figure 4.4: Comparison of the Power of the Knee (blue) and of the directly-actuated system (black) with $i_G = 60$, 120 and 160 depicted as dashed, dotted and continuous

A comparison of the power in Figure 4.4 shows additional peaks in power of the DA during the stance phase. The mechanical power is then approximately the same until 50 % of the gait cycle. During the pre-swing and swing phase of the gait cycle, the mechanical power of the DA system greatly deviates from the knee power. The two negative peaks in knee power are increased in amplitude and occur later in the gait cycle, while two additional positive peaks are observed correlating to necessary acceleration of the actuator inertia. The increase of the gear ratio leads to a higher reflected actuator inertia, thus affecting the required power, which can also be seen from Equation (4.3). Thus, a high moment of inertia of the actuator dominates the behaviour of the system, which is not desired, as the characteristics of the human gait are to be reproduced and leads to an increased power consumption. Hence, motor inertia and gear ratio should be selected as low as possible to reduce the impact of the actuation system.
After the analysis of the DA, the investigation of potential improvements by elastic actuation is examined in the course of this chapter, starting with the definition of the criteria for the optimization.

4.2 Criteria for the Analysis of the Potential of Elastic Actuation

As stated in Section 3.1, the actuation system of the active orthosis has to generate a natural gait cycle for the subject. Thus, desired knee angles and torques are given by the characteristic trajectories of the gait data. While elastic actuation systems show advantages regarding the robustness and shock absorption [31], the main focus on the potential of elastic actuation of this section is in reducing the required power and energy. Therefore, elastic models with compliances in series and parallel are examined and the values for each stiffness are optimised to minimize objective functions defined in Table 4.2.

The energy during one gait cycle E_{gc}, calculated from the absolute value of the power, represents the required energy to generate the desired gait cycle with duration t_{gc} in the absence of recuperation. The objective function $\min(E_{gc,rec})$ assumes that the negative power can be recuperated and stored for further use. Hence, E_{gc} and $E_{gc,rec}$ are minimised to find a configuration of the elastic actuation system with high efficiency and a comparison of these objective functions allow an evaluation of the potential of recuperation. The energy from positive power $E_{gc,+}$ and negative power $E_{gc,-}$ are used to examine the resulting behaviour of the system with optimal values. Thereby $\min(E_{gc,-})$ is equal to maximise the energy that can be recuperated. In addition, the minimisation of the required peak power, represented by the objective function P_{max}, may allow the selection of smaller actuators, which is advantageous due to lower weight and inertia. There is no distinction between systems with and without recuperation, as the actuator is required to either provide positive power or to recuperate a certain amount of power. The objective functions are used in the following section to find the optimal configuration with corresponding parameters of an elastic actuation system via optimisation.

Table 4.2: Objective Functions for the Optimisation

Objective Function	Description
$\min(E_{gc}) = \min\left(\int_0^{t_{gc}} \lvert P\rvert \,\mathrm{d}t\right)$	minimise the total energy required during one gait cycle
$\min(E_{gc,rec}) = \min\left(\int_0^{t_{gc}} P \,\mathrm{d}t\right)$	minimise the total energy required during one gait cycle with recuperation
$\min(E_{gc,+}) = \min\left(\int_0^{t_{gc}} P^+ \,\mathrm{d}t\right)$	minimise the total energy from positive power during one gait cycle
$\min(E_{gc,-}) = \min\left(\int_0^{t_{gc}} P^- \,\mathrm{d}t\right)$	minimise the total energy from negative power during one gait cycle
$\min(P_{max}) = \min\left(\max(\lvert P\rvert)\right)$	minimise the maximum required power

4.3 Optimisation of Elastic Actuation Systems

In this section, different configurations of elastic actuation systems with series and parallel stiffness are examined. Models of elastic actuated systems with parallel and series stiffness and increasing level of detail are presented and the respective values optimised to minimise the presented objective functions. As a first step, optimisations of the stiffness are performed neglecting the actuator inertia similar to the analysis in [29]. Next, the optimisations are performed considering the actuator inertia as in [7]. A more detailed model is examined in the last iteration and includes the electrical model of a DC-motor as well as efficiency factors for the gear unit, motor controller and power supply. The obtained results are analysed to generate an actuation concept to enable a SCI subject to perform a healthy gait while minimising the required energy of the actuator.

Optimisation neglecting the Actuator Inertia

The first investigation follows the principle of [29] and is based on the model given by Equations (2.1) and (2.2) with $I_a = 0$. Thus an actuator with elasticity in series as well as parallel to actuator would be represented by the equations of motion:

$$\begin{bmatrix} k_s + k_p & -k_s \\ -k_s & k_s \end{bmatrix} \begin{bmatrix} \theta_a \\ \theta_{ext} \end{bmatrix} = \begin{bmatrix} \tau_a + k_p \theta_{a,0} \\ -\tau_{ext} \end{bmatrix} \tag{4.4}$$

Hence, it is possible to calculate the power of the actuator $P_a = \tau_a \dot{\theta}_a$ necessary to generate a healthy gait for $\theta_{ext} = \theta_{knee}$ and $\tau_{ext} = \tau_{knee}$. From the lower part of Equation (4.4), one gets the relation:

$$\theta_a = \theta_{ext} + \frac{\tau_{ext}}{k_s} \tag{4.5}$$

which yields $\dot{\theta}_a$ after derivation according to:

$$\dot{\theta}_a = \dot{\theta}_{ext} + \frac{\dot{\tau}_{ext}}{k_s} \tag{4.6}$$

Thus the actuator power P_a is calculated from Equations (4.4) to (4.6) to:

$$P_a = \left[k_s(\theta_a - \theta_{ext}) + k_p(\theta_a - \theta_{a,0}) \right] \left[\dot{\theta}_{ext} + \frac{\dot{\tau}_{ext}}{k_s} \right] \tag{4.7}$$

As seen, P_a depends on the desired gait trajectory and the respective numerical derivatives, the values of the elasticities k_s, k_p as well as initial actuator position $\theta_{a,0}$. An optimisation is performed in *Matlab* using the *fmincon*-function constraining k_s and k_p to be positive. The *fmincon*-function is based on the Quasi-Newton method to find an extrema of a function. Specifically, a line search algorithm is employed and the respective direction to search is determined based on an approximation of the Hessian matrix [37]. Thus, the *fmincon*-algorithm calculates the gradient and Hessian of a function numerically at each iteration and is therefore only able to find local optima and thus depends on the selected initial values. To prevent high $\theta_{a,0}$, which lead to high deflections of the parallel spring, as a result of the algorithm, the constraint $-2\pi < \theta_{a,0} < 2\pi$ is applied. The optimisation is performed using three gait cycles, however the evaluation of the power uses only the data from the second cycle to avoid problems due to numerical derivation of τ_{ext} and θ_{ext}. The results are presented in Table 4.3 with k_s and k_p in $\mathrm{N\,m\,kg^{-1}\,rad^{-1}}$ and $\theta_{a0,}$ in radian. The resulting optimal values for the objective functions are given in $\mathrm{J\,kg^{-1}}$ for energy and in $\mathrm{N\,m\,kg^{-1}}$ for peak power. The optimal stiffness values are given in $\mathrm{N\,m\,kg^{-1}\,rad^{-1}}$ and the optimal offset in rad.

The optimisation results for $\min(E_{gc})$ and $\min(E_{gc,+})$ show similar results for the optimal stiffness values for $k_S \approx 4\,\mathrm{N\,m\,kg^{-1}\,rad^{-1}}$ and $k_p \approx 0$, thus minimizing the positive energy per gait cycle yields a similar result as optimising the total energy without recuperation. The results for $\min(E_{gc,rec})$ and $\min(E_{gc,-})$ yield high negative energies. The resulting value for k_p and $\theta_{a,0}$ lead to a system, that uses the parallel spring to drive the external load as well as the actuator, which is thus used as a generator during the complete gait cycle. In addition, the trajectory of the actuator shows very high peak power, e.g., $2.1344 \times 10^{10}\,\mathrm{W\,kg^{-1}}$ for the objective function $\min(E_{gc,rec})$, as the parallel spring produced very high torques. In contrast, $k_s \approx 0$ in $\min(E_{gc,-})$ leads to large movements of the actuator and thus high velocities leading to high recuperation. The minimisation of the peak power leads to $\min(P_{max}) = 0.0061\,\mathrm{N\,m\,kg^{-1}}$, which leads to a reduction of the peak power of approximately 6 %.

Table 4.3: Results of the Optimisation neglecting Actuator Inertia

Objective Function	Value	Optimal Parameters
$\min(E_{gc})$	$0.145\,\mathrm{J\,kg^{-1}}$	$k_s = 3.94$, $k_p \approx 0$, $\theta_{a,0} = 0.49$
$\min(E_{gc,rec})$	$-7.79 \times 10^{7}\,\mathrm{J\,kg^{-1}}$	$k_s = 1.28 \times 10^{9}$, $k_p = 2.9 \times 10^{9}$, $\theta_{a,0} = -6.28$
$\min(E_{gc,+})$	$0.0136\,\mathrm{J\,kg^{-1}}$	$k_s = 4.02$, $k_p = 0.017$, $\theta_{a,0} = 1.9$
$\min(E_{gc,-})$	$-3.18 \times 10^{9}\,\mathrm{J\,kg^{-1}}$	$k_s \approx 0$, $k_p = 13.14$, $\theta_{a,0} = -6.28$
$\min(P_{max})$	$6.1120 \times 10^{-5}\,\mathrm{N\,m\,kg^{-1}}$	$k_s = 181.17$, $k_p = 0.04$, $\theta_{a,0} = 0.05$

Extremely high torques can be observed in the results of $\min(E_{gc,rec})$ and high velocities in $\min(E_{gc,-})$, respectively, however are not feasible for the implementation in the orthosis and are thus not further considered. The minimisations of $\min(E_{gc})$ and $\min(E_{gc,+})$ lead to a reduction of the positive amount of energy for the gait cycle, mostly by utilisation of the series stiffness. The resulting behaviour over one gait cycle of a SEA with $k_s = 3.94\,\mathrm{N\,m\,kg^{-1}\,rad^{-1}}$ is depicted in Figure 4.5. The torque, angle and power of the gait data are depicted in blue and the respective trajectories of the actuator in red. Both systems exhibit the same torque trajectory, but the position differs displaying the elastic behaviour of the SEA, which mainly occurs in the stance phase. This is confirmed by the power of the spring depicted in green, showing a reduction of actuator power during the stance. The optimal stiffness $k_s = 3.94\,\mathrm{N\,m\,kg^{-1}\,rad^{-1}}$ is depicted in the torque over angle characteristic in green as the slope of a linear torque-angle relation. A high compliance between the optimal stiffness from the minimisation of the positive energy and the natural stiffness of the stance phase is derived from Figure 4.5. Comparing the slope of the torque-angle characteristic of the first half of the gait cycle depicted in red and the green line

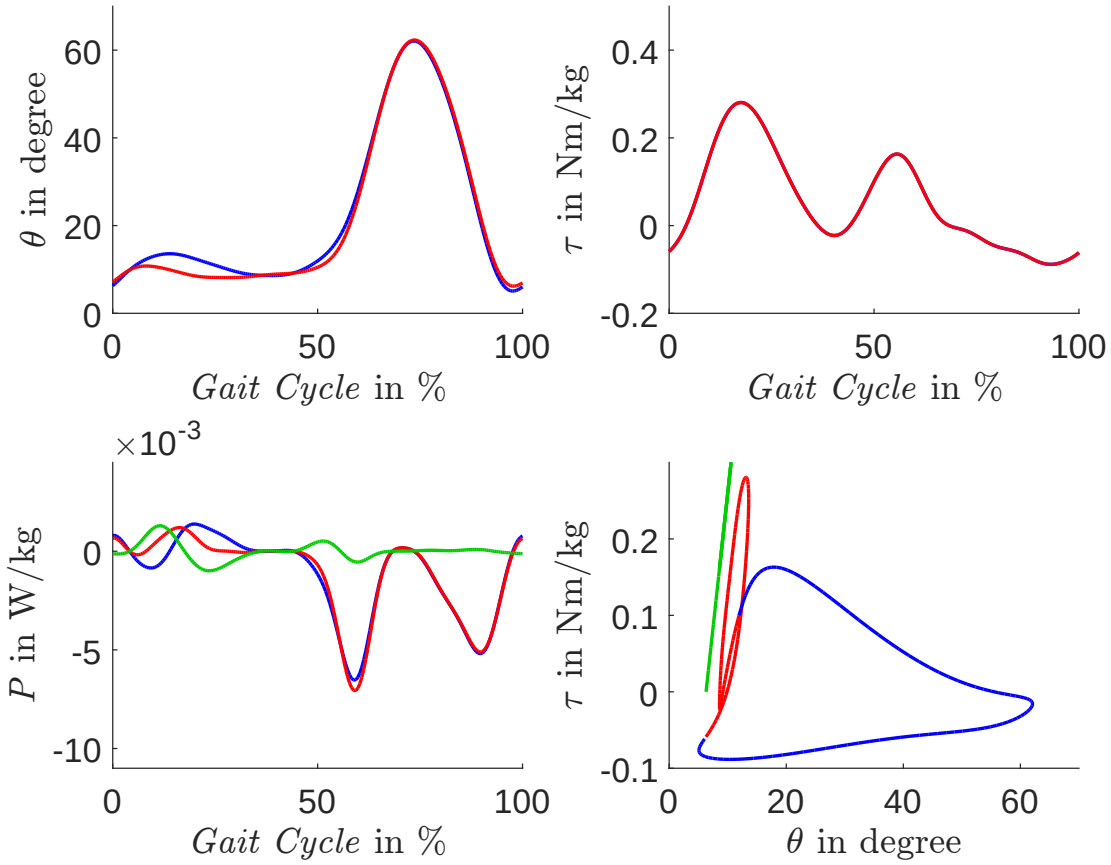

Figure 4.5: Resulting trajectory for a SEA without actuator inertia and $k_s = 3.94\,\mathrm{N\,m\,kg^{-1}\,rad^{-1}}$ / top left: knee (blue) and actuator (red) position / top right: knee (blue) and actuator (red) torque / bottom left: knee (blue), actuator (red) and spring (green) power / bottom right: torque-angle characteristic (red,blue), optimal stiffness for $\min(E_{gc})$ (green)

shows that the minimisation of the positive energy of the gait cycle leads to an optimal stiffness similar to the physiological stiffness of the knee.
To summarise, the optimisations $\min(E_{gc,rec})$ and $\min(E_{gc,-})$ do not lead to feasible results. The minimisation of E_{gc} and $E_{gc,+}$ yields an optimal series stiffness similar to the physiological characteristic of the knee, emphasizing a design centred on the natural human gait. Calculating E_{gc} for a SEA with $k_s = 3.94\,\mathrm{N\,m\,kg^{-1}\,rad^{-1}}$ yields $0.147\,\mathrm{J\,kg^{-1}}$, which shows very little reduction of the energy per gait cycle compared to the the SPEA with $E_{gc} = 0.145\,\mathrm{J\,kg^{-1}}$ with an additional parallel stiffness. Thus, the parallel stiffness only yields negligible advantages but increases the complexity of the system due to the additional component. Hence, in the following, focus is on a design based on a SEA.

Optimisation including the Actuator Inertia

To improve the results of the analysis, the moment of inertia of the actuator is included in the optimisations presented in this section. As a consequence, the torque of the human gait is scaled with an assumed mass of the human $m_h = 75\,\mathrm{kg}$ and the time of one gait cycle is set to $t_{gc} = 1.3\,\mathrm{s}$, so that power and energy can be calculated. An investigation of the influence of these parameters is conducted in Section 4.4. In addition, as the added moment of inertia of the actuator increases the required power, the results are compared with the directly-actuated system presented in Section 4.1.
The power of an elastic actuator including the moments of inertia is calculated from Equation (2.1) to:

$$P_a = \tau_a \dot{\theta}_a = \left(I_a \ddot{\theta}_a + \tau_{ext}\right) \dot{\theta}_a \tag{4.8}$$

Analogous to above, by inserting the relation $\theta_a = \theta_{ext} + \frac{\tau_{ext}}{k_s}$, the actuator power can be expressed in terms of the external position and torque:

$$P_a = \left[I_a \left(\ddot{\theta}_{ext} + \frac{\ddot{\tau}_{ext}}{k_s} \right) + \tau_{ext} \right] \left(\dot{\theta}_{ext} + \frac{\dot{\tau}_{ext}}{k_s} \right) \tag{4.9}$$

A brute-force search of Equation (4.9) and the objective functions from Table 4.2 is performed and the best value is selected from the results. Hence, the result does not depend on initial values as for the *fmincon*-function and the optimum with the lowest value in the examined range of parameters is determined with acceptable effort due to the analytic models. The optimisation is executed for stiffness values k_s between $1\,\mathrm{N\,m\,rad^{-1}}$ and $1000\,\mathrm{N\,m\,rad^{-1}}$ in increments of $1\,\mathrm{N\,m\,rad^{-1}}$. The influence of the actuator inertia is examined for the exemplary EC-motor *EC45 flat* as for the DA presented in Section 4.1 and gear ratios i_G between 1 and 200 in in-

Table 4.4: Results of the Optimisation with Actuator Inertia

Objective Function	Value SEA / DD	Optimal Parameters
$\min(E_{gc})$	10.93 J / 11.75 J	$k_s = 296\,\mathrm{N\,m\,rad^{-1}}$, $i_G = 32$
$\min(E_{gc,rec})$	−89.8502 J / −8.84 J	$k_s = 1\,\mathrm{N\,m\,rad^{-1}}$, $i_G = 200$
$\min(E_{gc,+})$	1.05 J / 1.46 J	$k_s = 296\,\mathrm{N\,m\,rad^{-1}}$, $i_G = 32$
$\min(E_{gc,-})$	-2.47×10^4 J / −21.69 J	$k_s = 1\,\mathrm{N\,m\,rad^{-1}}$, $i_G = 200$
$\min(P_{max})$	34.04 W / 34.14 W	$k_s = 1000\,\mathrm{N\,m\,rad^{-1}}$ $i_G = 44$

crements of 1. The found optimal gear ratio is used in the calculations for the power of the DA to allow the comparison of both systems. The results of the optimisations are presented in Table 4.4. Similar to the results of the optimisation without actuator inertia, the series elastic stiffness reduces power and thus the required energy compared to the directly-actuated system. Scaling the optimised stiffness from the analysis neglecting actuator inertia with m_h yields $3.94\,\mathrm{N\,m\,kg^{-1}\,rad^{-1}} \cdot 75\,\mathrm{kg} = 295.5\,\mathrm{N\,m\,rad^{-1}}$, which coincides with the result from the optimisation with actuator for $\min(E_{gc})$ and $\min(E_{gc,+})$. In addition, an optimal gear ratio is found at $i_G = 32$ in contrast to minimising the actuator inertia as an additional load. This yields a reduction of approximately 7 % of required energy compared to the DA in the absence of recuperation. While the series stiffness reduces positive power, it increases negative power, by maximising the potential and kinetic energy of the actuator and the minimum examined stiffness and maximum gear ratio is selected. This results in high recuperation induced by large movement and torque trajectories of the actuator. Thus the results for the objective functions $\min(E_{gc,rec})$ and $\min(E_{gc,-})$ yield similar behaviour as the optimisations without considering actuator inertia, accounting for different bounds of the parameters. The optimal stiffness for $\min(P_{max})$ is set to the maximum examined value, thus the SEA behaves similar to the DA and no potential of improvement can be identified from this result.

Figure 4.6 presents the resulting trajectory for the optimal values $i_G = 32$ and $296\,\mathrm{N\,m\,rad^{-1}}$. The trajectory of the DA is added in black to the torque and power over time. The result is similar to the analysis neglecting actuator inertia in Figure 4.5 and shows elastic behaviour mainly in the stance phase. To summarise, the consideration of the actuator inertia yields an optimal stiffness similar to the physiological stiffness of the knee joint in the first half of the gait cycle. These results are the same as from the analysis without inertia. Furthermore, an optimal gear ratio and thus reflected inertia is selected to minimise the energy consumption.

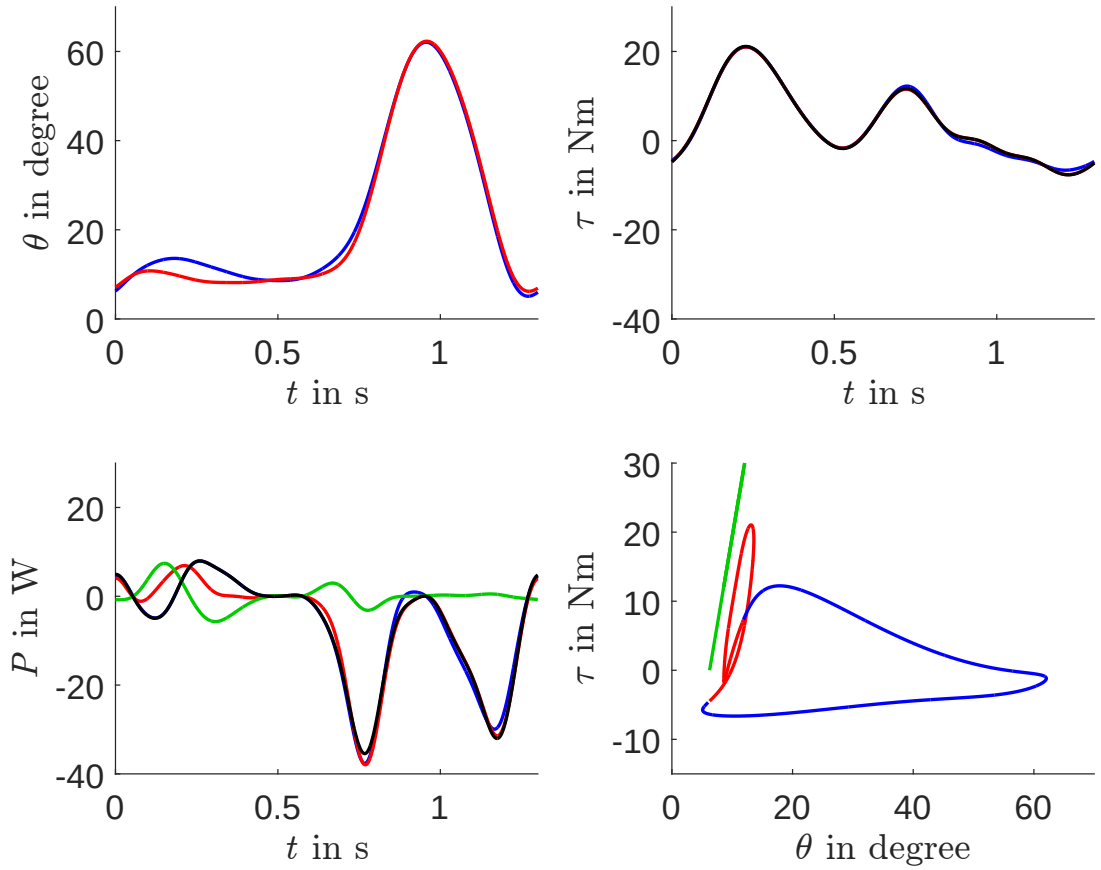

Figure 4.6: Resulting trajectory for a SEA with actuator inertia, $i_G = 32$ and $k_s = 296\,\mathrm{N\,m\,rad^{-1}}$ / top left: knee (blue) and actuator (red) position / top right: knee (blue), elastic actuator (red) and DA (black) torque, / bottom left: knee (blue), elastic actuator (red), spring (green) and DA (black) power / bottom right: torque-angle characteristic (red,blue), optimal stiffness for $\min(E_{gc})$ (green)

Analysis of the Natural Dynamics

To analyse the resulting optimal gear ratio of the optimisation, a natural dynamics analysis of the SEA is performed. As a simplification, the external torque is modelled as a simple pendulum with a fixed axis of rotation. This two-mass oscillator is described by the following equations of motion, which include the damping at the pendulum d_p and the actuator d_a:

$$\begin{bmatrix} I_a & 0 \\ 0 & I_p \end{bmatrix} \begin{bmatrix} \ddot{\theta}_a \\ \ddot{\theta}_p \end{bmatrix} + \begin{bmatrix} d_a & 0 \\ 0 & d_p \end{bmatrix} \begin{bmatrix} \dot{\theta}_a \\ \dot{\theta}_p \end{bmatrix} + \begin{bmatrix} k_s & -k_s \\ -k_s & k_s \end{bmatrix} \begin{bmatrix} \theta_a \\ \theta_p \end{bmatrix} = \begin{bmatrix} \tau_a \\ -m_p l_{p,cg} g \sin\theta_p \end{bmatrix} \tag{4.10}$$

Thus the pendulum describes the human leg and foot with moment of inertia I_p and gravitational torque $m_p l_{p,cg} g \sin\theta_p$. The respective parameters for the pendulum are calculated with anthropometric data given in [5] for an exemplary subject with mass $m_h = 68.5\,\mathrm{kg}$ and body

height $l_h = 1.71\,\mathrm{m}$, to match the mean values of the subjects in [6]. This ensures that the parameters of the subjects of model and gait data match. Thus, the folowing values are obtained and utilised in the analysis: $I_p = 0.536\,\mathrm{kg\,m^2}$, $m_p = 4.18\,\mathrm{kg}$ and $l_p = 0.295\,\mathrm{m}$. The damping coefficients are set to 0.001. This system is similar to the pendulum driven by an SEA investigated in [7]. In [7], the relation between actuator torque τ_a and position θ_a is described for the linearised system by the transfer function

$$\frac{\theta_a}{\tau_a} = \frac{I_p s^2 + d_p s + m_p l_{p,cg} g + k_s}{a_4 s^4 + a_3 s^3 + a_2 s^2 + a_1 s + a_0} \tag{4.11}$$

with the respective coefficients summarised in Table 4.5.

This transfer function is chosen in [7] to analyse the influence of the two resonance frequencies and the antiresonance onto the power consumption of the elastic actuation system. A respective amplitude response of the presented transfer function is depicted in Figure 4.7 for the stiffness value $k_s = 296\,\mathrm{N\,m\,rad^{-1}}$ and varying gear ratios. The first resonance occurs at approximately 0.744 Hz, which is similar for all depicted gear ratios and coincides with the base frequency of the Fourier-fit of the gait cycle. This value is given in Appendix A.1 as 0.0628, which equals 0.7688 Hz for $t_{gc} = 1.3\,\mathrm{s}$. The system shows anti-resonance at 3.82 Hz, which solely depends on the load, while the second resonance frequency depends on the gear ratio and thus on the moment of inertia of the actuator. Resonance is observed for $i_G = 26$ at 25 Hz, for $i_G = 31$ at 21.1 Hz and for $i_G = 36$ at 18.3 Hz. As these frequencies are higher than the frequencies observed from the Fourier-fit of the gait data, the optimal gear ratio of $i_G = 31$ from the performed optimisation can not be explained using the presented transfer function.

The presented model of the SEA with pendulum as external system can further be used to investigate the antiresonance as optimal operating frequency to minimize mechanical energy as in [7]. The antiresonance found in the presented transfer function equals the resonance of the single mass oscillator consisting of the spring and the pendulum. Thus an optimal stiffness can

Table 4.5: Coefficients of the Transfer Function $\frac{\theta_a}{\tau_a}$

a_4	$I_a I_p$
a_3	$I_a d_p + I_p d_p$
a_2	$I_a k_s + I_p k_s + I_a m_p l_{p,cg} g + d_p d_a$
a_1	$d_p k_s + d_a k_s + d_a m_p l_{p,cg} g$
a_0	$k_s m_p l_{p,cg} g$

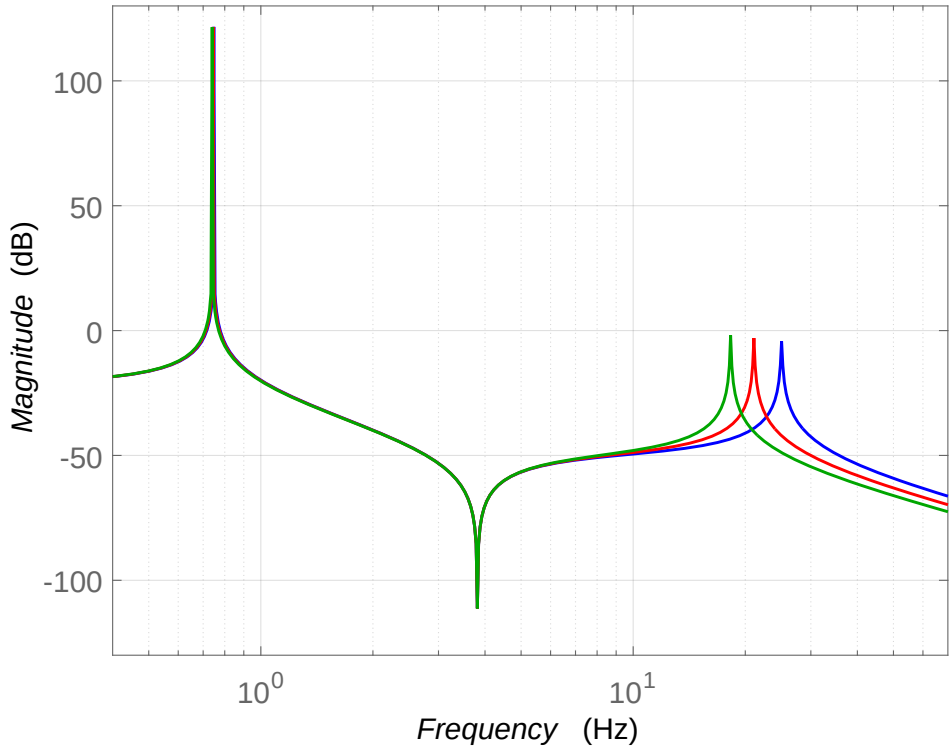

Figure 4.7: Amplitude response of the presented transfer function for $k_s = 296\,\mathrm{N\,m\,rad^{-1}}$ and $i_G = 26$ (blue), $i_G = 31$ (red) and $i_G = 36$ (green)

be calculated, so that resonance of the single mass oscillator matches with the base frequency of the gait cycle according to:

$$k_o = \omega_0^2 I_p - m_p l_{p,cg} g \tag{4.12}$$

This yields a value of $0.41\,\mathrm{N\,m\,rad^{-1}}$ for the optimal stiffness for $t_{gc} = 1.3\,\mathrm{s}$. For a slower gait, ω_0 decreases further while the moment of inertia of the foot and leg remains constant and the optimal stiffness would become negative. Due to the low series stiffness values, the use of the antiresonance is not further considered in this work. However, for higher velocities or running, it should be included in the analysis of the potential of elastic actuation systems.

Optimisation including Component Efficiency Factors

A further refinement of the used model of the SEA is the consideration of an imperfect actuation system. Therefore, an exemplary drive train is selected, consisting of an electric motor with a gear unit, motor controller and battery as the power supply. According to the analysis presented in [38], an estimation of the total efficiency of such a system is gained by considering the electrical model of the motor as well as efficiency of gear unit, motor drive and battery based on

the values given in the respective datasheets. The method to model an electric motor is taken from [38]. The electric power of an EC-motor is given by:

$$P_{el} = UI \tag{4.13}$$

with current I:

$$I = \frac{\tau_m + \nu_m \dot{\theta}_m}{k_m} \tag{4.14}$$

The voltage of the motor U is governed by a first order differential equation, however by neglecting the inductance of the motor, the calculation simplifies to:

$$U = RI + k_b \dot{\theta}_m \tag{4.15}$$

The parameters and extracted values from the datasheet in Appendix B.6 are summarized in Table 4.6. The extended model of the motor includes viscous motor damping $\nu_m \dot{\theta}_m$, with ν_m approximated by:

$$\nu_m = \frac{k_\tau I_{nl}}{\dot{\theta}_{nl}} \tag{4.16}$$

as well as resistive losses by the term RI and inducted voltage due to the velocity of the motor by $k_b \dot{\theta}_m$. Hence, an estimation of the voltage U and current I of the motor is possible when actuator torque τ_a and velocity $\dot{\theta}_a$ are known. Due to the transmission ratio of the gear unit, $\tau_m = \frac{\tau_a}{i_G}$ and $\dot{\theta}_m = \dot{\theta}_a i_G$ and thus the electrical power can be calculated from the actuator torque

Table 4.6: Parameters and Values for the Electrical Model of the EC-Motor

Parameter	Symbol	Value
Viscous Motor Damping	ν_m	see Equation (4.16)
Motor Constant	k_m	$0.0369\,\mathrm{N\,m\,A^{-1}}$
Terminal Resistance	R	$0.608\,\Omega$
Speed Constant	k_b	$27.12\,\mathrm{rad\,s^{-1}\,V^{-1}}$
Torque Constant	k_τ	$0.0369\,\mathrm{N\,m\,A^{-1}}$
No Load Current	I_{nl}	$0.234\,\mathrm{A}$
No Load Speed	$\dot{\theta}_{nl}$	$639.84\,\mathrm{rad\,s^{-1}}$

and trajectory. The motor efficiency results from a comparison of the mechanical and electrical power of the motor according to:

$$\eta_a = \begin{cases} \frac{\tau_a \dot{\theta}_a}{P_{el}} & \text{for } \tau_a \dot{\theta}_a > 0 \\ \frac{P_{el}}{\tau_a \dot{\theta}_a} & \text{for } \tau_a \dot{\theta}_a < 0 \end{cases} \tag{4.17}$$

The formulation of the actuator efficiency η_a increases the necessary power when the load is driven by the motor and decreases the recuperation if $\tau_a \dot{\theta}_a < 0$, occurring when the motor is driven by the load. The maximum efficiency of the motor is limited to 85 % as given in the datasheet.

The efficiency of the drive train is also influenced by the gear unit, the motor controller as well as the battery. As the components are not yet selected in detail, the efficiency of these components is assumed to be constant. Analogous to the motor, the required power is increased while the the recuperation is decreased. Hence, the resulting efficiency factor $\eta_{cmp,r}$ depending on the efficiency of the component η_{cmp} is written as:

$$\eta_{cmp,r} \begin{cases} \eta_{cmp} & \text{for } \tau_a \dot{\theta}_a > 0 \\ \frac{1}{\eta_{cmp}} & \text{for } \tau_a \dot{\theta}_a < 0 \end{cases} \tag{4.18}$$

Thus, with the values for the component efficiency given in Table 4.7, the resulting efficiency for the gear unit $\eta_{gb,r}$, motor controller $\eta_{mc,r}$ and battery $\eta_{b,r}$ can be calculated. This allows the estimation of the total efficiency η according to:

$$\eta = \eta_a \eta_{gb,r} \eta_{mc,r} \eta_{b,r} \tag{4.19}$$

The total efficiency according to Equation (4.19) is implemented in combination with the

Table 4.7: Efficiency Factors for the Components of the Drive Train

Component	η_{cmp}	Reference
EC Motor	-	from Equations (4.13) to (4.17)
Gear Unit	$\eta_{gb} = 0.7$	assumed value
Motor Controller	$\eta_{mc} = 0.92$	see Appendix B.5
Battery	$\eta_b = 0.8$	see [38]

Table 4.8: Results of the Optimisation including Component Efficiency

Objective Function	Value SEA / DA	Optimal Parameters
$\min(E_{gc})$	12.86 J / 14.76 J	$k_s = 168\,\mathrm{N\,m\,rad^{-1}}$, $i_G = 100$
$\min(E_{gc,rec})$	4.19 J / 5.87 J	$k_s = 168\,\mathrm{N\,m\,rad^{-1}}$, $i_G = 105$
$\min(E_{gc,+})$	8.55 J / 10.35 J	$k_s = 168\,\mathrm{N\,m\,rad^{-1}}$, $i_G = 104$
$\min(E_{gc,-})$	-2.47×10^4 J / -21.6946 J	$k_s = 1\,\mathrm{N\,m\,rad^{-1}}$, $i_G = 200$
$\min(P_{max})$	36.02 W / 40.49 W	$k_s = 238\,\mathrm{N\,m\,rad^{-1}}$, $i_G = 127$

model and optimisations utilised in Section 4.3. This yields the optimal parameters presented in Table 4.8. Due to the inclusion of efficiency factors, the optimal stiffness now yields $k_s = 168\,\mathrm{N\,m\,rad^{-1}}$ and the optimal gear ratio is chosen at $i_G = 100$, which approximately coincides for the objective functions $\min(E_{gc})$, $\min(E_{gc,rec})$ and $\min(E_{gc,+})$. Thus, including the efficiency factors of the components changes the behaviour of the system and reduced the recoverable energy. Hence, a SEA with recuperation requires approximately 28.6 % less energy per gait cycle than the DA with recuperation and the same gear ratio as seen from the results of $\min(E_{gc,rec})$. The behaviour as well as optimal parameters for $\min(E_{gc,-})$ do not change, but including the reduced efficiency alters the resulting value of the objective function. A comparison of the values of the peak power from Tables 4.4 and 4.8 show similar values, however the gained optimal parameters are completely different. For the results including efficiency, the SEA reduces the required peak power by approximately 11 %.

The resulting curves of the optimal parameters for $\min(E_{gc})$ are presented in Figure 4.8. The power of the actuator including the total efficiency is depicted in magenta and power of the DA is added in dashed-black using the same procedure to estimate the respective total efficiency. The non-continuous trajectory of the electric power is due to limiting the motor efficiency to $\eta_a < 85\,\%$. As seen, the torque curves now differ from the torque of the knee due to the increased gear ratio and therefore a higher reflected actuator inertia. The motion of the actuator also does not follow the motion of the knee during the stance phase due to the low stiffness of the series spring, which does not represent the physiological stiffness of the knee as seen in the torque-angle characteristic.

As expected from Equation (4.18), the efficiency factors reduce the negative power, and thus the recoverable energy during the swing phase. During the stance phase, a distinct peak in positive power is observed. This occurs due to the characteristic torque of the gait cycle, which leads with a low velocity to low mechanical power in this phase. However, to create the torque, an electrical current is required which yields voltage and thus electrical power as seen from Equa-

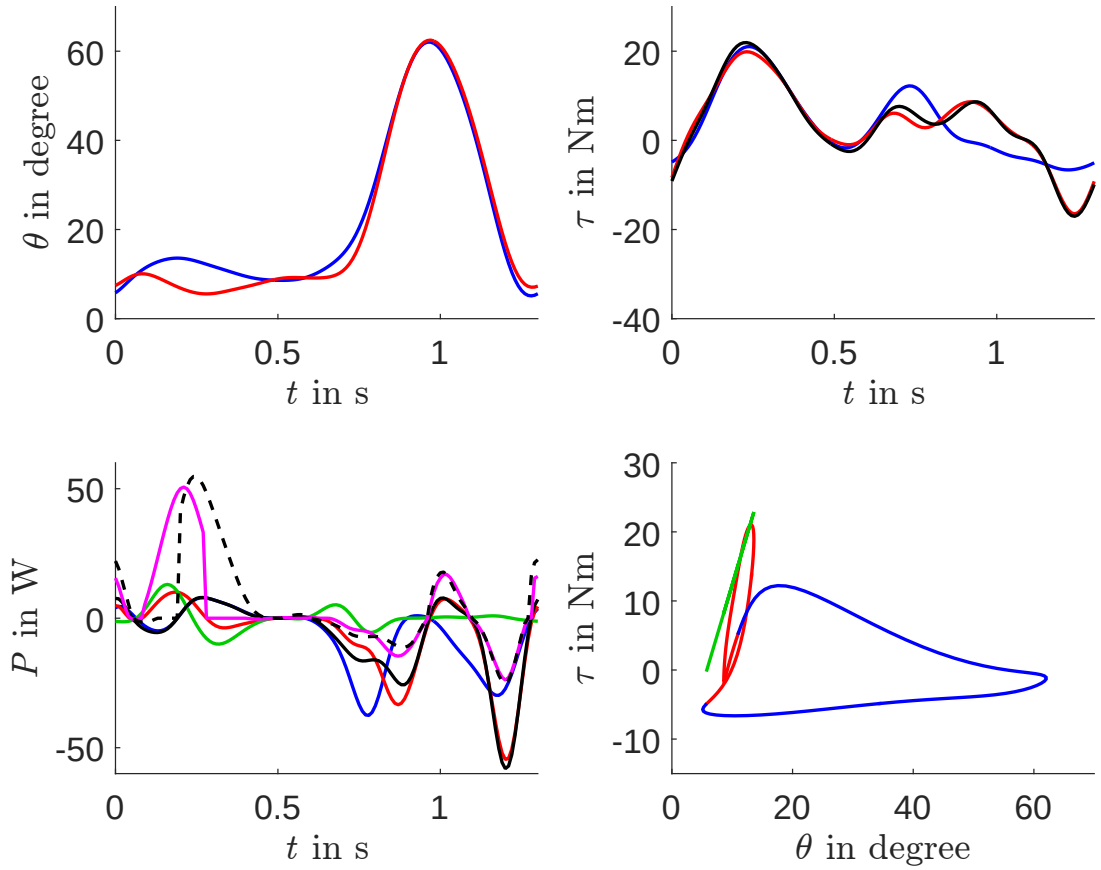

Figure 4.8: Resulting trajectory for a SEA with actuator inertia and total efficiency, $i_G = 100$ and $k_s = 168\,\mathrm{N\,m\,rad^{-1}}$ / top left: knee (blue) and actuator (red) position / top right: knee (blue), elastic actuator (red) and DA (black) torque, / bottom left: knee (blue), elastic actuator (red), spring (green) and DA (black) mechanical power, power including efficiencies of elastic actuator (magenta) and of DA (dashed-black) / bottom right: torque-angle characteristic (red,blue), optimal stiffness for $\min(E_{gc})$ (green)

tions (4.13) to (4.15). In addition, by increasing the gear ratio to the gained optimal values, the examined EC-motor operates in a torque-velocity region that yields high efficiency, exceeding the negative influence of high actuator inertia onto the required power.

Hence, the optimisation including the efficiency factors of components yields a characteristic curve of the electric power with an additional positive peak during the stance phase and drastically reduces recuperation. The optimal gear ratio differs from the optimal value gained from the mechanical model, increasing the reflected inertia. Thus, the influence of the actuator onto the system is increased and the optimal stiffness during the stance phase differs from the physiological stiffness of the human knee. This is not desired, as the stiffness of the knee joint is not mechanically reproduced and thus additional effort is required by the actuation system to mimic the human gait trajectory.

Impact of a Locked Actuator during the Stance Phase

As presented above, the electromechanical model shows a high positive power required by the SEA with an EC-motor in the stance phase to generate the required torque. In this section, the inclusion of a mechanism to lock the motor position during the stance phase and the respective influence onto the power curve is examined. Therefore, the motion of the actuator is locked by manually setting the position to a a fixed value of 0.12 rad, which is the angle at 50 % of the gait cycle. The resulting motion of the knee is then gained by applying Equation (4.5). As in Section 4.1, a fit to a Fourier Series of the 8th order is applied to generate a smooth and differentiable trajectory. This allows the calculation of the required actuator torque according to Equation (4.8). As it is assumed that the required torque is generated by a locking mechanism and the series spring, the torque is manually set to zero during the stance phase. Hence, adjusted gait trajectories are created, which are used to calculate the required power using the total efficiency of the components as above.

To mimic the characteristics of the human gait, the stiffness is selected to $k_s = 296\,\mathrm{N\,m\,rad^{-1}}$. An optimal gear ratio $i_G = 74$ is calculated from an optimisation with the objective function $\min(E_{gc,rec})$ using the model considering the efficiency of components and the adjusted trajectories. The resulting curves of a series elastic actuation system with locking during stance phase are presented in Figure 4.9. The small oscillations of the actuator position during the first half of the gait cycle occur due to the fit using a Fourier-Series, however these should not occur in the real system due to the locking mechanism. These were not removed manually to achieve smooth motions and the respective derivation to generate velocity and acceleration. Regarding the power over one gait cycle, the positive peak in power of the EC-motor during the stance phase is removed as the necessary torque is generated by the locking mechanism. This leads to a very low required actuator power.

A comparison of the values of the system with locking during stance and with the results from the optimisation from Table 4.8 as well as with the DA is presented in Table 4.9. Hence the locking during the stance phase as well as mimicking the physiological stiffness of the knee reduces the required actuator energy per gait cycle in the absence of recuperation by approximately

Table 4.9: Comparison of System with Locking and Optimisation with Efficiency Factors

System	E_{gc}	$E_{gc,rec}$	Optimal Parameters
with Locking	4.3 J	−3.67 J	$k_s = 296\,\mathrm{N\,m\,rad^{-1}}$, $i_G = 74$
without Locking	12.86 J	4.19 J	$k_s = 168\,\mathrm{N\,m\,rad^{-1}}$, $i_G = 95$
DA	14.86 J	6.3 J	$i_G = 95$

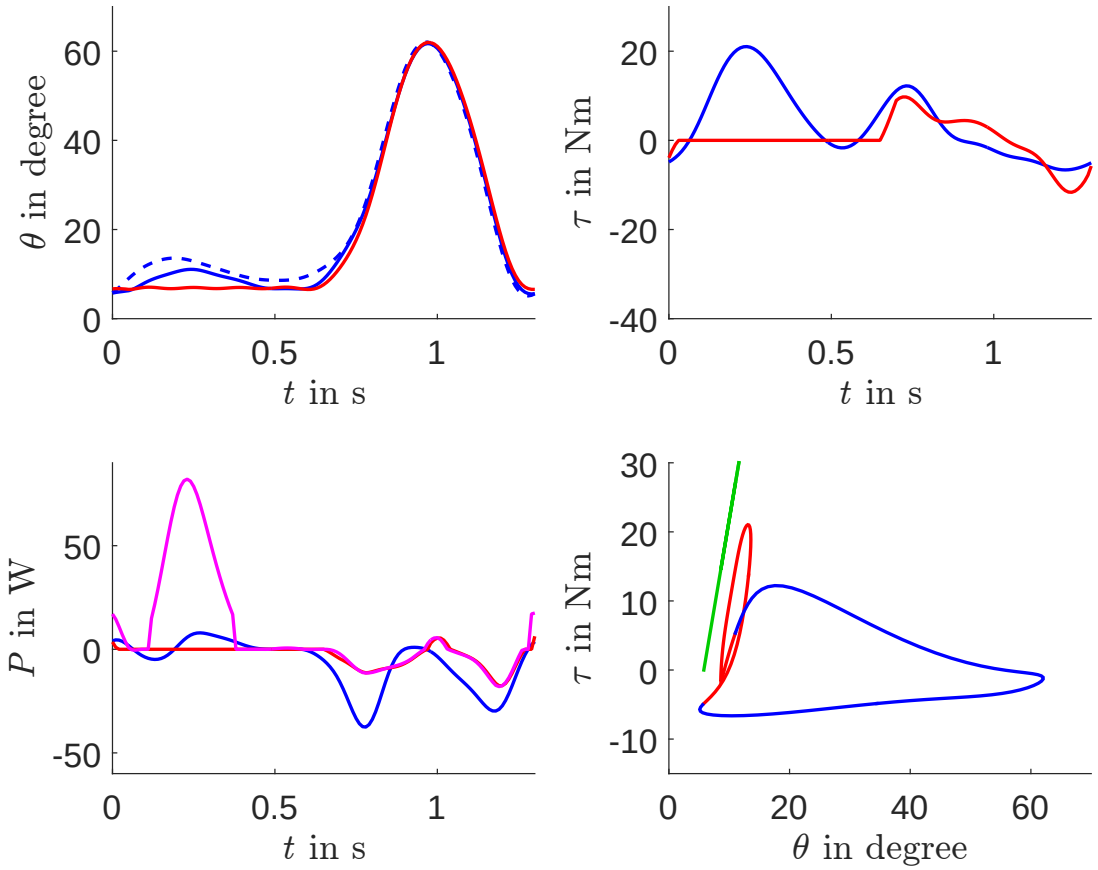

Figure 4.9: Resulting trajectory for a SEA with actuator inertia and total efficiency, $i_G = 74$ and $k_s = 296\,\mathrm{N\,m\,rad^{-1}}$ / top left: adjusted (blue), original (dashed-blue) knee and actuator (red) position / top right: knee (blue), elastic actuator (red) torque, / bottom left: knee (blue) power, power including efficiencies of elastic actuator (magenta) and of elastic actuator with locking (red) / bottom right: torque-angle characteristic (red,blue), optimal stiffness for $\min(E_{gc})$ (green)

66.5 %. Compared to the DA, the SEA with locking yields a reduction of 71 % when no energy is recuperated. In addition, the system with locked actuator during stance phase yields energy when recuperation is used, which can be used to charge the batteries. However, the locking mechanism itself may require power, which is not considered in the presented results. Comparing the values given in Table 4.9, a locking mechanism consuming approximately 7.9 J per gait cycle leads to a more efficient design compared to the DA, assuming further influences, e.g., increased moment of inertia can be neglected. In addition, the optimal gear ratio is selected to maximise the motor efficiency during the swing phase, where, compared to the stance phase, considerably higher velocities occur. Otherwise, the actuator efficiency is not optimal during one phase or a compromise regarding the total efficiency has to be found.

4.4 Impact of Variations in Subject and Gait Velocity on Optimal Values

The analysis of the potential of a SEA yields optimal values for stiffness and gear ratio and propose an elastic actuation system with a locking mechanism in the stance phase to increase energy efficiency. However, all optimisations were performed for constant mass of subject m_h and time of the gait cycle t_{gc}. To estimate influence of different parameters, the optimal stiffness and gear ratio are calculated for $60\,\mathrm{kg} \leq m_h \leq 90\,\mathrm{kg}$ in steps of $2.5\,\mathrm{kg}$ and $1\,\mathrm{s} \leq t_{gc} \leq 3\,\mathrm{s}$ in segments of $0.1\,\mathrm{s}$. Thus, the gait data is scaled in time and amplitude of the torque, but the curves themselves are not changed. However, for the natural human gait, the trajectories do change with increased velocity. This effect is not included in the analysis of the influence on optimal values.

In a first iteration, the impact of varying parameters onto the stiffness of the knee is examined by repeating the minimisation of E_{gc} of the model including actuator inertia presented in Section 4.3 for the selected range for m_h and t_{gc}. The result is presented in Figure 4.10 and a distinct correlation between m_h and the optimal stiffness is observed. This effect reflects the scaling of the torque with the mass of the subject. Thus, the optimal stiffness, representing the natural stiffness of the human knee varies between $k_s = 234\,\mathrm{N\,m\,rad^{-1}}$ and $k_s = 354\,\mathrm{N\,m\,rad^{-1}}$. Similar values are determined in the estimation of the stiffness of the human knee during the stance phase presented in [39]. In addition, [39] gives a model to assess the stiffness depending on body mass, body height and gait velocity, which could be utilised to design the desired stiffness for individual subjects. Figure 4.11 depicts the gear ratio to maximise recuperation for the SEA with locking during the stance phase considering component efficiencies. The optimal value increases with m_h as well as t_{gc} to maximise the motor efficiency for each motion

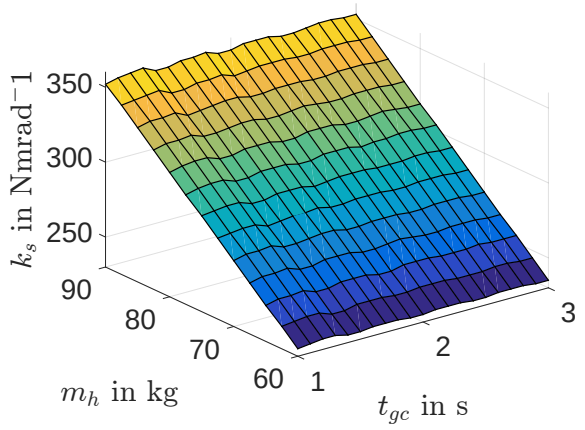

Figure 4.10: Optimal Stiffness of the Knee during the Stance Phase

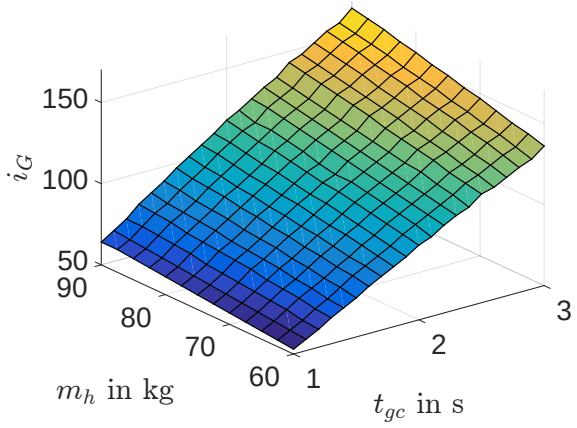

Figure 4.11: Optimal Gear Ratio of the Locked Actuation System with Recuperation

to match the actual torque-velocity ratio during the swing phase. The optimal gear ratio varies between $i_G = 53$ and $i_G = 166$, showing a large parameter spread. The performed assessment yields a range for optimal parameters, aiding in the definition of requirements and selection of component parameters.

4.5 Discussion

In the course of the analysis of the potential of elastic actuation system, the gait trajectory is analysed and fitted to a Fourier Series to achieve smooth trajectories and derivations. For comparison, a DA is presented and analysed to show the influence of high actuator inertia. To reduce the energy consumption, optimisations using models of elastic actuators with different level of detail are performed to calculate optimal values and examine the respective potential. In a first step, a model neglecting the actuator inertia is examined resulting in an optimal series stiffness value that is similar to the physiological stiffness of the knee during the stance phase. In addition, including a parallel spring does not show notable impact regarding the energy consumption of the system. An extension of the model by including the actuator inertia yields an optimal stiffness value similar to the physiological knee stiffness during the stance phase as well as an optimal gear ratio and an analysis of the natural dynamics of this system shows that the first resonance-frequency is close the base frequency of the Fourier-Series of the gait trajectory. The behaviour of the actuation system changes drastically when the electric model of an EC-motor as well as efficiency factors for motor controller, gear unit as well as battery are included. An additional positive peak in power is observed during the stance phase to counteract the characteristic torque during the gait cycle. The optimal stiffness value gained from this model does not coincide with the physiological stiffness of the knee. The additional peak in positive power can be removed by including a locking mechanism, so that the actuator position is locked during the stance phase. Hence, the actuator requires no power during the stance and the respective torque during this phase is generated by the locking mechanism. Thus, to mimic human-like characteristics, the stiffness of the series elastic actuators is selected appropriately. In summary, the analysis of the potential of elastic actuation systems shows a potential reduction of the energy per gait cycle of approximately 66.5 %, when compared to a DA and recuperation is not considered. This system generates 3.67 J per gait cycle when recuperation is included, which could be used to charge the batteries or power additional electronic components. However, this value does not include required power by the locking mechanism. The presented energy reduction per gait cycle is achieved by a series elastic actuator with a locking mechanism with $k_s = 296\,\mathrm{N\,m\,rad^{-1}}$ and $i_G = 74$ for a gait cycle according to the in [6] presented data with $t_{gc} = 1.3\,\mathrm{s}$ and scaled by the body mass $m_h = 75\,\mathrm{kg}$.

The results yielded by the optimisation clearly favour a SEA with locking during the stance phase, however at the merit of a non-exact reproduction of the gait data. Mimicking the stiffness of the human knee with a serial spring allows the reproduction of the characteristics of the human gait, however influencing the resulting motion with the actuator is not possible as consequence of the locking. Thus, the stability of the motion depends on a stable and smooth torque over the gait cycle, which can not be guaranteed due to the restrictions of the SCI subject. Furthermore, the exemplary gait data used for the analysis is captured from healthy subjects. As the goal is the reproduction of a natural gait, the data from [6] is used. However, the gait of a SCI subject may show distinct differences. Thus, the SEA with locking during stance phase as well as the obtained optimal parameters may not yield the advantages elaborated above. A review of the results is possible by selecting different gait data and repeating the presented procedure, for instance using captures from a subject utilising the prototype of the active orthosis with direct actuation. The calculated potential energy reduction depends next to the gait data on the selected efficiency values as well as on the selected, exemplary EC-motor. The electric efficiency modelling is verified in [38], however for gear unit, motor controller and battery, the efficiency is assumed to be constant in the presented analysis of the potential. Hence, the prediction of the total efficiency should be enhanced by including verified efficiency models for each component. Furthermore, this improves the selection and comparison of conceptual designs and individual components. Based on the analysis of potential, the next chapter presents the engineering design of a series elastic actuation system with locking of the actuator position during the stance phase.

5 Engineering Design of an Elastic Actuator

The analysis of the potential of an elastic actuation system has shown that a SEA with a locked actuator position during the stance phase presents an optimal solution to reduce energy consumption and mimic physiological behaviour during the gait cycle. This chapter presents the development of an exemplary design of an elastic actuation system. In the beginning, requirements are defined based on previous results and analysis, enabling the active orthosis to reproduce a human-like gait cycle for a SCI subject. A conceptual design based on the required functions for the elastic actuator is developed and components are selected as well as designed to fulfil the requirements. In the end of the chapter, the designed laboratory specimen is presented.

5.1 Definition of Requirements

The definition of requirements is the first step for the engineering design of the elastic actuator. These are based on the results above and on the data of the presented human gait trajectory. The requirements are presented in Table 5.1 in order of the priority. Each requirement is described and listed as desired (d) or as a wish (w). The most important requirement of the elastic actuation system is to enable the subject to perform a natural and healthy gait, which is the aim of this work. This is specified as a reproduction of the characteristic motion and torque of the healthy human knee. Due to the close interaction between human and robot, high attention has to be paid to the safety of the subject during all the time. A Failure Mode and Error Analysis should be performed to evaluate and reduce risks to ensure the safety for the subject.
The orthosis is supposed to work for different subjects, for the requirements of the actuation system characterized by the body weight as $60\,\mathrm{kg} \leq m_h \leq 90\,\mathrm{kg}$ and for a time per gait cycle up to 1 s. These values are used to scale the gait data to gain further parameters, e.g., the maximum required power. This value occurs for the highest body mass $m_{h,max}$ as well as the quickest gait $t_{gc} = 1\,\mathrm{s}$ and is calculated by a simulation of the SEA with locking with the optimal stiffness $352\,\mathrm{N\,m\,rad^{-1}}$ and optimal gear ratio $i_G = 65$ as 26 W. However, this value assumes that the subject achieves a healthy gait, so that the knee power is mostly negative during the swing phase as depicted in the gait data presented in Figure 4.1. Thus the actuator should at least provide the maximum and minimum peak power of the healthy human gait cycle, which equals 65.7 W from Table 4.1 for $m_{h,max}$. The maximum required torque is selected as the maximum torque of the knee during the swing phase, yielding $0.27\,\mathrm{N\,m\,kg^{-1}}$ in [6]. Thus, the minimal required

Table 5.1: Requirements for the Elastic Actuation System

Priority	Requirement	Description	Type
1	Reproduction of human gait	Reproduce characteristic motion and torque of the human knee during healthy, slow walking	d
2	Safety	Safe operation and human-robot interaction have to be ensured all the time	d
3	Weight of subjects	$60\,\mathrm{kg} \leq m_h \leq 90\,\mathrm{kg}$	d
4	Minimal time per gait cycle	$t_{gc,min} = 1\,\mathrm{s}$	d
5	Minimal required actuator power	$P_{a,min} = 65.7\,\mathrm{W}$	d
6	Minimal required actuator torque	$\tau_{a,min} = 24.3\,\mathrm{N\,m}$	d
	Minimal required actuator torque sit-to-stand motion	$\tau_{a,r,min} = 136.89\,\mathrm{N\,m}$	w
7	Minimal required locking torque	$\tau_{l,min} = 44.1\,\mathrm{N\,m}$	d
8	Range of optimal serial stiffness	$234\,\mathrm{N\,m\,rad^{-1}} \leq k_s \leq 354\,\mathrm{N\,m\,rad^{-1}}$	d

torque for $m_{h,max}$ is determined as 44.1 N m. However, to enable the subject to perform a sit-to-stand motion with the active orthosis, a peak torque of $1.17\,\mathrm{N\,m\,kg^{-1}}$ [40] is required, thus the minimal actuator torque increases to 136.9 N m. The facilitation of a sit-to-stand motion is a wish in the actual stage of the development, however subjects may benefit if the respective torque can be generated.

The maximum torque during the stance phase equals $0.49\,\mathrm{N\,m\,kg^{-1}}$, thus a torque of 44.1 N m is required to lock the actuator during the stance phase for m_h. Further requirements, e.g., regarding the cost, weight, total minimum efficiency, required lifespan or dimensions of the elastic actuation system as well as standards regarding comfort and safety were not specified in the course of this project as only a laboratory specimen is developed. A more detailed list of requirements has to be generated for the next iteration in the development. In addition, factors of safety, e.g., to compensate for modelling errors of deviations in the gait data are not considered in the list of requirements but are incorporated in the selection of components.

5.2 Selected Concept and Function Modelling

Based on the results of the performed optimisations , the advantage of a SEA with locking to reduce the energy consumption per gait cycle as well as the representation of the human knee during the stance phase is shown. Therefore, a deduction of the required functions is performed to select a concept for the actuation system. The basic function of the actuation system is the transformation of power and a control input to enable the user to perform a human-like gait cycle as depicted in Figure 5.1. Within the framework of this thesis, the existence of a high level controller is assumed, which uses user input and further information, e.g., the phase of the gait cycle to generate a control input for the actuation system. The type of input is not specified at this stage of the development, but could be a desired position or desired torque that the actuation system has to provide.

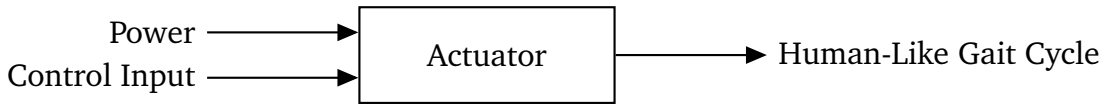

Figure 5.1: Basic Function of the Actuation Concept

A functional structure including subfunctions is presented in Figure 5.2. The control unit receives a control input from the high level controller, which is transformed into a control signal routed to the actuator. Thus, the required function by the control unit is the control of the actuator based on a control input, a control law and sensor signals, measured by sensors of the actuator or the orthosis. The requirements regarding the control law are discussed in more detail in Chapter 6. Based on the control signal, the actuator transforms power obtained from the power supply into actuating variables and allows recuperation by returning power back to the supply. The actuation variables include the required torque and position over time to achieve human-like motion as well as the required locking torque. The mechanical energy of the actuating variables is stored in the elastic element and transferred to the orthosis. In addition, the elastic element represents the stiffness of the human knee during the stance phase to allow a human-like gait cycle as well as the absorption of shocks and an increase of comfort and safety regarding the human-robot interaction. The mechanical energy transferred to the orthosis via an interface generates a human-like motion of the subject fulfilling the objective of the actuation system. Based on the discussed functional structure, a conceptual design is developed in the following section.

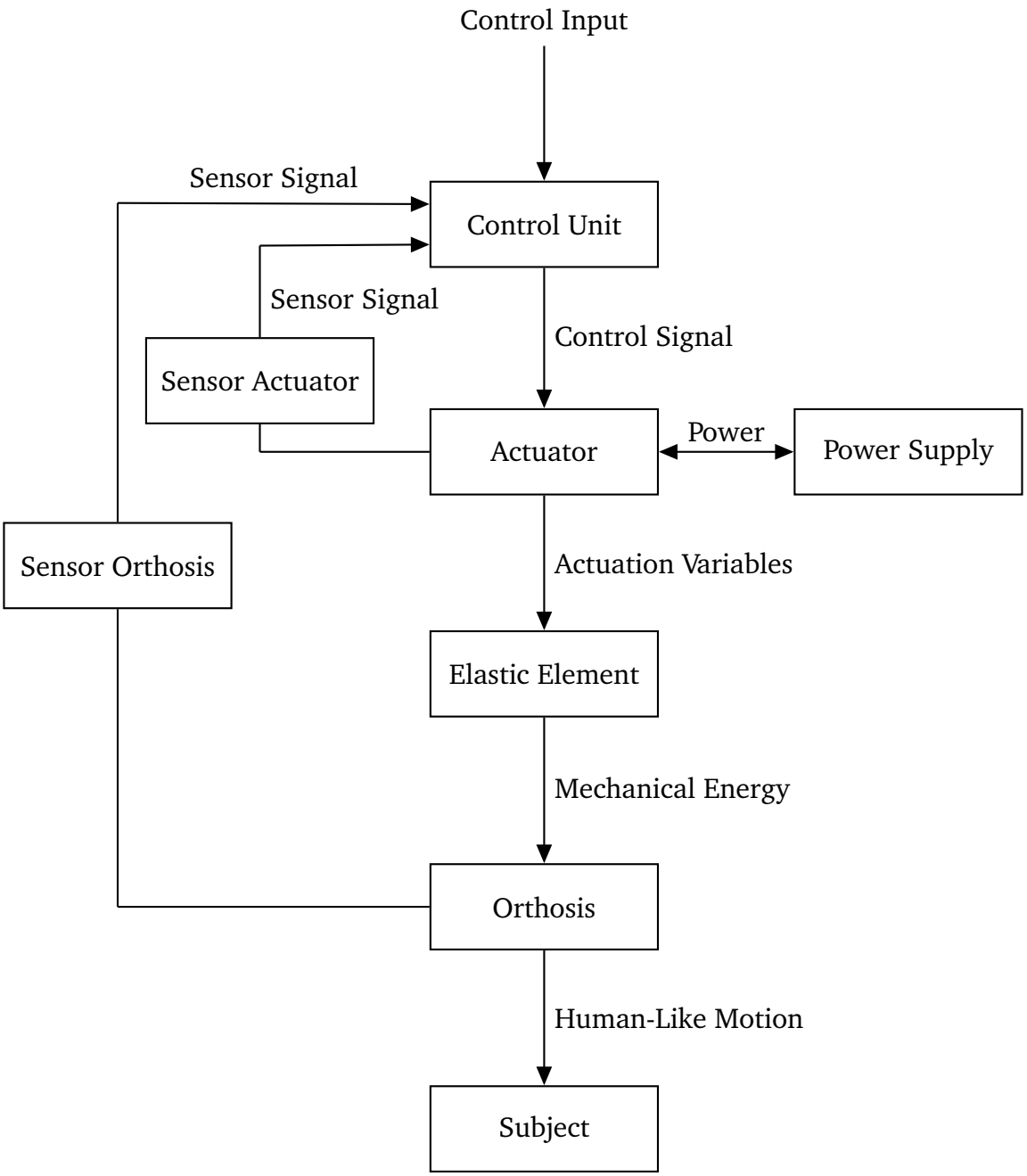

Figure 5.2: Subfunctions of the Actuation Concept

5.3 Conceptual Design

This section includes a conceptual design of a SEA with locking with and without recuperation. Two concepts are developed via brainstorming, however the utilization of further methods of product innovation, e.g., presented in [41], could improve the results of the next iteration of the product development. The first design is based on a self-locking actuation system, thus no additional locking mechanism is required, however recuperation is not possible. A conceptual SEA based on a ball screw is presented in Figure 5.3 and employs a lever arm at the knee joint

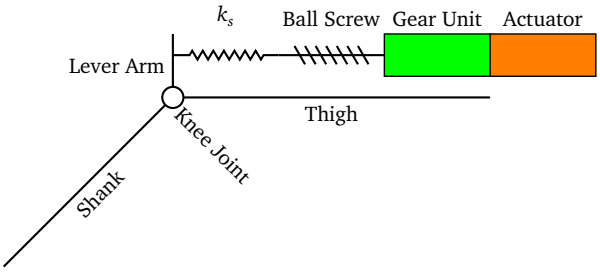

Figure 5.3: Conceptual Actuator Design based on a Ball Screw

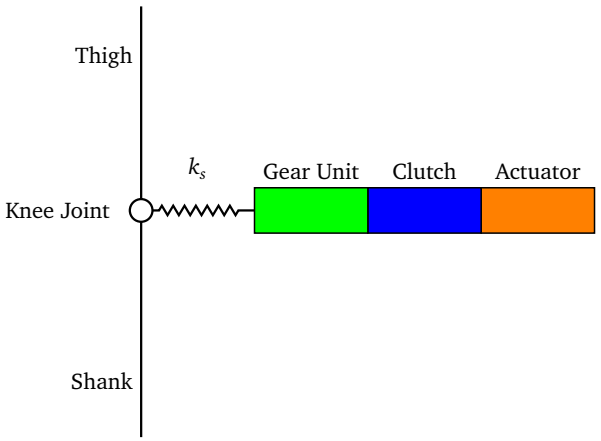

Figure 5.4: Conceptual Actuator Design based on a Rotary SEA with a Clutch

to transform translation into rotation. An electric motor combined with a gear unit is used to actuate the ball screw, so that the total transmission ratio equals the optimal gear ratio as determined by the analysis in Section 4.4.

The second concept presented in Figure 5.4 employs a rotary spring, gear unit and electric motor. The locking during the stance phase is achieved via an active clutch. In the proposed concept, the clutch is positioned between actuator and gear unit, thus for high gear ratios, the actual required locking torque is low, however the reflected moment of inertia is increased. Furthermore, the total weight of this concept is higher compared to the concept based on a ball screw, however allows recuperation of energy during the swing phase of the gait cycle.
As discussed in Section 4.3, a concept based on locked actuator during stance and recuperation shows the highest potential regarding a reduced energy consumption, therefore concept 2 is selected for the implementation as a laboratory specimen. A similar concept is presented in [27] and termed clutchabel series elastic actuator (CSEA). The next sections present the selection of components and final design of the CSEA to fulfil all discussed functions and requirements.

5.4 Selection of Components

The selection of components in this section is partitioned into two parts. At first, a component to fulfil the functions and requirements specified in the course of this chapter is proposed. However, to reduce cost and simplify the implementation, different and available components are utilised for the laboratory specimen.

Selection of Motor and Motor Controller

The criteria for the selection of the motor are based on the power requirement of $P_{a,min} = 65.7\,\mathrm{W}$. In addition, high motor efficiency as well as low moment of inertia is advantageous regarding the total efficiency of the system. Furthermore, a small motor size facilitates low dimensions of the complete CSEA. The nominal voltage is defined as 24 V to comply with the voltage of the battery supply used in the prototype of the gait-assistive orthosis. An EC-motor *EC45 flat* (*Maxon Motor AG, Sachseln, Switzerland*, Appendix B.6) with low weight of 141 g and low moment of inertia of $181\,\mathrm{g\,cm^2}$ providing 70 W is selected. However, due to the losses, as modelled in Section 4.3, the stated power may not be achieved without overloading the motor. An alternative motor of the same series is the *EC60 flat* (Appendix B.1), providing 100 W. However, the weight of 470 g and moment of inertia of $1210\,\mathrm{g\,cm^{-2}}$ are considerably higher. Therefore, the motor *EC45 flat* is suggested for the CSEA. Additional overloading of the motor should be considered to increase the peak power of the motor after consulting the respective manufacturer.

To utilize the motor, a respective drive has to be selected. The CSEA developed in [42] employs an intelligent drive, that is directly programmed with the impedance control. Thus, the low level controller and the motor drive required for the CSEA are integrated in the same component and the motor drive *iPOS4808 VX* (*Technosoft, Neuchâtel, Switzerland*, Appendix B.2) is proposed as well, as it fulfils all requirements. However the actual capabilities to program the impedance control were not reviewed in the course of this work. Due to availability, a motor drive from the same manufacturer as the motor *EPOS 24/5* (*Maxon Motor AG, Sachseln, Switzerland*, Appendix B.5) is utilized for the laboratory specimen.

Selection of Brake

The locking of the actuator position of concept 2 is implemented via a clutch. The required locking torque is $\tau_{l,min} = 44.1\,\mathrm{N\,m}$ and it has to be possible to activate and deactivate the clutch via the control. In addition, the required power dominates the efficiency during the stance phase. For this work, an electromagnetic friction brake of the model *Combinorm 02.02.120* (*KEB, Barntrup, Germany*, Appendix B.8) is selected. This component produces $0.75\,\mathrm{N\,m^{-1}}$ of friction torque and consumes 6 W. Thus, the minimal gear ratio $i_G = 58.8$ is required to generate $\tau_{l,min}$. To activate the brake, a Mosfet (*RFP50N06*) is utilized. The selected electromagnetic brake (EMB) generates a friction torque τ_{EMB} that can be modelled by Coulomb friction [43] according to:

$$\tau_{EMB} = \tau_{EMB,max} i_G \mathrm{sgn}(\dot{\theta}_a)\left(1 - \mathrm{e}^{-\frac{t}{t_{12}}}\right) a_{EMB} \tag{5.1}$$

where $\left(1-\mathrm{e}^{-\frac{t}{t_{12}}}\right) a_{EMB}$ is the activation signal for the brake including a first order time delay to consider the rise time given in the datasheet, see Appendix B.8. The activation signal is defined as:

$$a_{EMB} = \begin{cases} 1 & \text{if brake is activated} \\ 0 & \text{if brake is deactivated} \end{cases} \tag{5.2}$$

This assumes that the friction torque is constant and at maximum amplitude $\tau_{EMB,max}$ after the rise time, and the direction is against the movement of the actuator, determined by the sign of the angular velocity $\dot{\theta}_a$.
The brake consumes 6 W and is active for approximately 50 % of the gait cycle. Thus, for $t_{gc} = 1.3\,\mathrm{s}$, the brake requires 3.9 J per gait cycle. Hence, the energy per gait cycle for the concept of an elastic actuator with locking and recuperation presented in Table 4.9 is increased from −3.67 J to 0.23 J. This value can be reduced further by not fully activating the EMB, as, depending on the gear ratio, the maximum friction torque of the EMB may not be required.

Selection of Gear Unit

The selection of the gear unit influences the efficiency of the system significantly, especially as high backdrivability is required to maximise recuperation. In addition, the gear unit should employ a lightweight design while being robust to resist high peak torques during the gait cycle. According to concept 2, the locking torque of the clutch is amplified by the gear unit, thus the gear unit has to withstand repeating peak torques of $\tau_{l,min} = 44.1\,\mathrm{N\,m}$. The optimal gear ratio depends on t_{gc} and m_h as analysed in Section 4.4 and shows large range of values, with the mean at $i_G = 109.5$. The harmonic drive selected (*SHD-20-100-2SH, Harmonic Drive AG, Limburg/Lahn, Germany*, Appendix B.3) with a gear ratio of 100 allows a repeatable peak torque of 57 N m. However, an analysis of the locomotion should be performed to determine the optimal ratio and gear unit for a SCI subject.
The selected harmonic drive has the additional advantage of low dimensions and very low backlash. However due to the maximum allowed momentary peak torque of 95 N m, the harmonic drive is not suitable to achieve a sit-to-stand motion. Thus, the combination of the selected motor and gear unit can provide a continuous torque of 12.8 N m and repeatable peak torque of 57 N m due to the robustness of the harmonic drive. The stall torque of the motor is not reached in this torque interval. Hence, the combination of *EC45 flat* and *SHD-20-100-2SH* provides the required torque to perform a human gait cycle. Due to the availability of the component, a harmonic drive with gear ratio $i_G = 160$ (*SHD-20-160-2SH, Harmonic Drive AG, Limburg/Lahn, Germany*, Appendix B.7) is implemented in the laboratory specimen.

Design of the Torsional Spring

The torsional spring of the CSEA represents the compliance of the human knee during the stance phase. As a result from Chapter 4, the desired stiffness varies from 234 N m rad^{-1} to 354 N m rad^{-1}, and depends mainly on the mass of the subject as seen in Section 4.4. However, the model given in [39] includes the velocity of the motion as well. Thus, to achieve optimal results, the stiffness should be adjusted accordingly, requiring a respective mechanism. Possible concepts for variable elastic actuators are presented in Section 2.4, however, are deemed too complex to be realised during this work. Thus, a torsional spring with a fixed stiffness is developed in the following. Next to the desired stiffness, the elastic element's robustness is required to take the locking torque of $\tau_{l,min} = 44.1\,\mathrm{N\,m}$ as well as the maximum deflection occurring during the stance phase. In addition, low dimensions as well as weight are desired attributes.
The concept developed for the CSEA during this work is based on compression springs positioned in a circular arrangement around the centre of rotation as depicted in Figure 5.5. Hence, the rotational stiffness is calculated as $k_s = N k_{cp} r_s^2$ with the number of elements N, the stiffness of each compression spring k_{cp} and the radius r_s. It has to be remarked that the utilised equation for the calculation of the torsional stiffness is simplified and linearised and thus k_s is only an estimation. The generation of a geometrically detailed model is avoided, as a substantial amount of parameters needs to be included.

The torque is transferred from each spring to the output via cylindrical elements depicted in Figure 5.7 placed in the free space between two springs seen in Figure 5.6. To select the required parameters and dimensions to achieve the desired stiffness, a detailed 3D-model was developed in *Autodesk Inventor*. A design with $N = 6$, $r_s = 36\,\mathrm{mm}$ utilizing compression springs *D-263Q-03* (*Gutekunst Federn, Metzingen, Germany* Appendix B.9) provides a torsional stiffness

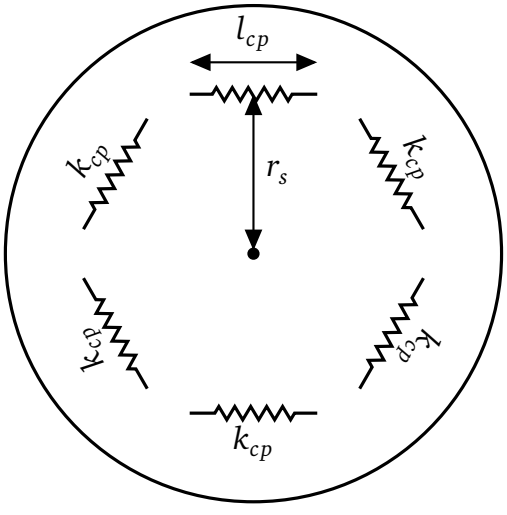

Figure 5.5: Conceptual Design of the Torsional Spring

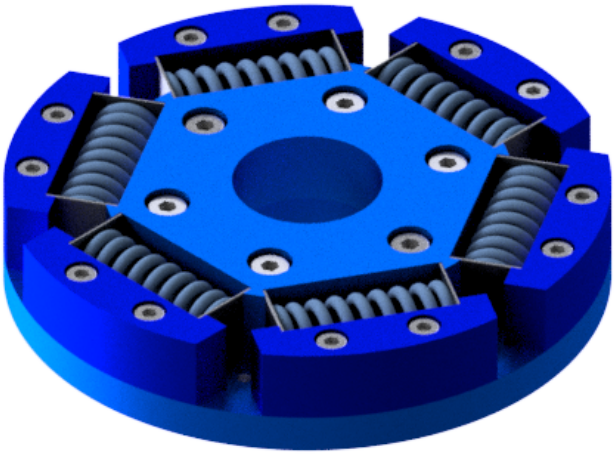

Figure 5.6: Part of the Torsional Spring containing the Compression Springs

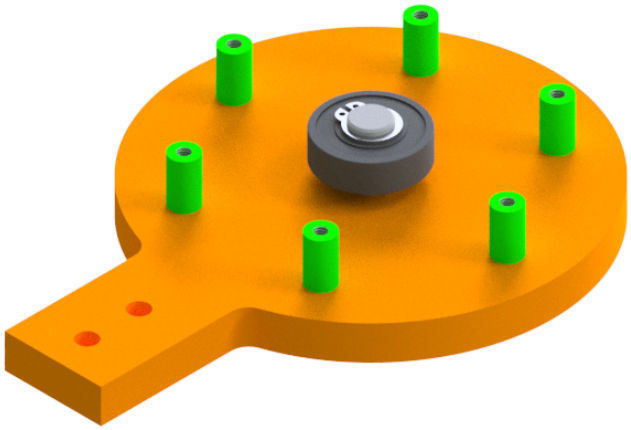

Figure 5.7: Part of the Torsional Spring containing the Cylindrical Interfaces

of 257.3 N m rad^{-1}. This stiffness value is at the lower end of the required stiffness range. However, was chosen as a compromise among stiffness, maximum dimensions and strength. Failure of the torsional spring occurs when a compression spring is loaded with the allowable, dynamical normal force, given as $F_{ndyn,min} = 269.3\,\text{N}$ in Appendix B.9. Hence, the allowable torque is calculated by $\tau_{s,a} = N r_s F_{ndyn,min} = 58.2\,\text{N m}$, which satisfies the strain occurring due to the maximum torque of 44.1 N m in the stance phase. However, to enable a sit-to-stand motion, a mechanical locking would be required to prevent full compression of the springs.
The finalised CAD-design of the torsional spring is depicted in Figures 5.6 and 5.7, presenting a disc containing the compression spring as well as the counterpart with cylindrical elements to transfer the torque. Additional plastic elements are utilized between compression springs and cylinders to create pretension and to reduce impact and noise occurring due to directional changes of the deflection. The counterpart with the cylindrical elements contains the bearings supporting the pendulum of the test bench. A similar design of a torsional spring is presented in [44]. The total weight of the torsional spring is with approximately 0.6 kg very high and could be reduced by applying lightweight construction techniques and materials.

Selection of Sensors

According to the functional model of the SEA with locking presented in Figure 5.2, one sensor for the actuator and one for the orthosis is required. Thus, both degrees of freedom of the SEA are observable. The encoder *MR Type L* (*Maxon Motor AG, Sachseln, Switzerland*, Appendix B.10) provides 4000 counts per rotation in quadrature mode, providing adequate precision regarding the position due to the selected gear unit. The high precision improves the estimation of the ve-

locity via differentiation. The second degree of freedom is observed via a inertial measurement unit (IMU) *SEN-10736* (*SparkFun Electronics, Niwot, Colorado*, Appendix B.4) that includes onboard processing of the sensor data. The IMU incorporates an accelerometer, a gyroscope and a magnetometer to generate an estimation of the angular position.

Selection of further Components

To operate the laboratory specimen, the hardware/software computer *myRIO* (*National Instruments, Austin, Texas*,Appendix B.5, evaluation unit) is selected. This component provides a cost efficient solution to achieve the required computation power and quantity of digital and analogue in-/outputs. The myRIO is programmed with the software *Labview 2015, National Instruments, Austin, Texas*. The power to all components is provided via a laboratory power supply unit.

5.5 Design Result

Next to the selected components, several parts for the CSEA were designed during this project and manufactured in the manufacturing lab of the UPC. The focus was thereby on simplifying and reducing the cost of the manufacturing process, thus lightweight construction techniques were not applied, resulting in a heavy actuation system. In addition, the laboratory specimen is designed for the test bench and therefore only suitable for a proof of concept. For the application at an active orthosis, the design of the conceptual actuator has to be revised.
The laboratory specimen is depicted in Figure 5.8 as the 3D model and in Figure 5.9 implemented in the test bench. In Figure 5.8, the motor depicted in yellow transfers the torque to the harmonic drive (red) via a shaft that is connected to the electromagnetic friction brake (magenta). The output torque of the harmonic drive is directly transferred to the first part of the torsional spring (blue) containing the compression springs. The cylindrical interfaces to the springs (green) are connected to the output component of the torsional spring (orange), which serves as attachment for the pendulum of the test bench. All parts depicted in grey were designed to mount and centre the components of the CSEA. The total length of the laboratory specimen, including the mounting, results in 142 mm and the maximum diameter at the torsional spring is designed to be 105 mm.

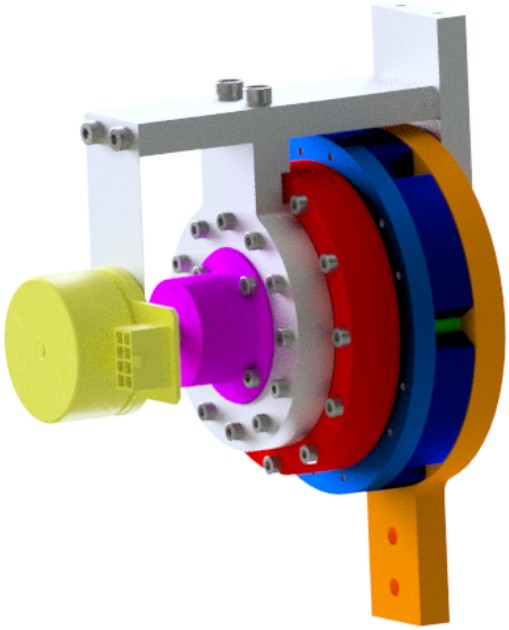

Figure 5.8: Design of the CSEA in the CAD-environment

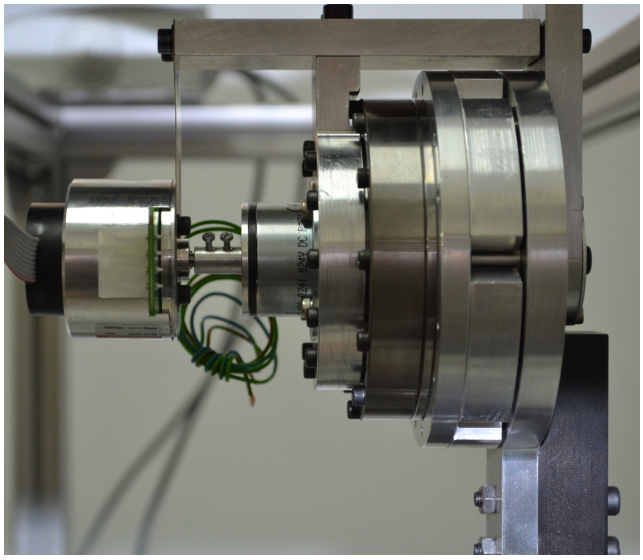

Figure 5.9: Implementation of the CSEA at the test bench

5.6 Discussion

The engineering design of the SEA with locked actuator during the stance phase is presented in this chapter. Requirements are defined in the beginning of the procedure. The required functions to operate the elastic actuator are analysed to develop and select conceptual designs. A rotatory series elastic actuator employing a clutch between an electric motor and a gear unit to provide the locked position during the stance phase is selected as the concept for this project. Components to fulfil the requirements are presented. However, to achieve the torque required for a sit-to-stand motion, defined as a wish, a more robust gear unit has to be selected. The selected components are incorporated into the design of the CSEA, further parts, e.g., parts of the torsional spring, are manufactured and the laboratory specimen is implemented at the test bench.

The proposed design and the selected components depend on the utilized gait data and the results of the analysis of the potential of elastic actuation. Thus, as discussed for Chapter 4, the procedure should be repeated including gait data for SCI subjects considering appropriate factors of safety in the requirements. Further requirements, that were neglected for the laboratory specimen, e.g., maximum weight and safety regulations should be included in virtue of possible influences on the design. In addition, the developed torsional spring is designed for a fixed stiffness, however the stiffness of the knee varies and an individual adjustment to each subject is not possible. More complex approaches, allowing variation of the compliance, should

be investigated to fit the actuated orthosis to each particular user. This would allow an individual adjustment of the stiffness of the system to not only consider energy efficiency but also feedback of the user regarding the comfort and satisfaction with the properties of the device.
The proposed design is generated via brainstorming, a more structured approach and appropriate methods may lead to a different concept with higher total efficiency. Human factors and quality function deployment should be investigated to ensure that the system fulfils not only the technical requirements but also leads to a design as desired by SCI subjects. A further enhancement of the design as well as the selected components could be achieved by conducting optimisations with combinations of different components while considering the respective efficiencies. Furthermore, lightweight construction methods or structural optimisation techniques are not applied due to the time frame of the project, however are deemed necessary to create a light actuation system, reducing the effort for the user during the locomotion. The presented design of the CSEA does fulfil all functions except the control. The next chapter presents the development of an appropriate control law for the operation of the CSEA and the simulation of the controlled system.

6 Control Design for the Developed Actuation System

The control represents a crucial component for the operation, as it determines the actions of the actuation system and thus the stability of the human gait. In addition, the human-robot interaction as well as the comfort depend on the selected control law with respective parameters. In the beginning of this chapter, criteria for the design and evaluation of the controlled system are presented. Based on these criteria, a control strategy is selected for the implementation at the test bench and the stability of the system is analysed. Further, a finite state machine (FSM) is developed to determine the activation of the locking mechanism. Simulations of the ideal system as well as of the system including external deviations and distortions to examine the control robustness are presented in the end of the chapter.

6.1 Criteria Control Design

To ensure the stability, safety and operability of the active orthosis, the control has to fulfil several requirements, which are presented in Table 6.1. The first requirement is the stability of the system, which has to be ensured all the time. This is especially important, as the presented

Table 6.1: Requirements for the Control System

Priority	Requirement	Description	Type
1	Stability	Ensure stability of the controlled system	d
2	Control error	Provide a minimal control error to ensure reproduction of stable gait cycle	d
3	Robustness	Ensure operation including distortions, environmental influences and parameter uncertainties	d
4	Human-robot interaction	Provide safe and comfortable human-robot interaction	d
5	Efficiency	Fulfil the specified function while minimising energy consumption	w

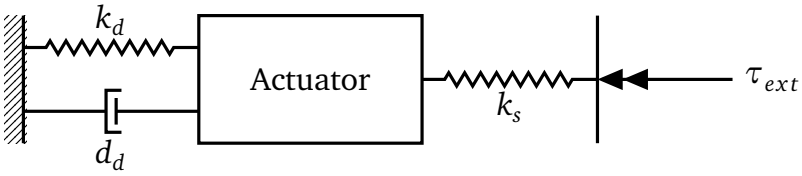

Figure 6.1: Structure of the SEA with Impedance Control as in [45]

CSEA and gait data include non-linear behaviour and may vary with the time. Thus, the system is nonlinear and time variant. The generation of a minimal control error is set as the second most important requirement to ensure safe locomotion for the subject, assuming that the reproduction of the healthy gait trajectory leads to a stable and human-like motion. This has to be ensured even when the system is experiencing external distortions, parameter uncertainties or effects that are not considered in the utilized control laws, hence the demand for a robust design. In addition, the selected control law is required to provide safe and comfortable human-robot interaction. To emphasize the energy efficiency, the control should be designed to minimise the energy consumption of the system. This is defined as a wish in the current stage of the development and the generation of a stable, robust locomotion has higher priority.
Several assumptions are made for the application of the control strategy. The observability as well as controllability of the system is ensured, which is the case for the selected components of the actuation system, however components are assumed to operate without failure. A loss of observability is for example not treated in this thesis. Furthermore, the electric model of the EC-motor is not included in the control law, instead it is assumed that the motor controller compensates the respective behaviour appropriately. The presented requirements lead to the utilisation of an impedance control law to model and influence the mechanical impedance of the active orthosis knee joint and ensure a desired disturbance response as a consequence of external disturbances [45]. The design of the control and an analysis of the stability is presented in what follows.

6.2 Impedance Control

This section contains the design of an impedance control law for the CSEA. In contrast to position or force control, the impedance control models the mechanical impedance of the system, which can thereby be described as a mapping from velocities to forces [45]. A desired impedance is achieved by modelling the desired dynamical behaviour of the system, represented by desired moment of inertia, damping and stiffness, subjected to external forces. This is achieved by determining the control signal depending on a desired stiffness k_d and desired damping d_d in series to motor and ground as depicted in Figure 6.1 for a SEA [45]. Thus, the desired dynamic behaviour is imitated by a respective motion of the actuator. For example, the

total stiffness k_t is a series connection of the physical stiffness k_s of the SEA and the desired stiffness k_d according to the model in Figure 6.1. Hence, the total stiffness is calculated as:

$$k_t = \frac{k_s k_d}{k_s + k_d} \tag{6.1}$$

The impedance control simulates this stiffness value by an appropriate control signal specifying the torque of the actuator, e.g., the arising deflection due to an external torque τ_{ext} depends on k_t and not only on k_s. This characteristic yields advantages for human-robot interaction and adjustability of the natural dynamics allows individual adaptation of the system behaviour via the control parameters.
The design of the control law follows the procedure in [45] and aims to create a passive system according to the definitions given in Section 2.5. To be able to perform the proof of passivity, the system is assumed to be time-invariant. This means that the motor brake of the CSEA is not activated and the control parameters are constant. Further, values for moment of inertia and stiffness are positive. The procedure for the design of the impedance control leads to closed loop equations resulting in a passive system. The control parameters are selected afterwards in Section 6.4.
The following system equations for a SEA introduced by Equation (2.1) are used in the following to design a passive impedance control law:

$$\begin{bmatrix} I_a & 0 \\ 0 & 0 \end{bmatrix} \begin{bmatrix} \ddot{\theta}_a \\ \ddot{\theta}_{ext} \end{bmatrix} + \begin{bmatrix} k_s & -k_s \\ -k_s & k_s \end{bmatrix} \begin{bmatrix} \theta_a \\ \theta_{ext} \end{bmatrix} = \begin{bmatrix} \tau_a \\ -\tau_{ext} \end{bmatrix} \tag{6.2}$$

Inertia Shaping

The first step in the design of the control law is a transformation of the actuator torque τ_a as in [45]:

$$\tau_a = \frac{I_a}{I_{a,d}} u_{ci} + \left(1 - \frac{I_a}{I_{a,d}}\right) k_s (\theta_a - \theta_{ext}) \tag{6.3}$$

Inserting Equation (6.3) in Equation (6.2) yields:

$$\begin{bmatrix} I_{a,d} & 0 \\ 0 & 0 \end{bmatrix} \begin{bmatrix} \ddot{\theta}_a \\ \ddot{\theta}_{ext} \end{bmatrix} + \begin{bmatrix} k_s & -k_s \\ -k_s & k_s \end{bmatrix} \begin{bmatrix} \theta_a \\ \theta_{ext} \end{bmatrix} = \begin{bmatrix} u_{ci} \\ -\tau_{ext} \end{bmatrix} \tag{6.4}$$

The resulting equations of motion for the system are written depending on the control input u_{ci}, which will be designed in the course of this section. Instead of the actuator inertia I_a, now the desired actuator inertia $I_{a,d}$ is in the equations of motion as a parameter of the control law and thus by selecting $I_{a,d}$, the dynamics of the system can be influenced. However, for $I_a \neq I_{a,d}$, a feedback of the spring-torque is necessary requiring a respective sensor or observer.

Passivity of the System

In the design of the impedance controller, a feedback system is generated and the control law is selected by applying Definition 5 given in Section 2.5, so that the resulting system is passive and thus L_2-finite-gain stable. Therefore, the passivity of each subsystem is shown. As a first step, the system equations are adjusted by extracting the inertial load from the external torque, which contains all loads or resistances acting on the knee, so that with

$$\tau_{ext} = \bar{\tau}_{ext} + I_{ext}\ddot{\theta}_{ext} \tag{6.5}$$

Equation (6.4) yields:

$$\begin{bmatrix} I_{a,d} & 0 \\ 0 & I_{ext} \end{bmatrix} \begin{bmatrix} \ddot{\theta}_a \\ \ddot{\theta}_{ext} \end{bmatrix} + \begin{bmatrix} k_s & -k_s \\ -k_s & k_s \end{bmatrix} \begin{bmatrix} \theta_a \\ \theta_{ext} \end{bmatrix} = \begin{bmatrix} u_{ci} \\ -\bar{\tau}_{ext} \end{bmatrix} \tag{6.6}$$

According to Definition 4 given in Section 2.5, a system is passive if a storage function S can be found, so that $S > 0$ and $\dot{S} < yu$ with the supply rate yu. Thereby, $\dot{S}$ denotes the derivative of the storage function S along the solution of the respective equation, in accordance with [35, 45]. The passivity of the external system can be shown using the storage function

$$S_{ext} = \frac{1}{2} I_{ext} \dot{\theta}_{ext}^2 > 0 \tag{6.7}$$

Thus, only kinetic energy is stored in the system. However, as discussed in [35], the storage function of a system can also contain virtual energy, e.g., introduced by a control law. As the storage function only depends on the time for the depicted system with constant inertia, the derivation along the solution of Equation (6.7) leads to:

$$\dot{S}_{ext} = \dot{\theta}_{ext} I_{ext} \ddot{\theta}_{ext} = \dot{\theta}_{ext} \left[-\bar{\tau}_{ext} + k_s(\theta_a - \theta_{ext}) \right] \tag{6.8}$$

For the output $y = \dot{\theta}_{ext}$ and the input $u = (-\bar{\tau}_{ext} + k_s(\theta_a - \theta_{ext}))$, $\dot{S} = yu$ and therefore the output system is passive and, in this case, lossless. The input u to the output system can be split into $-\bar{\tau}_{ext}$ of the environment, which contributes the power $-\bar{\tau}_{ext}\dot{\theta}_{ext}$ to the system, as discussed in modelling environmental influences in [35]. Following this, the output of the actuation system is $-k_s(\theta_a - \theta_{ext})$, so that the spring torque between two systems stays in equilibrium. The structure of the resulting system is illustrated in Figure 6.2 with the respective inputs and outputs. To proof the passivity of the system described by Equation (6.6), port matching has to be achieved, so the input to the actuation system has to be $\dot{\theta}_{ext}$ [35]. The passivity of the actuation system can be shown with the following storage function:

$$S_a = \frac{1}{2} I_a \dot{\theta}_a^2 + \frac{1}{2} k_s (\theta_a - \theta_{ext})^2 > 0 \tag{6.9}$$

which leads to the derivative:

$$\dot{S}_a = \dot{\theta}_a I_a \ddot{\theta}_a + (\dot{\theta}_a - \dot{\theta}_{ext}) k_s (\theta_a - \theta_{ext}) \tag{6.10}$$

and inserting the upper part of Equation (6.6) yields:

$$\dot{S}_a = \dot{\theta}_a [u - k_s(\theta_a - \theta_{ext})] + (\dot{\theta}_a - \dot{\theta}_{ext}) k_s (\theta_a - \theta_{ext}) \tag{6.11}$$

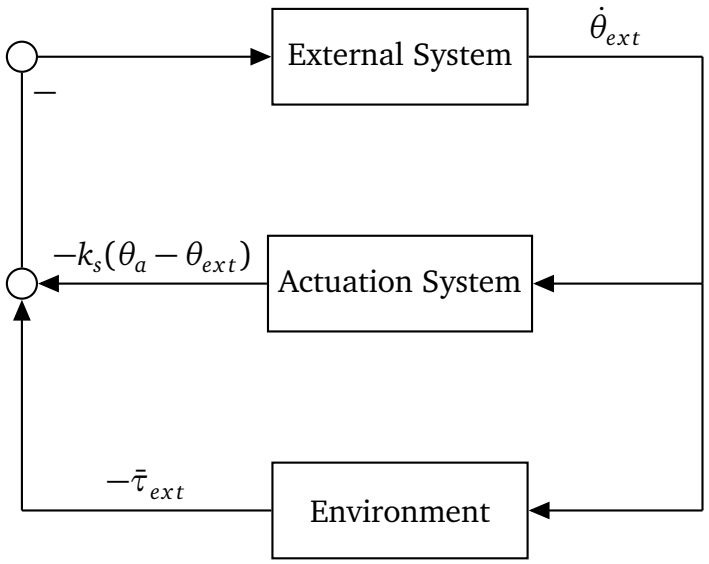

Figure 6.2: Structure of the Feeback System

Thereby, the passivity is shown with the inequality $\dot{S}_a \leq yu$ with $y = \dot{\theta}_{ext}$ and $u = -k_s(\theta_a - \theta_{ext})$:

$$\dot{\theta}_a \left[u_{ci} - k_s(\theta_a - \theta_{ext})\right] + (\dot{\theta}_a - \dot{\theta}_{ext})k_s(\theta_a - \theta_{ext}) \leq -\dot{\theta}_{ext}k_s(\theta_a - \theta_{ext}) \tag{6.12}$$

that simplifies to:

$$\dot{\theta}_a u_{ci} \leq 0 \tag{6.13}$$

Therefore the system is passive for $\dot{\theta}_a u_{ci} \leq 0$. This is for example satisfied for a simple derivative controller $u_{ci} = -d_d\dot{\theta}_a$ which leads to $-d_d\dot{\theta}_a^2 \leq 0$ and the system is passive for $d_d > 0$. For this controller, the system is input strictly passive by applying Definition 4 for $\delta = d_d$ and $d = 0$ and therefore according to Definition 5 the whole system is L_2-finite-gain stable for input $-\bar{\tau}_{ext}$ and output $\dot{\theta}_{ext}$.

Passivity Design of the Control for Position Tracking

In [45], a control law specified for tracking a desired position θ_d is designed to minimise the position error $\tilde{\theta} = \theta - \theta_d$, which will be presented in the following. A modified storage function for Equation (6.6) is thus given by:

$$\tilde{S}_{ext} = \frac{1}{2}I_{ext}\dot{\tilde{\theta}}_{ext}^2 > 0 \tag{6.14}$$

and the respective derivative along the solution of Equation (6.14):

$$\dot{\tilde{S}}_{ext} = \dot{\tilde{\theta}}_{ext}I_{ext}\ddot{\tilde{\theta}}_{ext} = \dot{\tilde{\theta}}_{ext}\left[k_s(\theta_a - \theta_{ext}) - I_{ext}\ddot{\theta}_{ext,d} - \bar{\tau}_{ext}\right] \tag{6.15}$$

which represents a passive mapping for the output $y = \dot{\tilde{\theta}}_{ext}$ and input
$u = \left[k_s(\theta_a - \theta_{ext}) - I_{ext}\ddot{\theta}_{ext,d} - \bar{\tau}_{ext}\right]$, as $\dot{S} \leq yu$.
Thus, similar to the procedure above, to achieve passivity, the actuation system has to be passive with the output $-\left[k_s(\theta_a - \theta_{ext}) - I_{ext}\ddot{\theta}_{ext,d} - \bar{\tau}_{ext}\right]$ and input $\dot{\tilde{\theta}}_{ext}$. In contrast to the procedure above, there is no split into environment and actuation system, however the influence of τ_{ext} is later considered in the generation of the desired trajectories.
The storage function selected in [45] to show passivity is given by:

$$\tilde{S}_a = \frac{1}{2}I_a\dot{\tilde{\theta}}_a^2 + \frac{1}{2}k_s(\tilde{\theta}_a - \tilde{\theta}_{ext})^2 + \frac{1}{2}k_d\tilde{\theta}_a^2 > 0 \tag{6.16}$$

Notice that the desired stiffness of the impedance law is present in the storage function and stores energy as well. Moreover, it fulfils the basic structure of the impedance control described by Figure 6.1. The derivative of the storage function can be expressed as:

$$\dot{\tilde{S}}_a = \dot{\tilde{\theta}}_a I_a \ddot{\tilde{\theta}}_a + k_s(\tilde{\theta}_a - \tilde{\theta}_{ext})(\dot{\tilde{\theta}}_a - \dot{\tilde{\theta}}_{ext}) + k_d \tilde{\theta}_a \dot{\tilde{\theta}}_a \tag{6.17}$$

and inserting Equation (6.6) yields:

$$\dot{\tilde{S}}_a = \dot{\tilde{\theta}}_a \left[u_{ci} - k_s(\theta_a - \theta_{ext}) - I_{a,d}\ddot{\theta}_{a,d}\right] + k_s(\tilde{\theta}_a - \tilde{\theta}_{ext})(\dot{\tilde{\theta}}_a - \dot{\tilde{\theta}}_{ext}) + k_d \tilde{\theta}_a \dot{\tilde{\theta}}_a \tag{6.18}$$

The control law for tracking given in [45] is as follows:

$$u_{ci} = I_{a,d}\ddot{\theta}_{a,d} + k_s(\theta_{a,d} - \theta_{ext,d}) - k_d\tilde{\theta}_a - d_d\dot{\tilde{\theta}}_a \tag{6.19}$$

It consists of a compensation of the desired actuator inertia and known external torque, described by the spring deflection, and an additional PD-control of the motor position based on the desired motion. By inserting Equation (6.19) into Equation (6.18), the derivative of the storage function results to:

$$\dot{\tilde{S}}_a = -d_d\dot{\tilde{\theta}}_a^2 - \dot{\tilde{\theta}}_{ext}k_s(\tilde{\theta}_a - \tilde{\theta}_{ext}) = -d_d\dot{\tilde{\theta}}_a^2 - \dot{\tilde{\theta}}_{ext}k_s[(\theta_a - \theta_{a,d}) - (\theta_{ext} - \theta_{ext,d})] \tag{6.20}$$

The condition for passivity

$$\dot{\tilde{S}}_a \leq uy = -\dot{\tilde{\theta}}_{ext}\left[k_s(\theta_a - \theta_{ext}) - I_{ext}\ddot{\theta}_{ext,d} - \bar{\tau}_{ext}\right] \tag{6.21}$$

thus leads to:

$$-d_d\dot{\tilde{\theta}}_a^2 - \dot{\tilde{\theta}}_{ext}k_s[(\theta_a - \theta_{a,d}) - (\theta_{ext} - \theta_{ext,d})] \leq -\dot{\tilde{\theta}}_{ext}\left[k_s(\theta_a - \theta_{ext}) - I_{ext}\ddot{\theta}_{ext,d} - \bar{\tau}_{ext}\right] \tag{6.22}$$

which can be transformed to:

$$-d_d\dot{\tilde{\theta}}_a^2 + \dot{\tilde{\theta}}_{ext}k_s[\theta_{a,d} - \theta_{ext,d}] \leq -\dot{\tilde{\theta}}_{ext}\left[-I_{ext}\ddot{\theta}_{ext,d} - \bar{\tau}_{ext}\right] \tag{6.23}$$

By assuming there exists a desired external torque $\tau_{ext,d}$, correlated to the desired external trajectory $\theta_{ext,d}$, the relation$\tau_{ext,d} = I_{ext,d}\ddot{\theta}_{ext,d} + \bar{\tau}_{ext}$ given in Equation (6.2) can be used, which leads to the selection of $\theta_{a,d}$ according to:

$$\theta_{a,d} = \theta_{ext,d} + \frac{\tau_{ext,d}}{k_s} \tag{6.24}$$

By inserting Equation (6.24) into Equation (6.23), the condition for passivity simplifies to:

$$-d_d\dot{\tilde{\theta}}_a^2 \leq 0 \tag{6.25}$$

which is fulfilled for any $d_d > 0$. As above, it can be shown that the system is input strictly passive by applying Definition 4 for $\delta = d_d$ and $d = 0$ and therefore, according to Definition 5 given in Section 2.5, the whole system is L_2-finite-gain stable for input $\bar{\tau}_{ext}$ and output $\dot{\tilde{\theta}}_{ext}$.
Inserting the control law for tracking given by Equation (6.19) into the system described by Equation (6.2), yields the following closed loop equations:

$$\begin{bmatrix} I_{a,d} & 0 \\ 0 & 0 \end{bmatrix}\begin{bmatrix} \ddot{\theta}_a \\ \ddot{\theta}_{ext} \end{bmatrix} + \begin{bmatrix} k_s & -k_s \\ -k_s & k_s \end{bmatrix}\begin{bmatrix} \theta_a \\ \theta_{ext} \end{bmatrix} = \begin{bmatrix} I_{a,d}\ddot{\theta}_{a,d} + k_s(\theta_{a,d} - \theta_{ext,d}) - k_d\tilde{\theta}_a - d_d\dot{\tilde{\theta}}_a \\ -\tau_{ext} \end{bmatrix} \tag{6.26}$$

In doing so, the desired external torque $\tau_{ext,d}$ is compensated by the term $k_s(\theta_{a,d} - \theta_{ext,d})$. However, in a real application, uncertainties or variations of the external torque occur. Hence, the unknown deviation $\tau_{ext,dev}$ can be described depending on τ_{ext} and the known $\tau_{ext,d}$ according to:

$$\tau_{ext} - \tau_{ext,d} = \tau_{ext,dev} \tag{6.27}$$

Inserting Equations (4.5) and (6.24), describing τ_{ext} and $\tau_{ext,d}$ depending on the actual or desired motor position into Equation (6.27) yields:

$$k_s(\theta_a - \theta_{ext}) - k_s(\theta_{a,d} - \theta_{ext,d}) = k_s(\tilde{\theta}_a - \tilde{\theta}_{ext}) = \tau_{ext,dev} \tag{6.28}$$

With this relation between position error and unknown component of the external torque, Equation (6.26) yields the following closed loop system for a SEA with impedance control in terms of the respective position error:

$$\begin{bmatrix} I_{a,d} & 0 \\ 0 & 0 \end{bmatrix} \begin{bmatrix} \ddot{\tilde{\theta}}_a \\ \ddot{\tilde{\theta}}_{ext} \end{bmatrix} + \begin{bmatrix} d_d & 0 \\ 0 & 0 \end{bmatrix} \begin{bmatrix} \dot{\tilde{\theta}}_a \\ \dot{\tilde{\theta}}_{ext} \end{bmatrix} + \begin{bmatrix} k_s + k_d & -k_s \\ -k_s & k_s \end{bmatrix} \begin{bmatrix} \tilde{\theta}_a \\ \tilde{\theta}_{ext} \end{bmatrix} = \begin{bmatrix} 0 \\ -\tau_{ext,dev} \end{bmatrix} \tag{6.29}$$

The closed loop equations show the tracking capabilities of the selected control law, as the position error is zero for $\tau_{ext,dev} = 0$. Hence, a error in position only occurs for unknown components of the external torque. These induce characteristic behaviour of the system according to the modelled impedance, which is described by the series stiffness k_s as well as the virtual, desired stiffness k_d, the virtual damping at the motor d_d as well as the desired actuator inertia $I_{a,d}$. The influence of unknown external torques is examined in the following.

Examination of the Influence of Unknown External Torques

The behaviour of the system under the influence of a deviation in the external torque can be examined using the model given by Equation (6.29). As both degrees of freedom are coupled by the series spring, inserting the lower part into the upper part results in:

$$I_{a,d}\ddot{\tilde{\theta}}_a + d_d\dot{\tilde{\theta}}_a + k_d\tilde{\theta}_a = -\tau_{ext,dev} \tag{6.30}$$

A Laplace transformation then leads to the transfer function:

$$\frac{\tilde{\theta}_a(s)}{-\tau_{ext,dev}(s)} = \frac{1}{I_{a,d}s^2 + d_d s + k_d} \tag{6.31}$$

which has two poles at $-d_d \pm \sqrt{d_d^2 - 4I_{a,d}k_d}$. As both poles have a negative real part, the position error of the actuator due to a deviation torque $-\tau_{ext,dev}$ is stable and behaves like a damped single mass oscillator.

Thus, for a bounded deviation torque $\tau_{ext,dev}$, the position error $\tilde{\theta}_a$ is also bounded as seen from Equation (6.31) and therefore from Equation (6.28) follows that the error at $\tilde{\theta}_{ext}$ is bounded as well. This shows that the system is BIBO-stable with respect to a deviation torque $\tau_{ext,dev}$. In addition, this complies with the design ideas of the impedance control presented in Section 6.2, as desired damping and stiffness are used to model the behaviour of the system loaded by the the torque $\tau_{ext,dev}$.

To avoid oscillations of the actuator error for $\tau_{ext,dev} \neq 0$, the desired damping d_d can be selected to generate a critical damped system with $D = 1$. Thus, to avoid oscillations introduced by $\tau_{ext,dev}$, for an equation of motion in the form of Equation (6.30), the resulting condition for a critical damped behaviour is [43]:

$$d_{d,cr} = 2\sqrt{I_{a,d} k_d} \tag{6.32}$$

6.3 State Machine

For the operation of the developed elastic actuator, activation of the EMB is implemented via a Finite State Machine (FSM). The FSM is defined according to Figure 6.3 and contains three states. State 1 corresponds to the stance phase of the gait and is initiated when a ground reaction force (GRF) is detected. In the simulation, the GRF of the gait data in [6] are used and state 1 is triggered as soon as the value $GRF \neq 0$ is detected. This corresponds to the heel strike in the gait cycle. In state 1, the EMB is active while the impedance control is deactivated, so the actuator is locked by the EMB, thus only the EMB requires power. The actuator is unlocked and the control activated (state 2) as soon as the swing phase begins, which is detected by a rise in the desired actuator position $\theta_{a,d}$. Using $\theta_{a,d}$ as a trigger for state 2 works well in the simulations, however does not include the actual position θ_{ext}. For the use in the active orthosis in a real application scenario, a different trigger should be used to ensure controllability and safety for the operator. During the evaluation of the simulations, it has been noticed that a low d_d is beneficial for the acceleration during the first half of the swing phase. However a higher damping is required afterwards to provide the required deceleration to adequately follow the trajectory before the stance phase. Hence, a third state is added in the FSM to reduce the

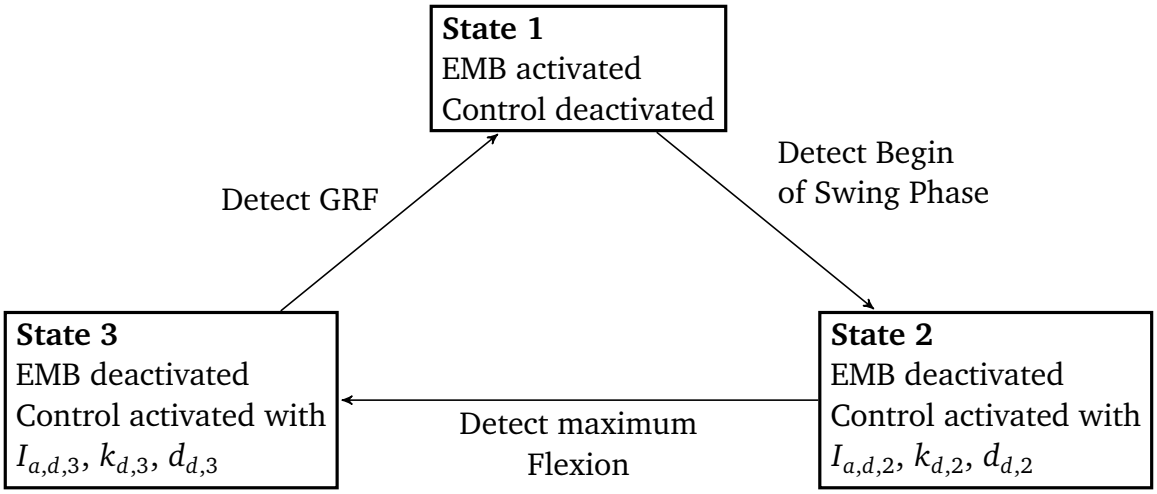

Figure 6.3: Developed Finite State Machine

control error, and is initiated after the full flexion, triggered by detecting $\dot{\theta}_{a,d} < 0$ as a typical occurrence during the gait cycle. Thus the model of the controlled elastic actuation system given in Equation (6.4) can be extended with the FSM to:

$$\begin{bmatrix} I_{a,d} & 0 \\ 0 & 0 \end{bmatrix} \begin{bmatrix} \ddot{\theta}_a \\ \ddot{\theta}_{ext} \end{bmatrix} + \begin{bmatrix} k_s & -k_s \\ -k_s & k_s \end{bmatrix} \begin{bmatrix} \theta_a \\ \theta_{ext} \end{bmatrix} = \begin{bmatrix} u_{ci} - \tau_{EMB} \\ -\tau_{ext} \end{bmatrix} \tag{6.33}$$

with

$$u_{ci} - \tau_{EMB} = \begin{cases} \text{State 1:} & a_{EMB} = 1, u = 0 \\ \text{State 2:} & a_{EMB} = 0, I_{a,d} = 0.9 I_a, k_d = 200, d_d = 8.45 \\ \text{State 3:} & a_{EMB} = 0, I_{a,d} = 0.9 I_a, k_d = 200, d_d = 16.9 \end{cases} \tag{6.34}$$

with u according to Equation (6.19) and τ_{EMB} according to Equation (5.1).

Influence of the FSM on the Passivity of the System

As shown by Equation (6.25), the passivity and thus the $L2$-finite-gain stability of the selected impedance control is ensured for any $d_d > 0$. Hence, the FSM with the selected control parameters does not influence the stability of the system. The activation of the EMB leads to a locked actuator and thus a system, which does only receive energy from the external torque, is generated. Assuming some sort of damping, e.g., friction of a bearing, the locked system is dissipative. Hence, all states of the FSM result in passive systems. However, the transition of states and thus of the control parameters is abrupt and may induce peaks in actuator torque, leading to uncomfortable human-robot interaction. As the investigated system is non-linear, additional oscillations may be introduced as well. Further, adjusting the parameters adds a dynamic component, as parameter vary with time and the system is therefore not time invariant. This means that the analytic proof of passivity presented above is no longer valid. As an alternative, the influence of the FSM respective the change of control parameters is investigated via simulation and experiments.

6.4 Simulation and Evaluation of the Controlled System

For the simulation, the model in Equations (6.33) and (6.34) is implemented in *Matlab/Simulink*, Figure 6.4 shows the resulting structure. The parameters used during the simulations are summarized in Table 6.2, the optimal values from the analysis performed in Section 4.3 are thereby applied to the model. The control parameters of the impedance control

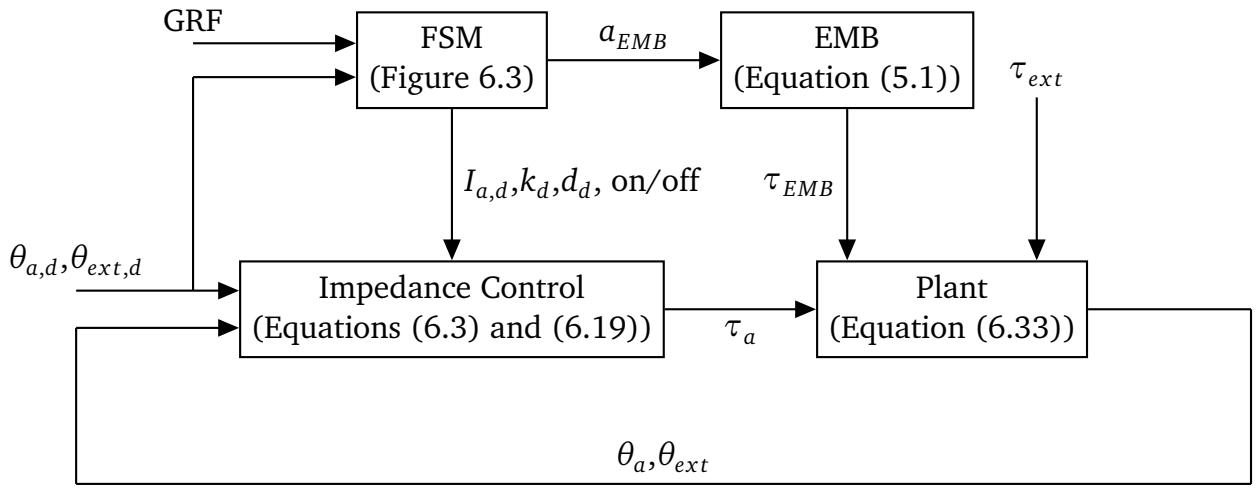

Figure 6.4: Structure of the implemented Impedance Control

are tuned manually after an implementation of the presented structure. An optimisation to minimise $[w(1)E_{gc,rec}^2 + w(2)\tilde{\theta}_{ext}^2]^T$ with the weights w only provided local minima, a global optimisation is not applied due to high effort and could improve the results as well as an automated procedure to select control parameters. Qualitative good results are achieved when the desired damping $d_{d,2}$ and $d_{d,3}$ is implemented depending on the critical damping $d_{d,cr}$ calculated by Equation (6.32). Thus, the utilised damping varies with desired actuator inertia $I_{a,d}$ and desired stiffness k_d.

The resulting simulation data is depicted in Figure 6.5. The curves present a good alignment of the desired and actual position of the knee that remains consistent for the simulated number of gait cycles. The FSM activates the EMB and the states correctly. The position errors $\tilde{\theta}$ only show notable deviations during the stance phase, which are due to the generation of the desired trajectories with locked actuator position during the stance phase. As discussed in Section 4.3, the Fourier-Series contains small oscillations during the stance phase, which are prevented by the locking system. However they are included in the desired position function to achieve smooth curves. Therefore, the actual position of the knee during state 1 is a reaction depending on the position of the locked actuator, the external torque and the series stiffness. Thus, the presented control error during the activated EMB can be neglected for the adjustment of the control parameters but has to be considered for the FSM. The maximum control error during the swing phase reaches to 0.19°, which is deemed acceptable for the simulation of the ideal system with the selected control parameters. The depicted torque and power over time confirm the results from Section 4.3, as high torques and power during the stance phase are generated by the EMB and not by the electric motor. The presented power of the simulation includes the required power of the motor as well as a the consumption of 6 W when the EMB is active. For the selected gait trajectory and parameters, a total energy of 1.52 J per gait cycle can be recuperated.

Table 6.2: Parameters of the Simulations

Parameter	Symbol	Value
Reflected Actuator Inertia	I_a	$0.0991\,\mathrm{kg\,m^2}$
Torsional Stiffness	k_s	$296\,\mathrm{N\,m\,rad^{-1}}$
Gear Ratio	i_G	74
Subject's Body Mass	m_h	75 kg
Time per Gait Cycle	t_{gc}	1.3 s
Simulated Gait Cycles	-	20
Desired Stiffness, State 1	$k_{d,2}$	$200\,\mathrm{N\,m\,rad^{-1}}$
Desired Stiffness, State 2	$k_{d,3}$	$200\,\mathrm{N\,m\,rad^{-1}}$
Desired Actuator Inertia, State 1	$I_{a,d,2}$	$0.9I_a$
Desired Actuator Inertia, State 2	$I_{a,d,3}$	$0.9I_a$
Desired Damping, State 1	$d_{d,2}$	$2d_{d,cr}$
Desired Damping, State 2	$d_{d,3}$	$4d_{d,cr}$
Solver	—	ode 45
Maximum Time Step	—	1×10^{-4} s

This includes the efficiency of each component as in Section 4.3.
The estimated position error of the actuator depicted in dashed-black is calculated from Equation (6.31) utilising the values of state 2, thus the change of the FSM are not considered to be able to implement a transfer function with constant parameters. As there is no unknown external torque, the estimated position error is approximately zero during the simulation.
To evaluate the behaviour of the controlled system exposed to external disturbances, an additional external deviation $\tau_{ext,dev}$ is applied to τ_{ext} of the gait data. The selected distortion is a rectangular signal with amplitude 10 N m from 3 s to 3.7 s of the simulation. The resulting trajectory is depicted in Figure 6.6, parameters for the simulation are not changed. The knee position distinctly deviates from the desired position during the period when the external disturbance is applied. The rectangular signal begins during the stance phase with activated EMB, thus the displacement of the knee only depends on the serial stiffness and is not actively influenced by the impedance control. This changes after state 2 is initialised and the motor error follows the estimated motor error, thus the behaviour of the system is dominated by the impedance control and the respective modelling of the interaction with the environment. The actual motor error follows thereby the estimated motor error, except for a delay observed at the removal of the external disturbance. However, this delay occurs to the calculation of the estimated motor error

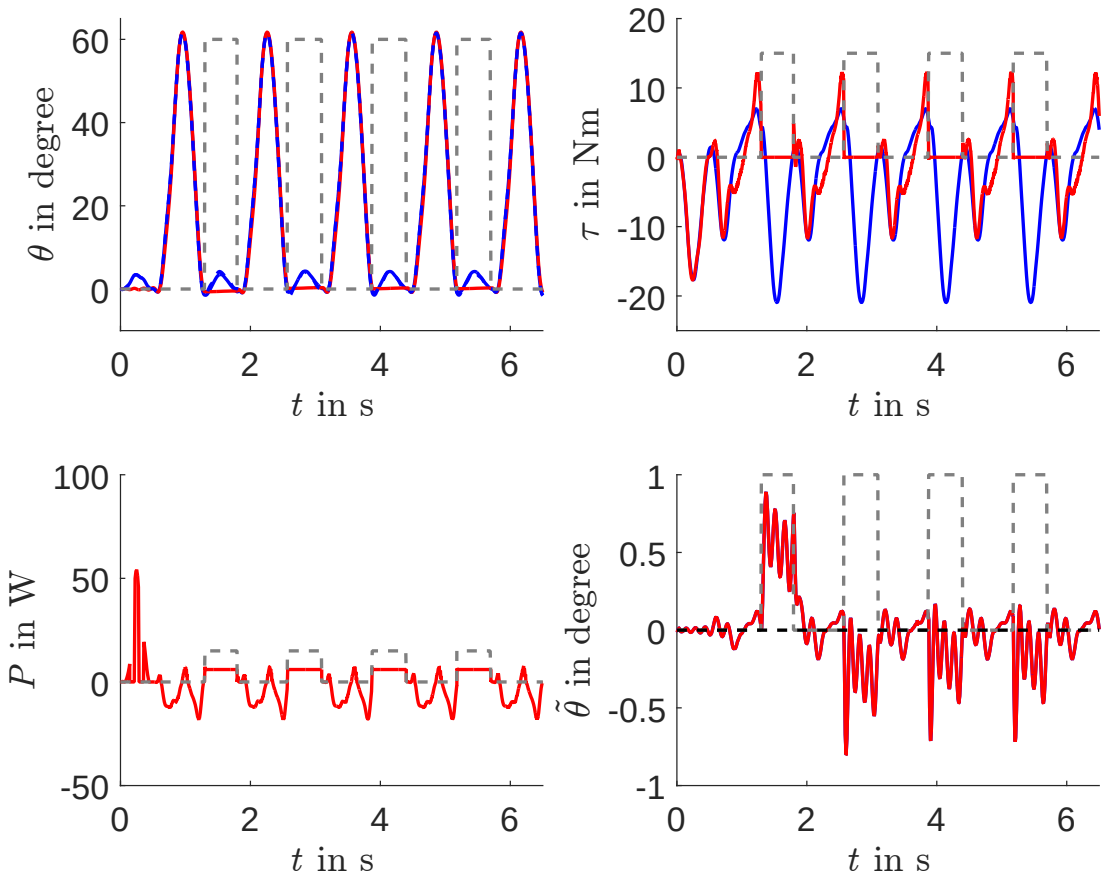

Figure 6.5: Resulting trajectory for the CSEA including impedance control and FSM / all: state of the EMB (dashed-grey) / top left: desired (dashed-blue) and actual (blue) position knee including brake impact, position actuator (red) / top right: knee (blue) and actuator (red) torque without brake / bottom left: actuator power (red) with brake / bottom right: position error knee (blue) and actuator (red)

via a transfer function with constant parameters, thus the increased damping of the system in state 3 is not included. Therefore, the behaviour of the system exposed to external disturbances is predicted according to the selected impedance control law with the respective control parameters, and the interaction with the environment is modelled accurately. The two peaks depicted in the power of the external system occur due to the application of the external torque as a step-signal, which induced sudden changes in the position and thus infinite values in the velocity. In addition, the compensation of the external disturbance leads to a noticeable increase in the required power, especially as the gear ratio is tuned for high motor efficiency at lower torques. To conclude, the requirements regarding stability and control error are fulfilled by the selected impedance control and FSM. The impedance of the robot-human-interaction is modelled by the parameters of the selected impedance control, which can be adapted to include user feedback. The required robustness of the system is investigated in the next section.

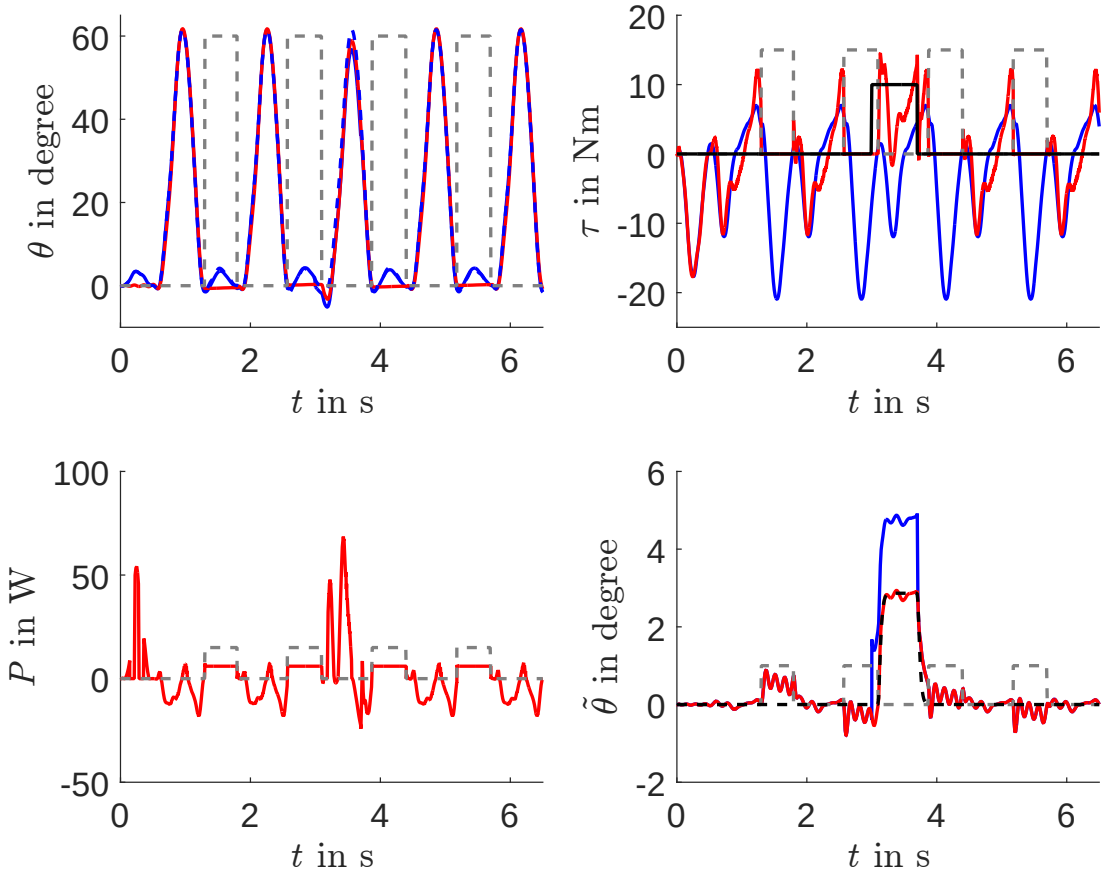

Figure 6.6: Resulting trajectory for the CSEA including impedance control and FSM exposed to external disturbance / all: state of the EMB (dashed-grey) / top left: desired (dashed-blue) and actual (blue) position knee including brake impact, position actuator (red) / top right: knee (blue) and actuator (red) torque without brake, external disturbance (black) / bottom left: actuator power (red) with brake / bottom right: position error knee (blue) and actuator (red), estimated motor error (black)

6.5 Examination of Robustness of controlled System

The presented system has to be robust to compensate for external disturbances, as well as parameter uncertainties and effects not considered in the model. Therefore, the simulation presented above is extended considering several effects. The distortion of the motor position due to an encoder is emulated by a quantisation. The quantisation interval is assumed to be from an encoder with 4000 counts per revolution enhanced by a gear ratio of 30. The selected resolution is decreased from the selected components in Section 5.4 to intensify negative effects. Noise influence of the IMU is directly implemented as white noise imposing the feedback of the external position with a noise power of 0.000002. This equals approximately a distortion of approximately ±0.06 rad. The external torque of the simulation is affected by a white noise as well, with a power of 0.001, resulting in a distortion of approximately ±2 N m. To include

parameter uncertainties, all parameters in the impedance control law are increased by the factor 1.2. This simulates a worst case scenario regarding the passivity, where more energy than required is induced into the system by the controller.

The data from this simulation are depicted in Figure 6.7, however two adjustments are implemented to improve the results. The first change is the application of a first-order low-pass filter with cut off frequency at 100 rad s^{-1} to the motor velocity, calculated by derivation of the quantised encoder signal. The second change is filtering of the estimation of the external torque via the deflection of the serial spring, as it includes distortions of both sensor signals and is utilised in the impedance law. By setting $I_{a,d} = I_a$, the feedback could be removed as seen from Equation (6.3), however then the desired actuator inertia can not be adjusted. Hence, a first-order low pass with cut off frequency 100 rad s^{-1} is implemented to improve the signal. Both filters are tuned manually to reduce induced phase lag. The in Figure 6.7 presented data show stabil-

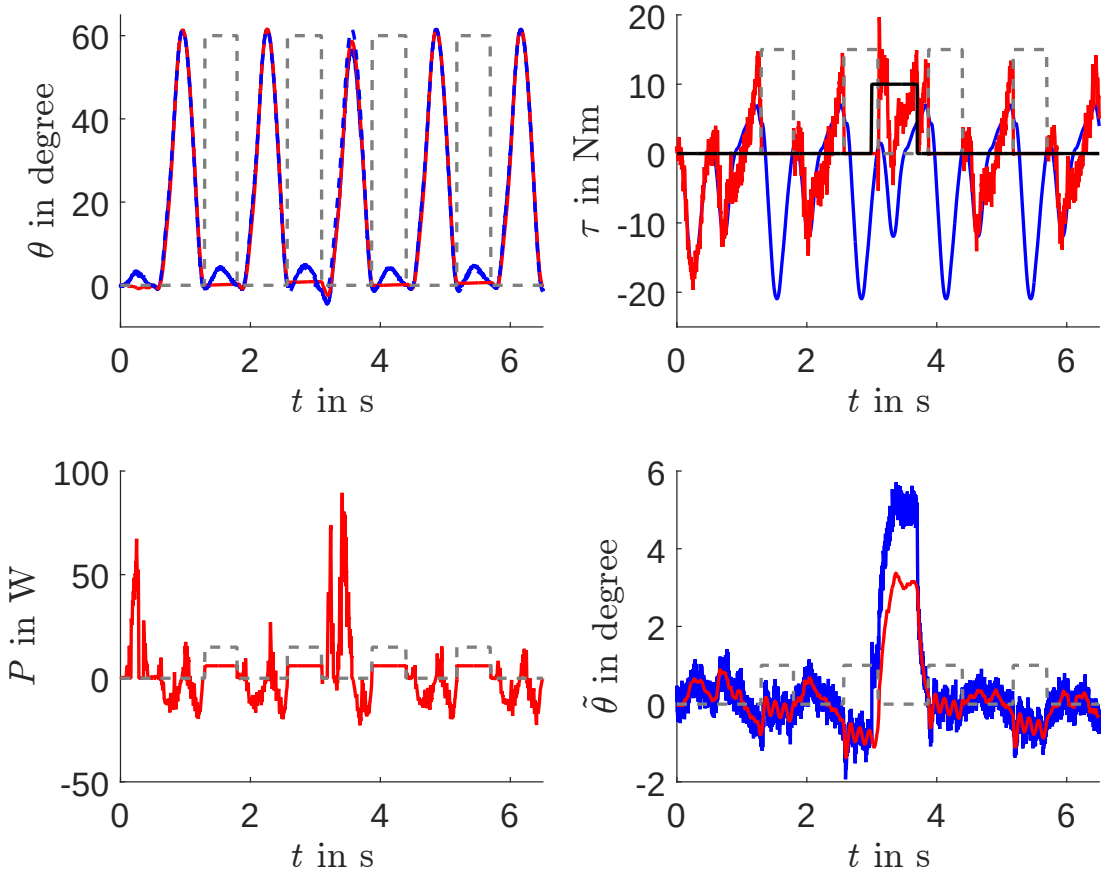

Figure 6.7: Resulting trajectory for the Examination of the Robustness of the System / all: state of the EMB (dashed-grey) / top left: desired (dashed-blue) and actual (blue) position knee including brake impact, position actuator (red) / top right: knee (blue) and actuator (red) torque without brake, external disturbance (black) / bottom left: actuator power (red) with brake / bottom right: position error knee (blue) and actuator (red)

ity of the system, although the performance is notably reduced. The torque signal reflects the induced noise and uncertainties, which are relayed to the required power. The position error of the motor shows a distinct increase, however tracking of the desired trajectory is maintained. During the analysis of the robustness, the importance of a qualitative high motor velocity and feedback of the external torque via the spring deflection is ascertained. This is achieved via low-pass filtering however additional uncertainties, e.g., calibration errors or offset errors are not examined and can therefore not be discovered or compensated in this case.

6.6 Discussion

The control design for the CSEA is presented in this chapter. In the beginning, requirements are specified to provide a basis for the selection and evaluation of an appropriate control strategy to ensure a stable and safe generation of locomotion. In addition, robustness and comfort of the human-robot interaction is focused on. The impedance controller proposed in [45] provides a modelling of the desired compliance of the actuation system, providing high potential as an appropriate control algorithm and was therefore implemented for the investigation of the controlled CSEA. In this chapter, a proof of passivity for tracking of a desired position via impedance control is conducted and the influence of deviations in the external torque is investigated. Furthermore, the impedance control is extended by a FSM to operate the EMB and lock the actuator position during the stance phase. A third state is included for the second half of the swing phase, as increased damping reduces the position error. The complete system is implemented and simulations are performed, using manually selected control parameters, reproducing the analytic behaviour of the CSEA obtained in Section 4.3. An investigation of external disturbances as well as effects not considered in the impedance control model is conducted to show the robustness of the selected control strategy. The simulations show that the control error is considerably small and robust behaviour is achieved. The stability of the system is retained even when exposed to considerably external disturbances and the human-robot interaction can be specified according to the desired impedance by adjusting the control parameters. Thus, all requirements are fulfilled by the selected control strategy consisting of impedance control and FSM. The wish to minimise the required energy consumption per gait cycle is not fulfilled, the performed minimisation to select appropriate control parameters only provided local minima and manual tuning achieved better overall results. The application of an adaptive or self-tuning controller could fulfil this wish.

The impedance control provides a suitable approach for the control of the CSEA and the proof of passivity is given. Thus, the system is L_2-finite-gain stable and the motor position error converges to zero in the absence of a deviation in the external torque. The L_2 finite-gain stability

states that the output of the system, the error in motor velocity, belongs to L_2, when the input, the control signal of the impedance control, belongs to L_2 as well. The control input contains the known external torque of the gait cycle, which is represented by a Fourier Series, which can be expressed as a sum of cosine and sine curves with a constant offset, as the coefficient a_0 is non-zero. The offset is similar to a step signal and does not belong to L_2, as the resulting signal is monotonically increasing. It is therefore not bounded and hence does not converge when integrated as seen from Definition 2 given in Section 2.5. Thus, the external torque only belongs to L_2, when the gait cycle ends at some point, reducing τ_{ext} to zero so that a bounded signal is created. The assumption that the gait cycle stops is valid, as the user of the active orthosis stops at some point in time, however it has to be discussed for the proof of passivity. In addition, the inclusion of the FSM requires the consideration of the EMB and varying control parameters, creating a time variant system.

In this work, the proof of stability of the extended model is only given by simulation, thus, the passivity of the non-linear, time varying system is not shown formally. Similarly, the robustness of the CSEA with impedance control and FSM is demonstrated by simulation and not analytically and only covers considered effects as described above. Further distortions, e.g. distinct changes in the external torque, time lags or friction are not investigated. An analysis of the influence of a distorted external torque should be performed, as for the human gait cycle, the external torque varies considerably depending on various factors, e.g., the ground reaction forces depend on the surface type and quality, and is also used to calculate the desired position of the motor. This is especially important for the application at the active orthosis to achieve a stable and safe locomotion. Hence, to generate the desired position of the knee, additional information of the external torque is required to determine the desired trajectory of the actuator. However, this is not limited to the proposed impedance control, but valid for all SEA, which have two degrees of freedom. Furthermore, the simulation and selection of control parameters is only performed for one time of the gait cycle and therefore influences of different gait velocities are not investigated.

7 Experimental Evaluation

To asses the laboratory specimen, several conducted experiments are presented in this chapter. The experimental evaluation is a crucial step in the validation of the developed concept of CSEA, the designed system and respective components as well as the selected control strategy. Criteria and experiments are defined in the beginning of the chapter as the basis for the evaluation. Thereby, the focus is on a comparison between DA and CSEA as well as on the relation between model-based and experimental results. The employed DA consists of the selected EC-motor combined with the selected harmonic drive, which are directly connected to the pendulum. Parameters of the directly-actuated and series elastic systems are identified for the implementation of the impedance control and for increased accuracy of the utilised models. Experiments are performed and evaluated as a proof of concept of the CSEA with the implemented laboratory specimen, presented in Figure 5.9, impedance control strategy and FSM. In the following, all values given for the actuator are with respect to the output of the gear unit. All experiments are conducted via the selected hardware/software computer and a custom program written in *Labview*, which is used for the control as well as data recording. The utilised sensors are calibrated. In addition, the auto-tuning capabilities of the motor controller are used to tune the parameters of the utilised PI current control to provide the torque desired by the impedance control law.

7.1 Definition of Experiments and Criteria for the Evaluation of the Elastic Actuator

The goal of the experimental evaluation is a proof of concept, thus several aspects, based on goals, criteria and requirements of Chapters 3 to 6 are investigated as suggested in [36]. The available test bench consists of a structure to mount the actuation system and a pendulum modelled after the human leg and foot. However, as additional torque can not be applied, the mimicking of the external torque according to gait data is not possible. Therefore, the proof of concept utilises the gait trajectories for the desired position and the resulting dynamics of the pendulum as the load. This allows the evaluation of the generation of a desired trajectory with the designed CSEA and the control strategy as well as the applied models. However, the measurement of the required energy per gait cycle and a comparison to the results of Section 4.3 is not possible for a human-like gait cycle.

To evaluate the capabilities to track the desired position, two test trajectories are selected. A

desired sine wave with an amplitude of 10° and frequencies from 0.1 Hz to 1 Hz in increments of 0.1 Hz is investigated. Furthermore, a gait trajectory with maximum amplitude of 30° and t_{gc} between 2 s and 10 s is applied and evaluated. The desired motion is associated with the pendulum, coinciding for actuator and pendulum for the DA. The respective desired actuator position is derived from Equation (6.24) for the CSEA depending on the desired trajectory of the pendulum. The restriction of the amplitude and time per gait cycle is required due to the friction, analysed in Section 7.3, and the resulting increase of the required power, which is not satisfied by the selected actuator. The selected control strategy and adjustment of the impedance via control parameters is investigated by manual deflection and examination of the response of the system as performed in [46]. Furthermore, a comparison of the power consumption between the EMB and the selected motor subjected to external torque is conducted.

7.2 Set up of the Test Bench

The experimental evaluation of the elastic actuation system is performed using the test bench developed in [47]. The test bench is modelled as a pendulum consisting of three sections representing the human knee, shank and foot as depicted in Figure 7.1. The knee-section consists

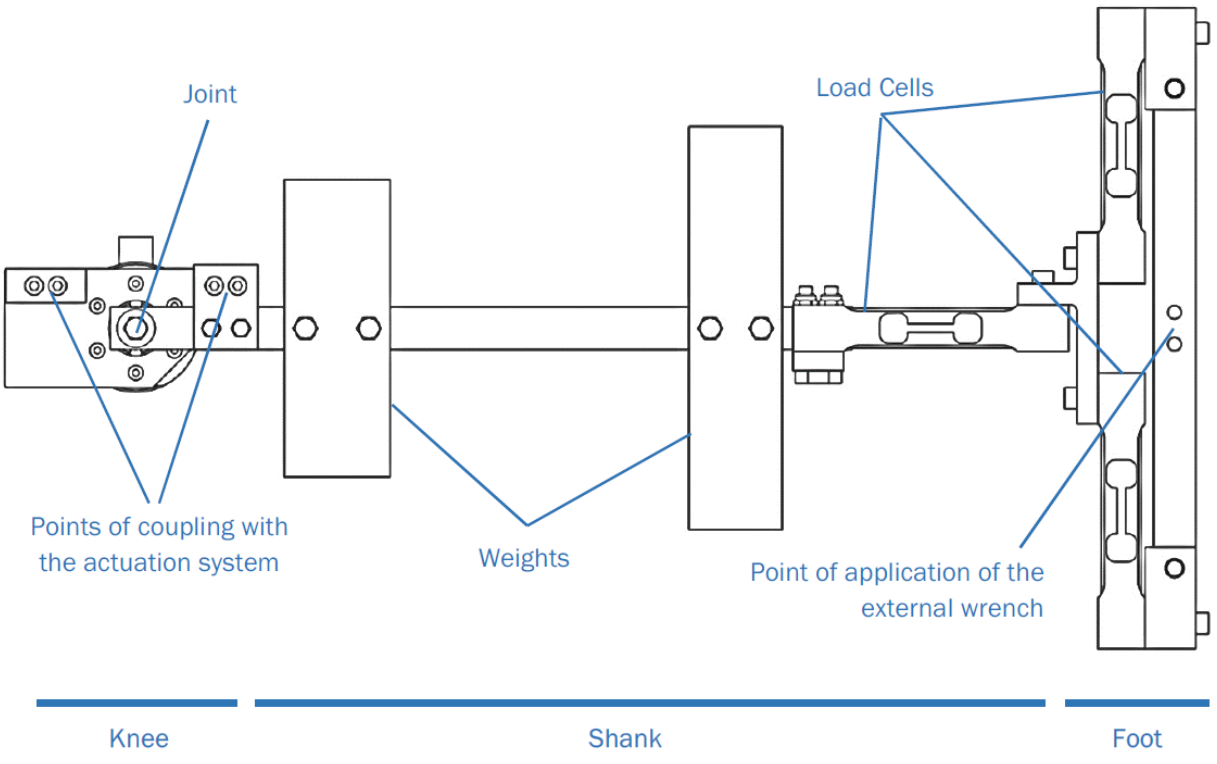

Figure 7.1: Structure of the Pendulum of the Test Bench from [47]

of the actuation system and the axis of rotation of the pendulum coincides with the knee joint. Thus, the knee-section varies depending on the implemented actuation system. The human shank is modelled as a rod with weights to provide the physiological moment of inertia. The foot consists of a structure to apply external loads via an external wrench. The load cells allow a measurement of inertial as well as external forces applied to the foot.
Thus, instead of applying the torque from the gait data, the external torque τ_{ext} consists of the inertial resistance and gravitational torque of the pendulum τ_p. Hence, Equation (4.10) is used as the model of the system for the application at the test bench.

7.3 Parameter Identification

The parameter identification of the system is required to conduct a model-based evaluation of the actuation system and to provide parameters for the impedance control. In the following, the parameters are identified for the DA and CSEA individually due to differences of the actuator and the mounting of the pendulum. The identified parameters are directly utilised in the following experiments.

Evaluation of the Moments of Inertia

The moments of inertia of the actuation system are composed of actuator inertia I_a and moment of inertia at the external side I_{ext}, which is equal to the moment of inertia of the pendulum of the test bench about the rotation axis I_p. The moment of inertia of the actuator side of the directly-actuated system consists of the reflected rotor inertia of the motor and the harmonic drive gear box, and are extracted from the respective datasheets. The corresponding moment of inertia of the CSEA includes the reflected rotor inertia of the EMB as an additional component. As the torsional spring is positioned after the harmonic drive, the moment of inertia is not increased by the gear ratio and thus not included in the inertia of the actuation side. The values for each component and the resulting total values are summarized in Table 7.1. Thereby, the total value represents the reflected moment of inertia, which is increased by the square of the gear ratio $i_G = 160$.

Evaluation of Inertia at External Side

The evaluation of the moment of inertia at the external side is performed experimentally in two steps. The first step consists of the estimation of the mass and centre of mass of the pendulum. This is performed by deflecting the pendulum with removed actuator and fixing it in several

Table 7.1: Moments of Inertia of the actuator side for the DA and CSEA

Component	Moment of Inertia	Reference
EC-motor	$I_{EC} = 1.81 \times 10^{-5}\,\mathrm{kg\,m^2}$	Appendix B.6
Harmonic Drive	$I_{HD} = 9 \times 10^{-6}\,\mathrm{kg\,m^2}$	Appendix B.7
EMB	$I_{EMB} = 2.1 \times 10^{-6}\,\mathrm{kg\,m^2}$	Appendix B.8
total for the DA	$I_{DA} = 0.6938\,\mathrm{kg\,m^2}$	$I_{DA} = (I_{EC} + I_{HD})i_G^2$
total for the CSEA	$I_{CSEA} = 0.7475\,\mathrm{kg\,m^2}$	$I_{CSEA} = (I_{EC} + I_{HD} + I_{EMB})i_G^2$

positions at the point of application of an external wrench depicted in Figure 7.1. Thus an equilibrium between gravitational torque $\tau_g = m_p l_{p,cg} g \sin(\theta_p)$ of the pendulum as in Equation (4.10) and reaction torque τ_r is created, which is measured by the load cells of the test bench according to the correlations provided in [48]. For the model-based comparison and the impedance control, the evaluation of the product $m_p l_{p,cg}$ is sufficient. The respective value is extracted from the relation

$$m_p l_{p,cg} = \frac{\tau_r}{g \sin(\theta_p)} \tag{7.1}$$

The measurements were repeated for several positions and yield $m_p l_{p,cg} = 1.1316\,\mathrm{kg\,m}$ with a standard deviation of $0.0375\,\mathrm{kg\,m}$. The moment of inertia of the pendulum around the axis of rotation is determined based on free oscillation experiments as proposed in [49]. Free oscillations are created by a manual deflection to approximately 30° and release of the pendulum. The position over time of the resulting oscillation is measured by an encoder *HS10-31312117-1024* (*Hohner Automáticos, Breda, Spain*) and a curve fit of the data to the model of a pendulum by means of a least squares method. The employed model represents a pendulum subjected to gravitational torque and damping at the axis of rotation according to:

$$I_p \ddot{\theta}_p + d_p \dot{\theta}_p = \tau_g \tag{7.2}$$

The model is fitted to the measurement data using a least squares method to estimate I_p and d_p. It is necessary to include the damping d_p, so that the amplitude of the oscillations of the model decline and a good fit is possible. The curve-fitting is performed using the *lsqcurvefit* function in *Matlab* utilising the Levenberg-Marquardt algorithm. This yields $I_p = 0.413\,\mathrm{kg\,m^2}$ with a standard deviation of $0.0012\,\mathrm{kg\,m^2}$ for the mean value of $m_p l_{p,cg}$. The damping is dermined as $d_p = 0.0182\,\mathrm{N\,m\,s\,rad^{-1}}$.

Due to the design of the CSEA, the moment of inertia changes slightly and is evaluated us-

ing the same procedure. The experiments yield a value of $m_p l_{p,cg} = 1.2806\,\mathrm{kg\,m}$ with a standard deviation of $0.0118\,\mathrm{kg\,m}$. Implementing this into the model and performing the least-squares optimisation using data from free oscillation experiments captured by the IMU selected in Section 5.4 yields $I_p = 0.4943\,\mathrm{kg\,m^2}$ with a standard deviation of $3.2128 \times 10^{-4}\,\mathrm{kg\,m^2}$ and $d_p = 0.0073\,\mathrm{N\,m\,s\,rad^{-1}}$. It has to be mentioned that the given standard deviations for I_p do not consider error propagation of the error of $m_p l_{p,cg}$ and thus only shows that the utilised method gives similar results for all experiments.

Evaluation of Friction at the Actuator Side

After the determination of the moments of inertia, the friction at the motor side is investigated. Therefore, experiments are performed using the motor directly connected to the harmonic drive. Any load attached to the harmonic drive, e.g., pendulum and interface between pendulum and harmonic drive is removed to allow continuous rotation of the system. This configuration enables the determination of the friction of the drive unit and of a respective compensation strategy. The friction is evaluated by measuring the output of a speed controller during a desired velocity increasing from $0\,\mathrm{rad\,s^{-1}}$ to $2.1\,\mathrm{rad\,s^{-1}}$ to $-2.1\,\mathrm{rad\,s^{-1}}$ to $0\,\mathrm{rad\,s^{-1}}$ in a total of 960 s, which covers the range of velocity of the test trajectories. The actuation system is set into motion before starting the measurement, to avoid the influence of large temperature differences. The resulting data is presented in Figure 7.2. The actuator velocity depicted in blue follows the desired value in red, except for very low desired values as seen in the bottom left of Figure 7.2, where stiction occurs. Furthermore, the relation between velocity and required torque is non-linear as seen from a comparison of velocity and output torque of the controller. The data presented in the bottom right plot show a distinct dependency of the required torque on the relative position of the harmonic drive. Therefore, the position is depicted in number of rotations and an oscillating pattern of the control output is observed. The described friction measurement is repeated several times and the results are shown in Figure 7.3 with different colours representing different experiments. In addition to the effects observed in Figure 7.2, hysteresis is observed when depicting the torque-velocity relation. Furthermore, large variations between the different experiments and hysteresis can be noticed, especially in the right hand side of Figure 7.3. The large friction torque observed in the experiments necessitates a respective compensation by the control strategy to ensure that the position tracking is fulfilled sufficiently and avoid distortion of the modelled impedance.

An exemplary friction compensation of an electric motor with harmonic drive is proposed in [50], superimposing the friction modelled by the dynamic LuGre model and a position depending term. This strategy compensates for all effects observed in the friction experiments except for non-symmetry. Nevertheless, the passivity of the LuGre model is only given without

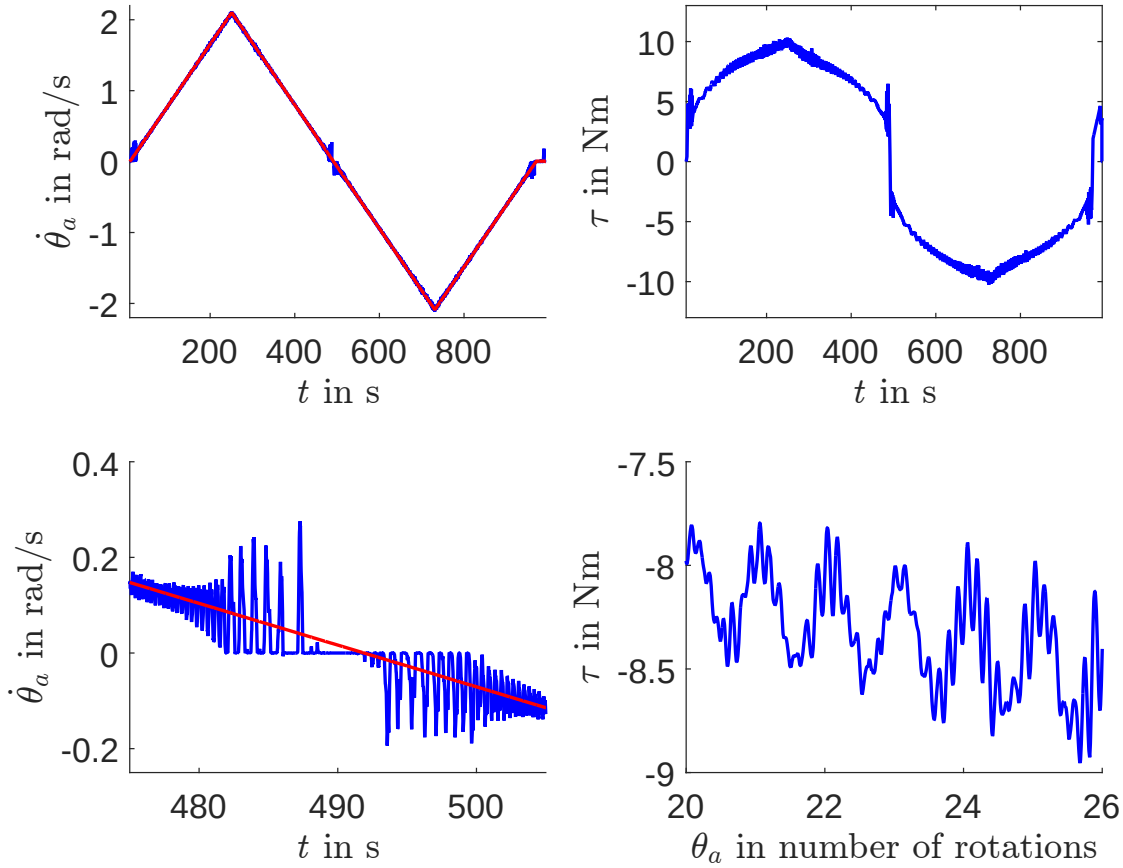

Figure 7.2: Exemplary measurement data for the evaluation of the friction at the actuator / left: actual (blue) and desired (red) actuator velocity / right: output torque of the controller (blue) / top: total time of the experiment / bottom: segment of the experiment to highlight stiction (bottom left) and dependency of the friction on the position (bottom right)

extensions in [51]. Several methods to analyse and compensate friction based on observers, adaptive control and neural networks are presented in [52], however are not utilised due the required proof of passivity and the given time frame of this work. Instead, the friction model proposed in [53] is implemented. The respective strategy compensates Coulomb friction by α_0, the required breakaway friction by $(\alpha_0+\alpha_1)$ and viscous friction is represented by α_2 according to [53]:

$$\tau_{fr,m} = \left[\alpha_0 + \alpha_1 \mathrm{e}^{-\beta_1|\dot{\theta}_a|} + \alpha_2\left(1-\mathrm{e}^{-\beta_2|\dot{\theta}_a|}\right)\right]\mathrm{sgn}(\dot{\theta}_a) \tag{7.3}$$

The requirements to maintain passivity of the actuation system are taken from Equation (6.13) and a controller with $\dot{\theta}u \leq 0$ leads to passive behaviour. The simple case of $u = -\tau_{fr}$ yields:

$$-\left[\alpha_0 + \alpha_1 \mathrm{e}^{-\beta_1|\dot{\theta}_a|} + \alpha_2\left(1-\mathrm{e}^{-\beta_2|\dot{\theta}_a|}\right)\right]\mathrm{sgn}(\dot{\theta}_a)\dot{\theta}_a \leq 0 \tag{7.4}$$

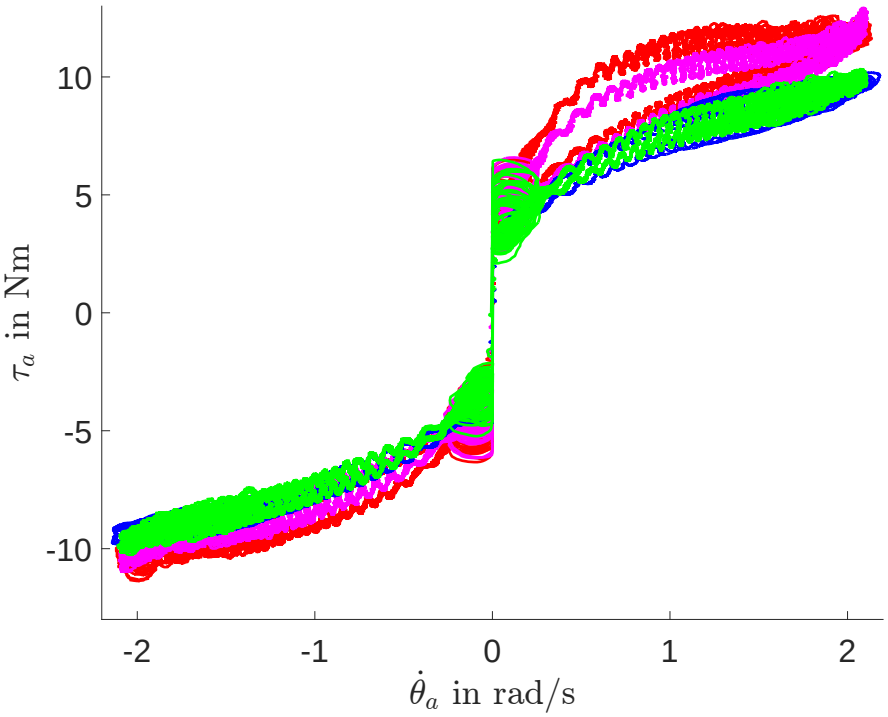

Figure 7.3: Measurement data for the evaluation of the friction at the actuator / colours indicate different experiments

As $\text{sgn}(\dot{\theta}_a)\dot{\theta}_a$ is always positive, $-\tau_{fr}\dot{\theta}_a \leq 0$ is fulfilled, when $\alpha_0 \geq 0$, $\alpha_1 \geq 0$, $\alpha_2 \geq 0$, $\beta_1 \geq 0$ and $\beta_2 \geq 0$, as e^{-x} is always in the interval [0,1]. Hence, the modelled friction torque $\tau_{fr,m}$ does not compensate non-symmetric behaviour, hysteresis and dependency on the position of the harmonic drive but maintains the passivity of the actuation system.

The evaluation of the friction model as well as identification of parameters is performed by the means of the complete DA system, including the pendulum. The pendulum is included in contrast to the experiments presented in Figures 7.2 and 7.3, as the resulting parameters of the friction model for this configuratione have provided improved results during the operation of the test bench. The test trajectory is a position controlled sine wave with amplitude of 10° and frequency of 1 Hz. A model-based comparison of the control signal and the required torque to generate the actual movement yields the friction. The selected controller is a PD-Controller with compensation of the gravitational torque of the pendulum, manually tuned to minimise the position error. The used model consists of the directly-actuated system of a driven pendulum according to:

$$(I_{DA} + I_p)\ddot{\theta}_a + \tau_g + \tau_{fr} = \tau_a \tag{7.5}$$

By assuming that the control signal equals τ_a, i.e., the current control of the EPOS is perfect and the torque constant of the motor does not vary, the friction torque τ_{fr} can be extracted from Equation (7.5) via inverse dynamics. The resulting torque over velocity of an exemplary

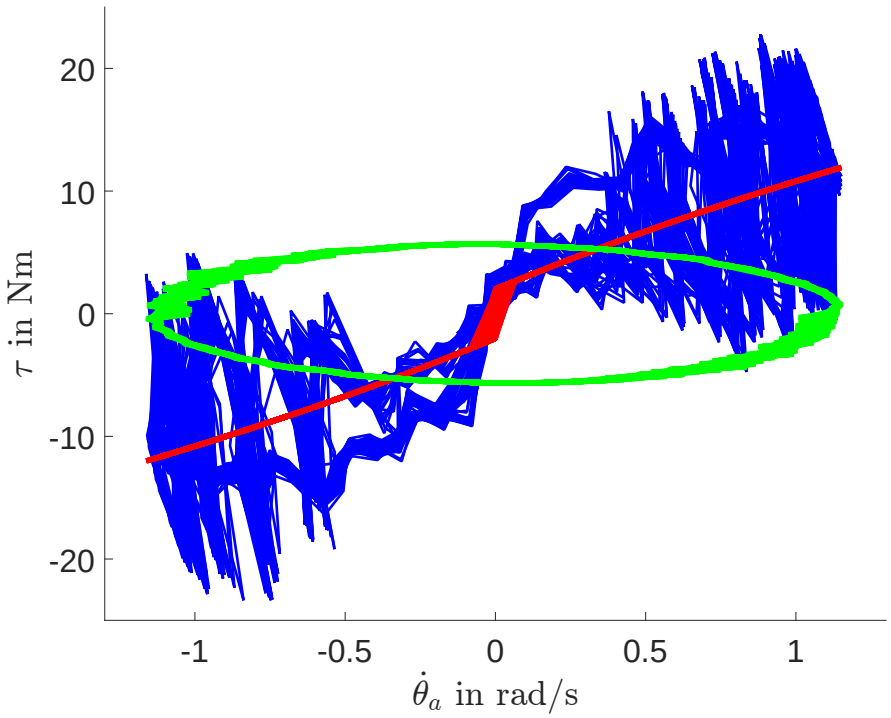

Figure 7.4: Torque over Velocity to Estimate the Friction / output signal of the controller (blue), mechanical torque of the actuated pendulum (green) and fitted friction model (red)

measurement is depicted in Figure 7.4. The output signal of the controller in blue represents τ_a and $(I_{DA}+I_p)\ddot{\theta}_a+m_p l_{p,cg} g \sin\theta_a$ as the mechanical torque is plotted in green. Hence, the friction torque τ_{fr} can be extracted from the recorded measurement data and Equation (7.5). Thus, τ_{fr} is used as data to fit the friction of the model $\tau_{fr,m}$ from Equation (7.3) via a least squared minimisation utilising the *fmincon*-function in *Matlab*. The mean of several measurements for each identified parameter is presented in Table 7.2. The compensation with the presented system maintains the passivity and is simple to implement and thus used in the further experiments, where it distinctly improves the results of the position tracking.

Table 7.2: Identified Parameters of the Friction Model

Parameter	α_0	α_1	α_2	β_1	β_2
Value	0.15	1.86	37.39	0.2847	0.2843

Evaluation of the Series Stiffness of the Elastic Actuator

A further parameter to determine is the series stiffness of the elastic actuation system, dominated by the torsional spring. Therefore, the procedure presented in [49] for the static stiffness is applied. Thereby, the motor is positioned at a fixed position by the actuator. The resulting

deflection of the spring is expressed by the position of motor and pendulum and depends in the static position on the gravitational torque. Thus, by knowing the constant position of both degrees of freedom as well as the moment of inertia of the pendulum identified above, the stiffness can be calculated from Equation (4.10) according to:

$$k_s = \frac{\tau_g}{\theta_a - \theta_p} \tag{7.6}$$

For the evaluation, the motor is positioned from 0° to 30°, then to −30° and back to 0° in increments of 1° and fixed for 4 s. The stiffness is determined from Equation (7.6) via a linear regression to compensate offset errors. In addition, only values above 10° are considered, as otherwise the resulting deflection is small and absolute errors of the position signals distort the result due to the structure of Equation (7.6). In addition, effects that are not considered, e.g., friction in the bearing dominate the gravitational torque, which is low for small angles. In Figure 7.5, results from an exemplary measurement are presented in blue. There are no measurement values for low deflections, as only values positions above 10° are considered. Noticeable is an offset in the deflection to positive values. This shift is observed in all measurements into the direction of the first movement, e.g., into positive deflection for the trajectory above. The offset occurs in negative direction, when the position is varied from 0° to −30° to

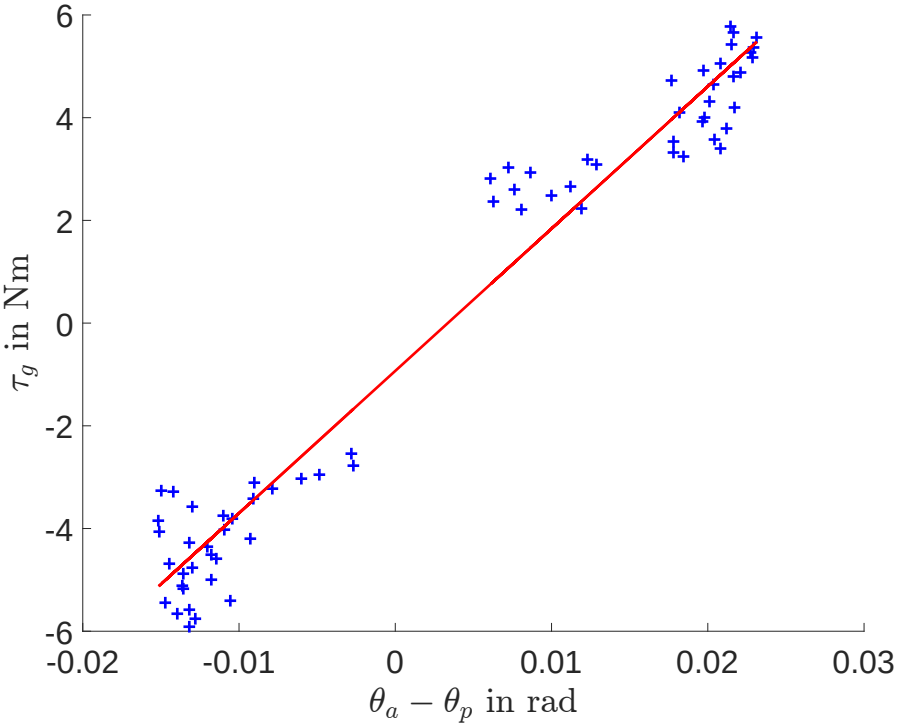

Figure 7.5: Exemplary measurement data (blue) and linear regression (red)

30° and back to 0°. The presented offset is compensated by the linear regression, depicted in red. The resulting series stiffness is determined to 269.95 N m rad^{-1} with a standard deviation of 8.53 N m rad^{-1}. The standard deviation amounts to approximately 3.2 % of the mean value, which is sufficient for the application of the impedance control, however could be reduced by a direct measurement of the spring torque via appropriate sensors.
The determined stiffness is slightly higher than the stiffness of the torsional spring designed to be 257.3 N m rad^{-1} in Section 5.4. This is not expected, as the experimental value includes the compliance of further components, e.g., the harmonic drive in series to the torsional spring, reducing the resulting stiffness. A more detailed mechanical model for the design of the torsional spring as well as the application of a finite element analysis could improve the estimation of the stiffness in the design phase. In addition, the individual stiffness of the implemented compression springs should be measured individually for the investigation of the increased resulting stiffness.

7.4 Experimental Evaluation of the Directly Actuated System

After the identification of parameters, experiments to evaluate the tracking of a desired trajectory by the DA system are performed. The results are utilised for a comparison between DA and CSEA, presented in the end of this chapter. The motion of the DA is controlled by a feed-forward compensation of the desired gravitational torque and actuator inertia and pendulum. The friction compensation presented above and a PD-controller assist in the reduction of the tracking error. The parameters of the PD-controller are tuned manually to achieve a low position error and summarised in Table A.1. The experiments are performed for the desired trajectories described in Section 7.1 and the control parameters are not adjusted individually. An exemplary measurement with a desired gait cycle with maximum amplitude of 30° and $t_{gc} = 3.33\,\mathrm{s}$ is presented in Figure 7.6. The system follows the desired position, the control error is between −0.1° and 0.3° with the highest value occurring at the maximum knee flexion, hence the desired trajectory, depicted as a dashed red line, is overlapped by the actual position and not visible in Figure 7.6. The output-torque of the controller, required to achieve the tracking, is considerably higher than the mechanical torque depicted in red, calculated from the inverse dynamics of the desired motion by means of Equation (4.1). The prediction of the control output is improved by including the friction in the inverse dynamics according to the model presented in Equation (7.5) with the friction torque of the model $\tau_{fr,m}$, however considerable differences are still observed in the amplitude of the respective torque. The high oscillations of the control signal during the stance phase are due to a high gain of the controller, to compensate the differences between modelled and actual friction. This is because the parameters of the control scheme are tuned to minimise the tracking error without considering a smooth control output.

A comparison of the required power shows similar differences, as the general shape of actual and modelled power coincides, however the amplitudes exhibit differences. In addition to the power calculated by control output multiplied with the velocity of the motor (blue), the power from the inverse dynamics (red) with and without friction (yellow), the electric power, calculated from the measured current, is presented in magenta. The current is evaluated between power supply and motor controller via a current probe and filtered with a zero-lag low-pass. An estimation of the power over time is received by multiplication with the supply voltage, assuming the laboratory supply provides constant 24 V. The electric power exhibits large differences during the first half of stance phase, where high acceleration in one direction occurs. A review of the experiments while recording current and voltage with different measurement equipment may provide different behaviour of the electric power and further insight in the behaviour of the system. In addition, in experiments tracking a gait trajectory with $t_{gc} = 4\,\mathrm{s}$, the output torque

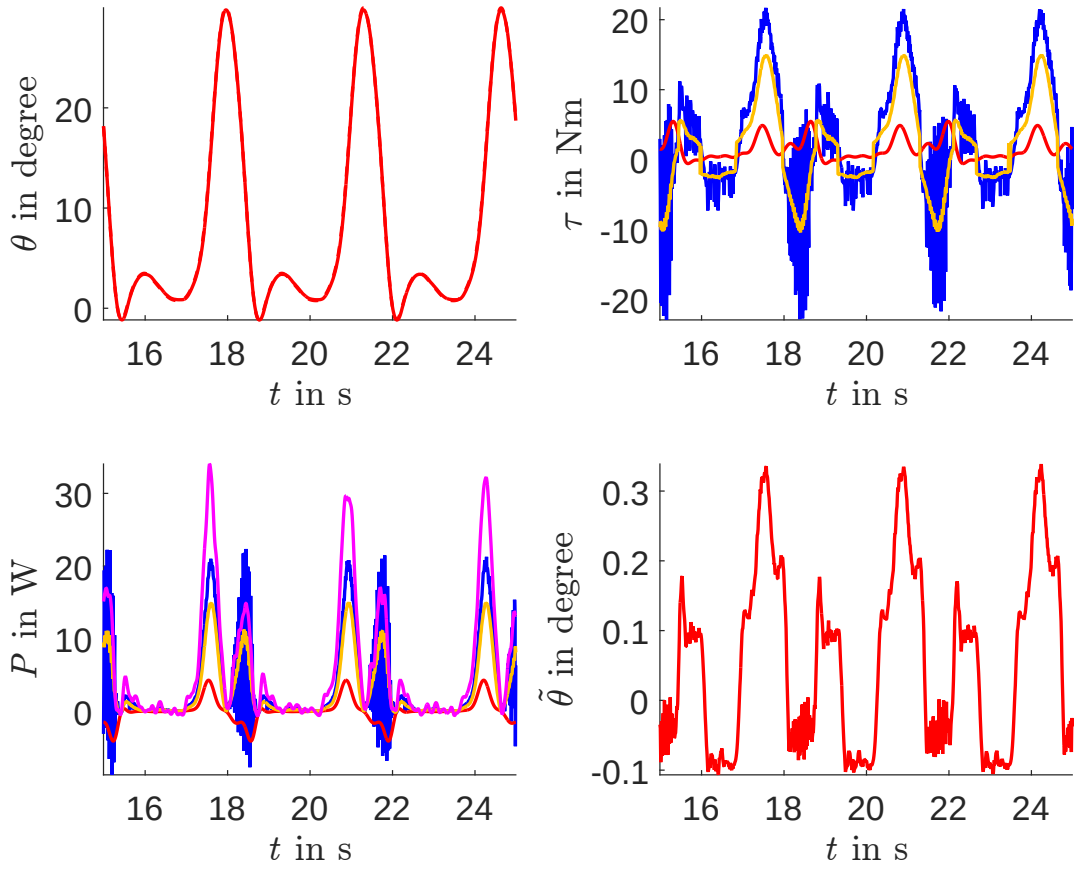

Figure 7.6: Exemplary Measurement of the Directly-Actuated System: Gait trajectory with maximum amplitude of 30° and $t_{gc} = 3.33\,\mathrm{s}$ / top left: desired (dashed-red) and actual (red) position actuator / top right: output signal (blue), mechanical torque (red) including friction (yellow) / bottom left: power calculated from output signal (blue), mechanical power (red) including friction (yellow), electrical power (magenta) / bottom right: position error actuator (red)

exceeds a limitation of 30 N m. This limit is implemented in the control algorithm to avoid overheating the motor. Furthermore, the motor driver *EPOS 24/5* includes a restriction to the allowed continuous current, but there is no feedback when this is applied, while the restriction via the control is observable. The increased control error is depicted in Table 7.3, which includes a summary and comparison of maximum control error and energy per period of the sine wave respectively gait cycle for DA and CSEA.

7.5 Experimental Evaluation of the Elastic Actuator

The experiments described in Section 7.1 are conducted for the implemented CSEA in the next step. At first, FSM and EMB are deactivated throughout the execution. The utilised control law includes compensation of friction according to Equation (7.3) in addition to the impedance control law from Equation (6.19). The desired trajectory is defined for the pendulum and the respective desired motion of the actuator is calculated from the relation given in Equation (6.24), with $\tau_{ext} = I_p \ddot{\theta}_{p,d} + m_p l_{p,cg} g \sin(\theta_{p,d})$. The utilised control parameters are summarised in Table A.2. As for the directly-actuated system, the control parameters are not tuned for individual motions.

Tracking of a Desired Position

In Figure 7.7, a desired gait cycle with maximum amplitude of 30° and $t_{gc} = 3.33$ s is presented as an exemplary result for the tracking of a desired motion. A comparison between Figure 7.6 and Figure 7.7 indicates a similar behaviour regarding the control error of the actuator as well as the required electrical power. The control output torque is smoother than for the DA. However this depends on the tuning of the controller as well. Electrical power, power estimated from control output and power from inverse dynamics including friction approximately coincide with the results of the DA, except for a large deviation during the first half of the swing phase. Noticeable is the high control error of the position of the pendulum compared with the error of the actuator position. This indicates the existence of an unknown external torque as discussed in Section 6.2, e.g., due to parameter uncertainties and neglect of friction at the external side. A thorough summary of the maximum position errors as well as energy per gait cycle respectively period of the sine wave is presented in Table 7.3.

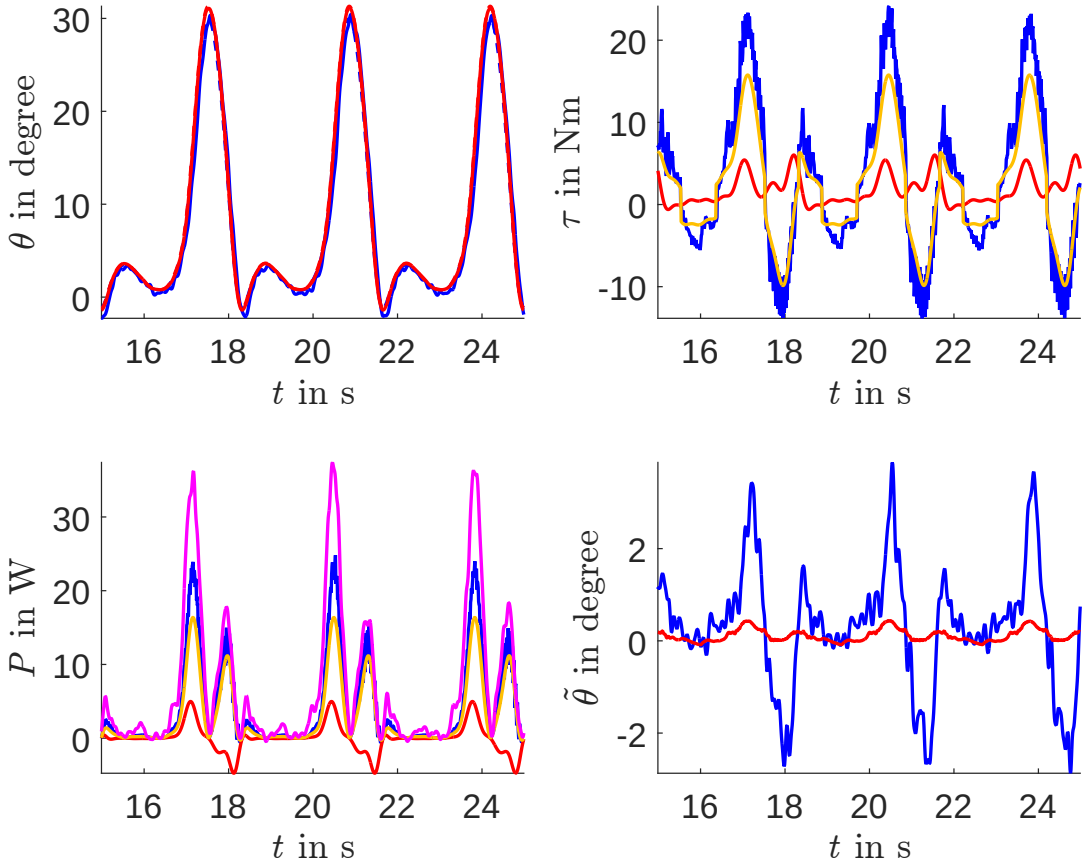

Figure 7.7: Exemplary Measurement of the CSEA: Gait trajectory with maximum amplitude of 30° and $t_{gc} = 3.33\,\mathrm{s}$ / top left: desired (dashed-red) and actual (red) position actuator, desired (dashed-blue) and actual (blue) position pendulum / top right: output signal (blue), mechanical torque (red) including friction (yellow) / bottom left: power calculated from output signal (blue), mechanical power (red) including friction (yellow), electric power (magenta) / bottom right: position error pendulum (blue), position error actuator (red)

Evaluation of the Resulting Impedance

The resulting impedance of the system, as modelled in the impedance control law, is examined by manual deflection of the pendulum. Therefore, the resulting response is investigated as proposed in [46]. The left curve of Figure 7.8 presents the characteristic of the impedance control with a constant desired position $\theta_{p,d} = 0°$ and therefore a static case in the absence of external disturbances. Different control parameters for the desired stiffness in the impedance control are evaluated. In the depicted experiment, $k_d = 100,\ 200,\ 500$ and 1000 are applied from left to right. Furthermore, the desired inertia $I_d = 0.5 I_a$ as well as the desired motor damping $d_d = 55$ are utilised. The depicted deviations are applied manually until the control output amounts approximately 20 N m. As seen from the results, the system does not try to

force the tracking of the desired position of $\theta_{p,d} = 0°$ as a pure position controller would do. Instead, a compliant behaviour of the system according to Figure 6.1 is observed and low values of k_d yield higher deflection of the pendulum by adjusting the motor position appropriately. Hence, the impedance control is implemented correctly. The actual total stiffness of the elastic system with impedance control is investigated in the following. The external torque consists of the gravitational torque as well as the torque in the spring for a static deflection. Thus the actual total stiffness $k_{t,a}$, consisting of the physical stiffness and the emulated behaviour by the impedance control yields [46]:

$$k_{t,a} = \frac{m_p l_{p,cg} g \sin(\theta_p) + k_s(\theta_p - \theta_a)}{\theta_p - \theta_{p,d}} \tag{7.7}$$

This equation is utilised to calculate the external torque of the manual deflection depicted in the left hand side of Figure 7.8. The resulting total stiffness $k_{t,a}$ from the experiments is depicted in blue in the right hand side of Figure 7.8. For comparison, the total stiffness, as modelled by the impedance control, is presented in red, shows distinct differences between experiment and model. The modelled total stiffness is thereby calculated with the applied desired stiffness $k_d = 100,\ 200,\ 500$ and 1000 and the identified stiffness of the torsional spring $269.95\,\mathrm{N\,m\,rad^{-1}}$ according to Equation (6.1). Hence, a further investigation regarding the influence of the friction and uncertainties of the model should be performed for an accurate selection of the control parameters. The depicted peaks in the stiffness occur due to dynamic movement or no deflection of the spring, for which Equation (7.7) is not valid. Hence, the implementation of the impedance control is successful, although the desired total stiffness is not sufficiently reproduced.

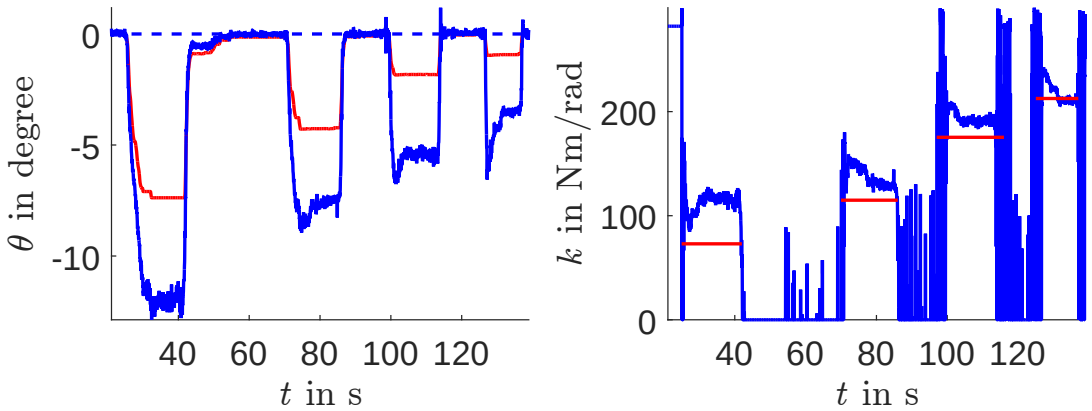

Figure 7.8: Manual deflection of the pendulum with $\theta_{p,d}$ / left: position of the pendulum (blue) and desired position of the pendulum (dashed-blue), position of the actuator (red) / right: actual total stiffness (blue) and modelled total stiffness (red)

Comparison of the Required Power to Lock the Position

The analysis performed in Section 4.3 leads to a concept with locked actuator position during the stance phase and optimised gear ratio for the swing phase. To show the difference in required power between the selected EC-motor and the EMB, the pendulum is manually deflected, while either the impedance control is set to maintain a desired position of 0° or the EMB is activated. A manual deviation of approximately −8.5° and the resulting required power, calculated from the measured current at the power supply, are presented in Figure 7.9. The comparison of the required power, depicted in magenta, clearly shows a reduced consumption when the EMB is active, which is indicated in grey though the deflection is not exactly the same. Thus, for the presented experiment, the application of the active locking, which requires approximately 6 W is more efficient. The depicted required power is slightly higher than that, as the power consumption of the motor controller is included in the measured current. However, the advantages of the EMB decrease for lower deflections as the required locking torque decreases, reducing the motor power while the power of the EMB is independent of the load. In addition, the necessary torque to lock the actuator depends on the selected gear unit as well. The gear ratio of the harmonic drive utilised in the laboratory specimen is $i_G = 160$, which is higher than the optimal value for recuperation as obtained from the optimisations in Section 4.3. Thus, for a lower gear ratio, the required torque of the motor increases to achieve the same locking torque, leading to higher electrical power. Hence, the difference in efficiency between locking by motor and locking mechanism rises for the same deflection, favouring the utilised EMB.

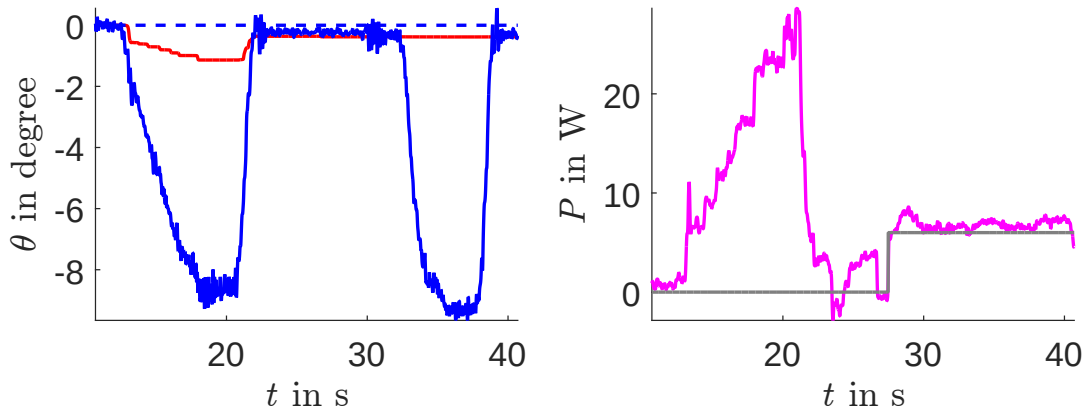

Figure 7.9: Manual deflection of the pendulum with impedance control to 0° and activated EMB / left: position of the pendulum (blue) and desired position of the pendulum (dashed-blue), position of the actuator (red) / right: electrical power (magenta), 6 W power consumption of the EMB (grey)

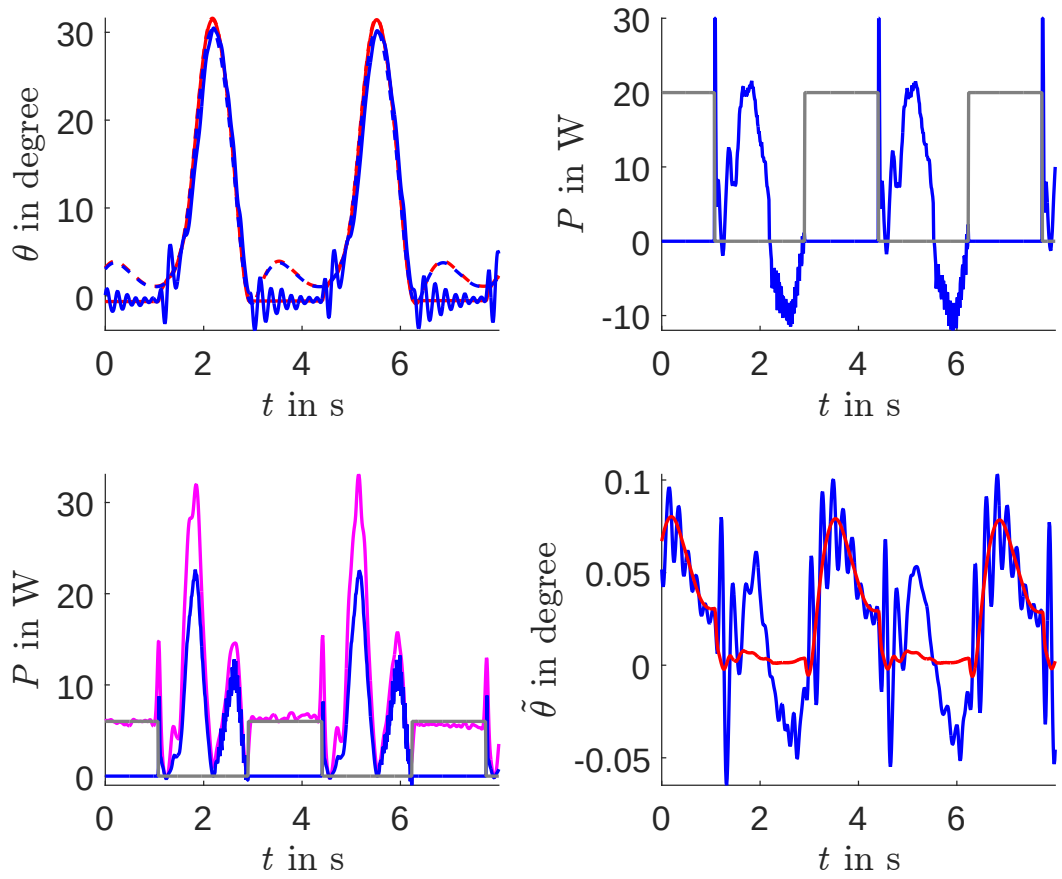

Figure 7.10: Exemplary Measurement of the CSEA: Gait trajectory with maximum amplitude of 30° and $t_{gc} = 3.33\,\mathrm{s}$ / top left: desired (dashed-red) and actual (red) position actuator, desired (dashed-blue) and actual (blue) position pendulum / top right: output signal (blue), status of the EMB (grey) / bottom left: power calculated from output signal (blue), status of the EMB (grey), electrical power (magenta) / bottom right: position error pendulum (blue), position error actuator (red)

Tracking of a Desired Gait Cycle with Activated Finite-State-Machine

The presented experiments above do not utilise the FSM to switch states of the controller during each gait cycle. The effect of changing control parameters and activation of the EMB is examined via position tracking of a gait trajectory with amplitude of 30° and $t_{gc} = 3.33\,\mathrm{s}$ presented in Figure 7.10. The FSM discussed in Section 6.3 is implemented at the test bench, however the conditions for the transition of states are changed. Instead of using the ground reaction forces and desired position, the chronological progression of each gait cycle is utilised. State 1 lasts from 0 % to 50 % of each cycle, representing the single support phase of the gait cycle. The second state is active between 50 % to 75 % of the gait cycle followed by the third state. This change is implemented as a simplified method, to avoid fine-tuning each condition for the transition to the next state. The utilised control parameters are summarised in Table A.3.

The activation of the EMB or the change in control parameters does not lead to unstable behaviour, however oscillations are introduced at the pendulum position, while the motor position remains smooth. A slight step in the output signal at approximately 3.46 s occurs due to the transition of state 2 and 3, but does not considerably influence the motion or yield a peak in the torque of the actuator for the selected control parameters. It has to be mentioned, that the depicted control error during the activated FSM is not correct due to the modelling of the desired trajectories as discussed in Section 4.3. Thus, activation of the FSM and variation of control parameters do not influence the stability of the system. A fine tuning of the deactivation of the EMB could remove the visible peak in the torque at approximately 2.3 s. In addition, the oscillations of the pendulum would not occur with an external torque according to the gait data, as the torsional spring is strained by the respective external torque. However this also implies, that if oscillations are introduced externally, the system can not compensate them properly when the EMB is activated. Therefore, an additional safety mechanism to unlock the brake and activate the impedance control in such a case may be required. In addition, the detection of faults or unstable locomotion should be implemented to achieve a safe state of the system to protect the user for the real application.

7.6 Comparison of Experimental Results

In Section 7.4 and Section 7.5, characteristic behaviour of the DA and CSEA during the tracking of a desired gait trajectory are presented. The results from further experiments, as defined in Section 7.1 is summarised in Table 7.3. All experiments are carried out as described in Section 7.4 and Section 7.5, thus the FSM and EMB are not utilised, as the test bench can not emulate the ground reaction forces in a controlled manner and therefore the comparison of the gait trajectories is not useful. Similarly the FSM and EMB do not yield any advantages for a sine wave. Instead, the presented analysis allows a comparison of the DA and CSEA in hindsight of the increased complexity due to the additional degree of freedom and components of the elastic actuation concept. The values presented in Table 7.3 are extracted from experiments lasting for 12 periods of the sine wave or 12 gait cycles, whereby the first and last cycle are not included in the evaluation. In total, three sets for every test trajectory are conducted without changing control parameters or set-up of the system.
Before the beginning of each experiment, the system is tested to achieve operating temperature. Table 7.3 presents the maximum control error per oscillation or gait cycle of the actuator $\tilde{\theta}_a$ and in case of the CSEA for the pendulum $\tilde{\theta}_p$. The depicted electrical energy E_{el} is calculated from the measured current as $E_{el} = \int P_{el} \mathrm{dt}$ and is given per oscillation or gait cycle. The standard deviation for each value is given in brackets. The position tracking of the DA yields low errors

Table 7.3: Summary of the Experimental Comparison DA and SEA with mean value and standard deviation given in brackets

	Directly-Actuated System		Series Elastic Actuator		
Trajectory	$\tilde{\theta}_a$ [degree]	E_{el} [J]	$\tilde{\theta}_a$ [degree]	$\tilde{\theta}_p$ [degree]	E_{el} [J]
Sine 0.1 Hz	0.22 (0.006)	23.78 (5.06)	0.24 (0.007)	1.3 (0.08)	21.07 (6.51)
Sine 0.2 Hz	0.21 (0.004)	18.91 (6.56)	0.22 (0.003)	1.61 (0.61)	18.64 (7.31)
Sine 0.3 Hz	0.2 (0.002)	15.6 (6.74)	0.22 (0.003)	1.67 (0.78)	15.1 (7.48)
Sine 0.4 Hz	0.17 (0.003)	14.21 (5.43)	0.19 (0.003)	1.6 (0.09)	11.37 (3.47)
Sine 0.5 Hz	0.14 (0.004)	11.11 (1.66)	0.15 (0.003)	1.88 (0.18)	11.14 (0.55)
Sine 0.6 Hz	0.15 (0.002)	11.22 (1.96)	0.15 (0.004)	2.16 (0.57)	11.18 (0.74)
Sine 0.7 Hz	0.17 (0.003)	11.23 (1.33)	0.18 (0.005)	2.53 (0.37)	10.51 (1.18)
Sine 0.8 Hz	0.2 (0.006)	11.33 (1.88)	0.22 (0.006)	3.04 (0.37)	12.05 (1.21)
Sine 0.9 Hz	0.24 (0.005)	12.09 (0.97)	0.26 (0.005)	3.52 (0.27)	11.54 (1.28)
Sine 1 Hz	0.28 (0.005)	11.86 (2.01)	0.33 (0.004)	4.29 (0.36)	11.55 (1.11)
Gait 10 s	0.42 (0.02)	23.29 (5.34)	0.45 (0.015)	1.74 (0.29)	25.02 (4.63)
Gait 5 s	0.34 (0.02)	18.53 (4.37)	0.37 (0.018)	2.14 (0.16)	19.92 (0.55)
Gait 3.33 s	0.32 (0.06)	19.22 (4.13)	0.38 (0.064)	3.26 (0.29)	21.73 (0.32)
Gait 2.5 s	0.51 (0.08)	21.02 (2.89)	0.69 (0.12)	4.81 (0.37)	22.8 (1.34)
Gait 2 s	1.96 (0.47)	23.15 (3.17)	2.6 (0.84)	24.38 (9.18)	31.51 (2.20)

between desired and actual position, which are rather constant during the experiments as seen from the low standard deviation. An increase in the position error occurs at very low velocities and for the gait cycle with $t_{gc} = 2\,\mathrm{s}$, as the restriction of the torque to 30 N m limits the control output for this trajectory. The mechanical energy of a sine wave of a pendulum is zero in average for a system without friction, thus the presented values occur due to friction and other losses. In addition, the standard deviation of the energy is considerably high compared to the mean value, thus the values do not present a reliable prediction of the actual required power.
The control error of the CSEA at the motor side is comparable to the DA while the error at the pendulum is considerably higher and always above 1.3°, as seen from a comparison of the values in Table 7.3. In addition, the control error at the pendulum $\tilde{\theta}_p$ increases with the velocity of the test trajectory. This indicates that the external torque, in this case described by the inertial and gravitational torque of the pendulum, is not modelled adequately and a velocity based parameter, e.g., damping is required to improve the tracking. However the damping at the bearing of the pendulum is small, as identified in Section 7.3, and should not yield such large differences in the control error. In addition, a control error of 24.38° at the gait trajectory with $t_{gc} = 2\,\mathrm{s}$ while the error at the actuator side amounts 2.6° would imply considerable errors of the model and parameters. An investigation of the position acquired by the selected IMU at high velocities was not conducted at the actual state of the project, although it could lead to an explanation of the high position error at the external side for experiments with high velocity test trajectories.

The required energy is similar to the DA, however the minimum occurs at 0.7 Hz.In summary, the performed experiments show a similar position error at the actuator for both systems while requiring approximately the same energy per gait cycle respective sine oscillation. The control error at the pendulum has to be investigated for further improvements. Thus, the CSEA yields similar tracking capabilities as the DA for a similar amount of effort regarding the utilised control laws and tuning of respective parameters. Hence, the challenge in the design of elastic actuators due to the additional degree of freedom as well as the compliant behaviour of the elastic actuator is controlled. However, the control error at the pendulum does not satisfy the required tracking capabilities to ensure the generation of a stable and safe gait trajectory by the active orthosis and has to be investigated further.

7.7 Discussion of the Experimental Results

Chapter 7 presents the experimental evaluation of the CSEA, which serves as a proof of concept, as an assessment of the mechanical design and control strategy. Furthermore, the review of the fulfilment of requirements and functions according to the V-model is performed as proposed by [36]. Criteria and experiments to perform are defined in the beginning followed by a presentation of the test bench. For a model-based evaluation, a parameter identification is conducted to gain values for the moment of inertia at the actuator side, pendulum side and the stiffness of the elastic actuator. In addition, the friction at the actuator side is analysed and a compensation strategy is proposed. After the identification of parameters, the test trajectories are tracked by the directly-actuated system to provide a comparison with the elastic actuator. The capability of the system to follow a gait trajectory or sine wave with different frequencies with satisfactory control error was shown. Substantial differences between predicted and actual required power show a deficit of accuracy in the utilised model, even when a friction model is considered. The measurements also present large differences between electrical power, evaluated via a current probe and assuming constant supply voltage, and the actuator power estimated from the control output. The CSEA shows a similar behaviour regarding the required power and control error at the actuator side, however large deviations between desired and actual position of the pendulum are observed. The successful implementation of the impedance control is evaluated experimentally. A comparison of required power to lock the system with the actuator or the EMB is conducted, and favours the brake for a minimisation of power consumption, confirming the developed concept. The CSEA with impedance control and FSM is operated successfully at the test bench, showing that the stability of the system is preserved. However, during the stance phase, the locking via the EMB prevents active influence of the position of the pendulum.
A review of the requirements defined in Section 5.1 shows that a human-like gait cycle can be

tracked at the test bench, however the minimal time of $t_{gc} = 1\,\mathrm{s}$ can not be achieved due to the applied restriction of the actuator torque. The safety is not explicitly tested, thus gait cycles with potential events, e.g., stumbling should be investigated. Further, special attention should be given to the lost controllability during the first half of the gait cycle due to the locked actuator.

The evaluation of the friction provided high influence on the performance and the efficiency of the system, thus the minimal required actuator power of $P_{a,r,min} = 65.7\,\mathrm{W}$ and minimal torque of $\tau_{a,r,min} = 24.3\,\mathrm{N\,m}$ are not sufficient to generate the desired gait trajectories. The actual power requirements have to be evaluated again including the friction and the electrical efficiency of the system. Due to the non-linear and varying characteristic of the friction, the respective compensation is not sufficient. In the presented experiments, this is compensated by increasing the gain of the controller to achieve good tracking. In return, this means that the friction of the system poses a lower limit for the desired stiffness of the impedance control. The additional restriction regarding the adjustability of the system is not desired. To summarise, the experimental evaluation presents an operational CSEA at a test bench. Further experiments emulating the complete dynamics of a human-like gait cycle are required for the final proof of concept. The reduction of the friction is identified as a key objective to reduce effort for a high quality compensation, increase the efficiency of the actuator and reduce the tracking error.

8 Economic Study and Social Impact of the Project

A discussion of the contribution of this thesis to the national project presented in Section 2.1 as well as the social impact is given. Furthermore, an economic study of the thesis is given in this chapter, estimating the occurred project cost, which consists in expenses for building the laboratory specimen and personnel costs.

8.1 Social Impact

The social impact of the project is high, as the developed and investigated CSEA aims at the improvement of the actuation systems utilised in exoskeletons, orthoses as well as prostheses actuating the knee joint. Furthermore, by applying the procedure used in this project, the examination of the potential of elastic actuation for all joints is conceivable. Hence, rehabilitation devices profit from the performed investigations, which focus on mimicking the physiological behaviour and human-robot interaction. The additional increase in efficiency allows for lighter products or extended time of operation. The laboratory specimen designed and tested throughout this work can serve as a basis for further developments to obtain an actuation system for the active orthosis for SCI subjects developed in the national project. Thus, this thesis contributes to the development of rehabilitation devices with the aim to improve the quality of live of disabled people. In particular, the project supports the ongoing development of the active orthosis to provide SCI subjects with a cost-efficient and reliable device to improve their mobility.

8.2 Economic Study

An estimation of the cost of the project is outlined in the following. The overview is divided into personnel costs, which include one engineer for the full time of the project as well as one senior engineer giving support. The number of hours of the engineer correspond to the number of hours expected from a master's thesis at Technical University Darmstadt. The support and supervision of the thesis equal the working hours of a senior engineer and is estimated to 100 h. A listing of the expenses to implement the laboratory specimen includes manufactured and bought components. Thereby, the price of each component is given by the manufacturer and

does not include taxes or shipment. A summary of the items listed in Table 8.1 yields a total cost of the project of 35739,40 €.

The majority of the total cost is due to the working hours. A review of the design of the prototypic actuation system shows that the harmonic drive gear box causes approximately 39 % of the total design cost. Hence, the utilisation of an alternative gear unit should be investigated to reduce the expenses for the real application. The second highest matter of expense is the manufacturing of the prototype in the workshop. However, an increase of the effort for the manufacturing may occur due to the application of lightweight construction techniques to improve the design, resulting in a further increase of the manufacturing cost.

A further extension of the project to optimise the mechanical design, implement the actuation system at the active orthosis and perform experiments with a healthy wearer is estimated as further 400 h of effort in engineering and additional manufacturing of two elastic actuators. This yields further cost of approximately 20000 € for the advancement of the actuation system.

Table 8.1: Estimated Costs of the Project

Item	Cost	Quantity	total Cost
Engineer	30 €/h	900 h	27000 €
Senior Engineer	50 €/h	100 h	5000 €
Personnel Cost			32000 €
EC-Motor EC45 flat	116,73 €	1	116,73 €
Motor Controller EPOS 24/5	475,18 €	1	475,18 €
Encoder MR, Type L	92,91 €	1	92,91 €
EMB Combinorm 02.02.120	181,6 €	1	181,6 €
Harmonic Drive SHD-20-160-2SH	1462€	1	1462 €
Compression Spring D-263Q-03	2,74 €	6	16,44 €
Hardware/Software Computer MyRIO	300 €	1	300 €
Small Parts	-	-	200 €
Manufacturing Cost Workshop	-	-	1000 €
Total Cost Design			3739,40 €
Total Cost Project			35739,40 €

9 Conclusion and Discussion

The final chapter of this thesis presents a summary of the conducted design of an elastic actuation system for a gait-assistive orthosis for incomplete spinal injured subjects. A conclusion of the previous chapters is given for the following discussion and outlook for future works.

9.1 Conclusion

In the course of this thesis, an elastic actuation system for a gait-assistive orthosis for incomplete spinal injured subjects is designed. After an analysis of the state of the art and the presentation of the theoretical background, the aim of the thesis is defined. The focus for the design of the actuation system is to enable the subject to perform a human-like gait cycle, which is robust against disturbances and uncertainties. Additional goals are a comfortable and energy efficient system. To achieve the aim, the potential to reduce energy consumption and peak power by the implementation of elastic actuators is investigated via optimisations of defined objective functions with increasing level of detail of the utilised models. The objective is to minimise peak power, energy per gait cycle and energy per gait cycle including recuperation to find the optimal configuration and parameters of the elastic actuation system. The analysis of the potential of elastic actuation yields the following results:

- The optimal series stiffness from a minimisation of energy per gait cycle calculated from positive or absolute power is similar to the physiological stiffness of the knee during the stance phase, when actuator inertia is not considered. A parallel spring at the actuator does not yield considerable improvements.
- The minimisation including the actuator inertia yields an optimal gear ratio and an analysis of the natural dynamics shows that the first resonance frequency of the system equals the first frequency of the Fourier Series of the gait trajectory.
- The inclusion of component efficiency change the minimisation results considerably and is therefore considered as a crucial step of this work.
- The locking of the actuator by means of an additional mechanism allows the selection of the compliance of a series spring similar to the physiological stiffness of the knee to model a human-like gait cycle during the stance phase. An optimal gear ratio is determined to maximise recuperation by an electric motor during the swing phase.

Two conceptual designs are presented based on the functional modelling of the series elastic actuator with locking during the stance phase. From the proposed concepts, a clutchable series elastic actuator (CSEA) based on a torsional spring and an active brake is selected, designed and implemented at a test bench. For the operation of the CSEA, a control scheme based on impedance control is selected to fulfil specified criteria. The control law for the impedance control is derived to ensure passivity of the system. The behaviour of the system subjected to external distortions is analysed, yielding a bounded response and a condition for critical damping. An extension of the impedance control law by a finite state machine is implemented to operate the locking mechanism during the stance and vary control parameters throughout the swing phase of the gait cycle.

The designed control strategy is implemented at the test bench and several experiments are conducted to proof the concept, compare DA and CSEA, and evaluate the control strategy. An identification of parameters of the system is performed. The friction of the motor side is analysed and a respective compensation is implemented.

The evaluation of the tracking of test trajectories yields similar, low position errors at the actuator side for the DA and CSEA, however the external position of the CSEA is not followed with sufficient accuracy. In addition, both systems require high energy per period or gait cycle due to the substantial amount of friction, thus reducing the efficiency. The implemented impedance control and modelling of the desired stiffness as well as a comparison of the required power to lock the system between motor and brake are shown experimentally by manual deflection of the pendulum. Finally, successful tracking of a gait trajectory shows the operability and stability of the CSEA with impedance control and finite state machine, hence the main goals for this thesis are achieved and experimentally evaluated as far as possible, while the implemented laboratory specimen has to be improved to address the presented issues before it can be utilised at the active orthosis.

9.2 Discussion and Outlook

The gait data from [6] utilised as a basis to determine the potential of elastic actuation and to analyse the control represent trials with healthy subjects. Even though the aim of this project is the reproduction of healthy gait, the characteristic motion of SCI subjects may vary distinctly. Thus, the procedure used for the determination of optimal configuration and parameters of the elastic actuator should be repeated utilising respective gait data and, if necessary, adjust the concept of the actuation system. Furthermore, as the test bench does not reproduce human-like external torque, the energy efficiency and robustness of the actuation system is only shown by simulation. Thus, experiments with applied external load according to appropriate gait data should be performed. In addition, the actuation system should be implemented at the active orthosis to allow experiments under real conditions and evaluate the whole system.

However, before this, the actuation system should be improved in several aspects to provide efficient and safe operation as well as a device that is accepted by the user. During the design phase, focus is on the reproduction of a human-like gait cycle, which is reflected in the defined requirements. However, these mainly represent requirements from the side of the engineer and do not consider aspects that might be important to SCI subjects. Hence, respective human factors should be investigated and included into the design criteria for the actuation system. Thus, questionnaires should be developed and surveys performed to focus on the needs of subjects. For example, the compliant behaviour of the CSEA may feel unsafe to the subject, who can not directly control the deflection during the stance phase. An interdisciplinary approach to include engineering, medical and psychological knowledge as well as a strong focus on each individual subject may be beneficial to ensure success of the project.

Furthermore, the safety of the user of the active orthosis has to be ensured. Therefore, a failure mode effects analysis should be performed to develop a respective safety concept. For example, the device has to ensure the safety as well as stability when the user stumbles or walks on slippery ground.

Lightweight construction techniques and structural optimisation should be utilised to minimise the weight of the actuation system to design a reduce the impact of the orthosis on the user. Furthermore, an aesthetic design of the active orthosis with CSEA may improve the acceptability of the device by the subject. Global optimisation methods may be utilised to aid in the selection of concept and components leading to an actuation system with higher efficiency. Adaptive or intelligent control strategies should be examined to automatically identify parameters, tune control parameters or compensate the friction while maintaining the passivity. Furthermore, a review and testing of the overall system, including the orthosis, power supply as well as high-level control should be performed to ensure high performance of the overall system.

Bibliography

[1] N. A. Erosa, J. W. Berry, T. R. Elliott, A. T. Underhill, and P. R. Fine, "Predicting quality of life 5 years after medical discharge for traumatic spinal cord injury," *British Journal of Health Psychology*, vol. 19, no. 4, pp. 688–700, 2014.

[2] P. L. Ditunno, M. Patrick, M. Stineman, and J. F. Ditunno, "Who wants to walk? Preferences for recovery after SCI: a longitudinal and cross-sectional study," *Spinal Cord*, vol. 46, pp. 500–506, Jan. 2008.

[3] World Health Organization, "WHO global disability action plan 2014-2021." as of the 17.04.2016.

[4] J. M. Font-Llagunes, R. Pàmies-Vilà , J. Alonso, and U. Lugrís, "Simulation and design of an active orthosis for an incomplete spinal cord injured subject," *Procedia {IUTAM}*, vol. 2, pp. 68 – 81, 2011. {IUTAM} Symposium on Human Body Dynamics.

[5] D. A. Winter, *Biomechanics and motor control of human movement [Elektronische Ressource] David A. Winter*. Hoboken, N.J.: Wiley, N.J. : Wiley, 2009.

[6] G. Bovi, M. Rabuffetti, P. Mazzoleni, and M. Ferrarin, "A multiple-task gait analysis approach: kinematic, kinetic and emg reference data for healthy young and adult subjects," *Gait Posture*, vol. 33, no. 1, pp. 6–13, 2011.

[7] P. Beckerle, *Human-machine-centered design and actuation of lower limb prosthetic systems*. Forschungsberichte Mechatronische Systeme im Maschinenbau, Aachen: Shaker Verlag, 2014.

[8] K. Shamaei and A. Dollar, "On the mechanics of the knee during the stance phase of the gait," in *Rehabilitation Robotics (ICORR), 2011 IEEE International Conference on*, pp. 1–7, June 2011.

[9] H. Herr, "Exoskeletons and orthoses: classification, design challenges and future directions," *Journal of NeuroEngineering and Rehabilitation*, vol. 6, no. 1, p. 21, 2009.

[10] A. Zoss, H. Kazerooni, and A. Chu, "Biomechanical design of the berkeley lower extremity exoskeleton (bleex)," *Mechatronics, IEEE/ASME Transactions on*, vol. 11, pp. 128–138, April 2006.

[11] A. M. Dollar and H. Herr, "Active orthoses for the lower-limbs: Challenges and state of the art," in *Rehabilitation Robotics, 2007. ICORR 2007. IEEE 10th International Conference on*, pp. 968–977, 2007.

[12] Francesco Giovacchini, Federica Vannetti, Matteo Fantozzi, Marco Cempini, Mario Cortese, Andrea Parri, Tingfang Yan, Dirk Lefeber, and Nicola Vitiello, "A light-weight active orthosis for hip movement assistance," *Robotics and Autonomous Systems*, vol. 73, pp. 123–134, 2015.

[13] F. Sergi, D. Accoto, G. Carpino, N. Tagliamonte, and E. Guglielmelli, "Design and characterization of a compact rotary series elastic actuator for knee assistance during overground walking," in *Biomedical Robotics and Biomechatronics (BioRob), 2012 4th IEEE RAS EMBS International Conference on*, pp. 1931–1936, June 2012.

[14] K. Shamaei, M. Cenciarini, A. Adams, K. Gregorczyk, J. Schiffman, and A. Dollar, "Design and evaluation of a quasi-passive knee exoskeleton for investigation of motor adaptation in lower extremity joints," *Biomedical Engineering, IEEE Transactions on*, vol. 61, pp. 1809–1821, June 2014.

[15] J. Blaya and H. Herr, "Adaptive control of a variable-impedance ankle-foot orthosis to assist drop-foot gait," *Neural Systems and Rehabilitation Engineering, IEEE Transactions on*, vol. 12, pp. 24–31, March 2004.

[16] K. Shibata, Y. Inoue, and H. Satoh, "Intelligent ankle-foot orthosis by energy regeneration for controllable damping during gait in real time," in *Human-Computer Interaction â€" INTERACT 2015* (J. Abascal, S. Barbosa, M. Fetter, T. Gross, P. Palanque, and M. Winckler, eds.), vol. 9299 of *Lecture Notes in Computer Science*, pp. 563–568, Springer International Publishing, 2015.

[17] J. Beil, G. Perner, and T. Asfour, "Design and control of the lower limb exoskeleton kit-exo-1," in *Rehabilitation Robotics (ICORR), 2015 IEEE International Conference on*, pp. 119–124, 2015.

[18] H. Tran, H. Cheng, H. Rui, X. Lin, M. Duong, and Q. Chen, "Evaluation of a fuzzy-based impedance control strategy on a powered lower exoskeleton," *International Journal of Social Robotics*, pp. 1–21, 2015.

[19] Ü. Önen, F. Botsali, M. Kalyoncu, M. Tinkir, N. Yilmaz, and Y. Sahin, "Design and actuator selection of a lower extremity exoskeleton," *Mechatronics, IEEE/ASME Transactions on*, vol. 19, pp. 623–632, April 2014.

[20] M. Tucker, J. Olivier, A. Pagel, H. Bleuler, M. Bouri, O. Lambercy, J. d. R. Millán, R. Riener, H. Vallery, and R. Gassert, "Control strategies for active lower extremity prosthetics and orthotics: a review," *Journal of NeuroEngineering and Rehabilitation*, vol. 12, no. 1, 2015.

[21] J. Nikitczuk, B. Weinberg, P. Canavan, and C. Mavroidis, "Active knee rehabilitation orthotic device with variable damping characteristics implemented via an electrorheological fluid," *Mechatronics, IEEE/ASME Transactions on*, vol. 15, pp. 952–960, Dec 2010.

[22] P. P. Pott, H. Graefenstein, J. Fischer, R. Mueller, H. F. Schlaak, and E. Abele, "Series elastic actuators for man-machine cooperation," in *Innovative Small Drives and Micro-Motor Systems, 2013. 9. GMM/ETG Symposium*, pp. 1–5, Sept 2013.

[23] S. Talbi, B. Daachi, and K. Djouani, "Rbf-based neuro-adaptive controller for a knee joint rehabilitation orthosis," in *Neural Information Processing* (M. Lee, A. Hirose, Z.-G. Hou, and R. Kil, eds.), vol. 8226 of *Lecture Notes in Computer Science*, pp. 257–266, Springer Berlin Heidelberg, 2013.

[24] H.-T. Tran, H. Cheng, X. Lin, M.-K. Duong, and R. Huang, "The relationship between physical human-exoskeleton interaction and dynamic factors: using a learning approach for control applications," *Science China Information Sciences*, vol. 57, no. 12, pp. 1–13, 2014.

[25] H.-B. Kang and J.-H. Wang, "Adaptive robust control of 5 dof upper-limb exoskeleton robot," *International Journal of Control, Automation and Systems*, vol. 13, no. 3, pp. 733–741, 2015.

[26] L. Flynn, J. Geeroms, R. Jimenez Fabian, B. Vanderborght, and D. Lefeber, "Cyberlegs beta-prosthesis active knee system," in *ICORR 2015 IEEE International Conference on Rehabilitation Robotics*, pp. 410–415, 2015.

[27] E. J. Rouse, L. M. Mooney, and H. M. Herr, "Clutchable series-elastic actuator: Implications for prosthetic knee design," *International Journal of Robotics Research*, vol. 33, pp. 1611–1625, Nov. 2014.

[28] S. Au and H. Herr, "Powered ankle-foot prosthesis," *Robotics Automation Magazine, IEEE*, vol. 15, pp. 52–59, September 2008.

[29] M. Grimmer, *Powered Lower Limb Prostheses*. PhD thesis, Technische Universität, Darmstadt, February 2015.

[30] B. Vanderborght, R. Van Ham, D. Lefeber, T. Sugar, and K. Hollander, "Comparison of mechanical design and energy consumption of adaptable, passive-compliant actuators," *International Journal of Robotics Research*, vol. 28, pp. 90–103, 1 2009.

[31] J. Pratt, B. Krupp, and C. Morse, "Series elastic actuators for high fidelity force control," *Industrial Robot: An International Journal*, vol. 29, no. 3, pp. 234–241, 2002.

[32] G. Tonietti, R. Schiavi, and A. Bicchi, "Design and control of a variable stiffness actuator for safe and fast physical human/robot interaction.," in *ICRA*, pp. 526–531, IEEE, 2005.

[33] J. J. Park, Y. J. Lee, J. B. Song, and H. S. Kim, "Safe joint mechanism based on nonlinear stiffness for safe human-robot collision," in *Robotics and Automation, 2008. ICRA 2008. IEEE International Conference on*, pp. 2177–2182, May 2008.

[34] R. V. Ham, T. G. Sugar, B. Vanderborght, K. W. Hollander, and D. Lefeber, "Compliant actuator designs," *IEEE Robotics Automation Magazine*, vol. 16, pp. 81–94, September 2009.

[35] B. Brogliato, R. Lozano, B. Maschke, and O. Egeland, *Dissipative Systems Analysis and Control : Theory and Applications*. Communications and Control Engineering, London: Springer, 2007.

[36] Verein Deutscher Ingenieure, "VDI 2206: Design methodology for mechatronic systems," June 2004.

[37] A. Schumacher, *Optimierung mechanischer Strukturen: Grundlagen und industrielle Anwendungen*. Springer Vieweg, Springer, 2013.

[38] T. Verstraten, G. Mathijssen, R. Furnémont, B. Vanderborght, and D. Lefeber, "Modeling and design of geared DC motors for energy efficiency: Comparison between theory and experiments," *Mechatronics*, vol. 30, pp. 198 – 213, 2015.

[39] K. Shamaei, G. S. Sawicki, and A. M. Dollar, "Estimation of quasi-stiffness of the human knee in the stance phase of walking," *PLoS ONE*, vol. 8, pp. 1–10, 03 2013.

[40] M. K. Mak, O. Levin, J. Mizrahi, and C. W. Hui-Chan, "Joint torques during sit-to-stand in healthy subjects and people with parkinsonâ€™s disease," *Clinical Biomechanics*, vol. 18, no. 3, pp. 197 – 206, 2003.

[41] G. Pahl, W. Beitz, J. Feldhusen, and K.-H. Grote, *Engineering Design: A Systematic Approach*. Springer, 3rd ed., Jan. 2007.

[42] E. J. Rouse, L. M. Mooney, E. C. Martinez Villalpando, and H. M. Herr, "Clutchable series-elastic actuator: Design of a robotic knee prosthesis for minimum energy consumption," in *Rehabilitation Robotics (ICORR), 2013 IEEE International Conference on*, pp. 1–6, 2013.

[43] K.-H. Grote and J. Feldhusen, *Dubbel*. Wiesbaden: Springer Berlin Heidelberg, 2007.

[44] S.-S. Yoon, S. Kang, S.-k. Yun, S.-J. Kim, Y.-H. Kim, and M. Kim, "Safe arm design with mr-based passive compliant joints and visco—elastic covering for service robot applications," *Journal of Mechanical Science and Technology*, vol. 19, no. 10, pp. 1835–1845.

[45] C. Ott, *Cartesian Impedance Control of Redundant and Flexible-Joint Robots*. Springer Publishing Company, Incorporated, 1 ed., 2008.

[46] M. Lendermann, B. R. P. Singh, F. Stuhlenmiller, P. Beckerle, S. Rinderknecht, and V. P. Manivannan, "Comparison of passivity based impedance controllers without torque-feedback for variable stiffness actuators," in *2015 IEEE International Conference on Advanced Intelligent Mechatronics*, July 2015.

[47] D. Callejo Goena, "Design of a test bench to evaluate the dynamic performance of the actuation system of an active knee-ankle-foot orthosis," Master's thesis, Escola Tècnica Superior d'Enginyeria Industrial de Barcelona, 2014.

[48] S. Orozco Martin, "Estudi del model dinàmic del banc d'assaig i del sistema d'actuació d'una ortesi activa de genoll per a lesionats medul lars.," 2015. Bachelor's Thesis.

[49] M. Lendermann, F. Stuhlenmiller, P. Erler, P. Beckerle, and S. Rinderknecht, "A systematic approach to experimental modeling of elastic actuators by component-wise parameter identification," in *IEEE/RSJ International Conference on Intelligent Robots and Systems*, October 2015.

[50] P. S. Gandhi, F. H. Ghorbel, and J. Dabney, "Modeling, identification, and compensation of friction in harmonic drives," in *Decision and Control, 2002, Proceedings of the 41st IEEE Conference on*, vol. 1, pp. 160–166 vol.1, Dec 2002.

[51] H. Olsson, K. J. Astrom, C. C. de Wit, M. Gafvert, and P. Lischinsky, "Friction models and friction compensation," *Eur. J. Control*, vol. 4, no. 3, pp. 176–195, 1998.

[52] D. Schröder, *Intelligente Verfahren: Identifikation und Regelung nichtlinearer Systeme (German Edition)*. Springer, 1st edition. ed., June 2010.

[53] T. Nef and P. Lum, "Improving backdrivability in geared rehabilitation robots," *Medical & Biological Engineering & Computing*, vol. 47, no. 4, pp. 441–447, 2009.